



Catalysis Reviews

Science and Engineering

ISSN: (Print) (Online) Journal homepage: <https://www.tandfonline.com/loi/lctr20>

A comprehensive and critical review on recent progress in anode catalyst for methanol oxidation reaction

Afdhal Yuda, Anchu Ashok & Anand Kumar

To cite this article: Afdhal Yuda, Anchu Ashok & Anand Kumar (2022) A comprehensive and critical review on recent progress in anode catalyst for methanol oxidation reaction, Catalysis Reviews, 64:1, 126-228, DOI: [10.1080/01614940.2020.1802811](https://doi.org/10.1080/01614940.2020.1802811)

To link to this article: <https://doi.org/10.1080/01614940.2020.1802811>



© 2020 The Author(s). Published with license by Taylor & Francis Group, LLC.



Published online: 30 Aug 2020.



Submit your article to this journal [↗](#)



Article views: 9611



View related articles [↗](#)




View Crossmark data [↗](#)



Citing articles: 28 View citing articles [↗](#)

A comprehensive and critical review on recent progress in anode catalyst for methanol oxidation reaction

Afdhal Yuda, Anchu Ashok, and Anand Kumar 

Department of Chemical Engineering, Qatar University, Doha, Qatar

ABSTRACT

The synthesis of anode electrocatalyst with high activity and durability for methanol oxidation reaction has been one of the main focuses of researchers in recent years. Several works are reviewed in this paper to summarize and compare the performance of electrocatalysts comprising of noble and non-noble metals. The effect of manipulating catalysts by introducing nanostructured morphology, metal alloys, support materials, acidic or basic electrolyte, and synthesis methods are also examined. The paper finally concludes with details of challenges that are generally faced in making direct methanol fuel cell (DMFC) a reliable source of energy for future prospects, and the approach to be taken to reduce the complexity in synthesizing new generations of anode electrocatalysts.

ARTICLE HISTORY


Received January 21, 2020
Revised June 10, 2020
Accepted July 23, 2020

KEYWORDS

Methanol oxidation;
CO poisoning; Supports;
DMFC

1. Introduction

The increase in human population and the growing importance of technology have both contributed to the upsurge in the demand of energy. Data obtained by the US Energy Information Administration (EIA) have shown that energy utilization was roughly equal in 2007 between Organization for Economic Co-operation and Development (OECD) and non-OECD countries. However, from 2007 to 2035, OECD countries have been estimated to increase their energy use by 14%, while that of non-OECD countries is forecasted to grow by 84%.^[1] Currently, energy applications in the form of electricity is predominant amongst electronic devices such as chargers for laptops, cameras, and mobile phones. These chargers or rechargeable batteries have a disadvantage of needing to charge using an external electrical power source. This dependency is an obstacle to their usage due to the requirement of an existing electrical source and the battery itself is limited in capacity. Therefore, remote areas without any source of electric power can face problems using devices operating on such batteries. Furthermore, the sources of electric power are mostly derived from fossil fuels, which has a negative impact on the environment as the number of technology users

CONTACT Anand Kumar  akumar@qu.edu.qa Department of Chemical Engineering, Qatar University, P O Box 2713, Doha, Qatar

© 2020 The Author(s). Published with license by Taylor & Francis Group, LLC.
This is an Open Access article distributed under the terms of the Creative Commons Attribution License (<http://creativecommons.org/licenses/by/4.0/>), which permits unrestricted use, distribution, and reproduction in any medium, provided the original work is properly cited.

depending on electricity continue to escalate. It was reported that nearly 6.2 billion tons of carbon dioxide was released into the atmosphere in 2000 and out of this about 40% was due to emissions from electricity production.^[2] As a result, researchers are encouraged to find alternative power sources that are renewable and eco-friendly.

Recently, advances in the field of direct alcohol fuel cells (DAFCs) have been a trend amongst researchers and manufacturers to find an alternative fuel in generating electrical energy. This is also due to a desire to exploit the benefits of alcohol fuel cell technologies; particularly its environmentally friendliness, low cost, portability, and the high-energy density of alcohols such as methanol and ethanol. Direct methanol fuel cell (DMFC), for example, requires no electricity to recharge, have low temperatures operability, can be developed to have an extended lifetime, and utilizes a swift refueling system.^[3-6] However, there are still challenges presented by DMFCs that need to be addressed. The issues that are encountered in DMFCs can stem from situations such as high cost, methanol crossover issues through the proton exchange membrane, and problems in managing heat and water and maintaining long-term stability and durability in operation.^[7] Other challenges that arise can also include the assembly of membrane electrode, catalyst loading, membrane thickness, diffusion layer, and low power density. Moreover, the slow reactions that occur on the cathode (oxygen reduction) and the anode (methanol oxidation) have posed a challenge to direct methanol fuel cell operations. Increasing the catalyst loading has been generally implemented to achieve high methanol conversion in MOR in Micro-DMFC consisting of platinum-based catalyst. However, methanol crossover can occur due to higher loading and there is also an increase in cost as more of platinum-based electrocatalyst is used. To overcome this problem many studies have been performed to identify catalysts with suitable functionality and cost to enhance the operations and commercialization of fuel cells as alternative sources of energy.

Synthesis of catalysts containing platinum has been studied by many researchers as Pt promotes high catalytic efficiency, excellent electrical properties and is highly resistant to corrosion. This, therefore, made it extensively suitable to be used by chemical, petrochemical, pharmaceutical, electronic, and automotive industries.^[8,9] However, because platinum being one of the noble and rare metals, recent studies have been directed toward synthesizing catalysts containing reduced quantities of platinum. This includes alloying platinum with other noble or non-noble metals, such as ruthenium, palladium, nickel, iron, and cobalt, or embedding platinum on metal oxides such as MnO_2 and RuO_2 . These combinations help enhance the performance of the synthesized catalyst in oxidizing methanol and improving the efficiency of DMFC.^[10-16]

Another reason to avoid the use of a pure platinum catalyst is that it has been observed to be deactivated by the carbon monoxide generated during the electro-oxidation of methanol. The adsorbed carbon monoxide intermediates degrade the platinum catalyst and reduce its lifetime when used in fuel cells. Additional metals can prevent such circumstances and upgrade the anti-CO poisoning ability of a catalyst by modifying the CO adsorption site.

Attention has also been given to the fabrication of nano-sized catalysts that involve developing functional platinum-based materials with specified geometrical layout, shape, and composition. For example, incorporating porous platinum-based nanostructures with narrow pore-size and extremely ordered network arrangements offers an advantage over the solid or bulk counterparts. This not only optimizes the surface area for great mass transfer efficiency of reactant molecules, but also enhances the mobility of electrons in the solid ligaments.

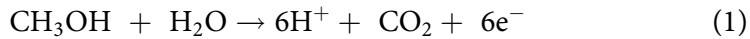
The addition of catalyst supports that are mesoporous and conductive are frequently conducted to promote catalyst durability and charge transfer efficiency. The categories of support materials include carbonaceous materials, such as carbon nanotubes, activated carbon and graphene, and noncarbonaceous materials, namely metal oxides and mesoporous silica. Pores can also be introduced to the support materials of electrocatalysts, however control is required to obtain the right pore size. Although small pores can increase the surface area, they can reduce the mass transport rate. Overall, the support materials must possess certain key characteristics, as listed below, to make them suitable for practical applications ^[17]:

- Good electrical conductivity
- Large surface area
- Strong link between the support and the catalyst
- Mesoporous structure
- Excellent water handling
- Acceptable resistivity toward corrosion
- Simple catalyst recovery

In this review paper, the focus will be given to the various electrocatalysts recently synthesized that are comprised of noble or non-noble metals for methanol oxidation reactions (MOR) occurring on the anode of DMFC. In addition, the influences of catalyst size and shape, electrolyte conditions (acidic or alkaline), the type of support materials, as well as the effect of synthesis method will also be reviewed. Recent challenges encountered in the development of micro-DMFC for commercialization will also be discussed in this paper.

2. Mechanism of methanol oxidation reaction

Within the direct methanol fuel cell, the electro-oxidation of methanol occurs on the anode. This anodic reaction can be depicted by the following equation:



Complex reactions are involved in producing carbon dioxide indirectly, where several intermediates are formed following various pathways.^[18] A representation of the possible reaction pathways along with their intermediates is shown in Figure 1.

Based on Figure 1, it can be observed that a pair of proton and electron are produced from each carbonaceous compound. There are also intermediate species undergoing reactions that do not generate electron/proton pair, which are illustrated by the light blue arrows. The water molecules present in the medium surrounding the anode also produce electron/proton pair in the form of hydroxyl groups and get combined with some of the intermediates. Carbon monoxide is one of the intermediates being produced that restricts the rate of methanol oxidation in the anode due to its relatively higher stability.^[19] After a series of adsorption and deprotonation that takes place on the anode catalyst carbon monoxide is formed that blocks the active sites of the catalyst.^[20] The presence of CO suppresses any other reaction from occurring and their formation is represented on Figure 2. The formation of CO occurs as a result of an indirect mechanism in which CHO or COH are directly dehydrogenated. Such incidents are not observed in the direct mechanism. When formyl or COH has been formed from formaldehyde or hydroxymethylene that undergoes hydrogen abstraction, a proton/electron pair is taken away from a water molecule that

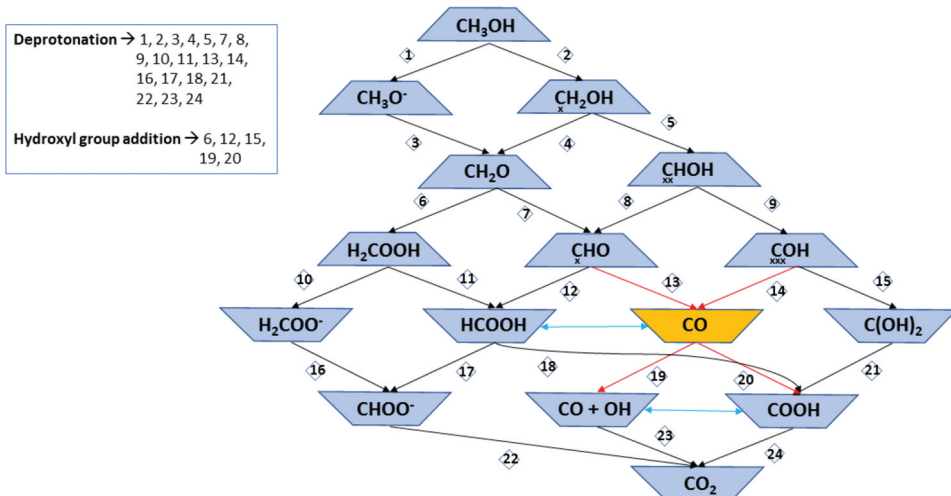


Figure 1. The possible reaction products and reaction paths (reaction scheme) for methanol oxidation.

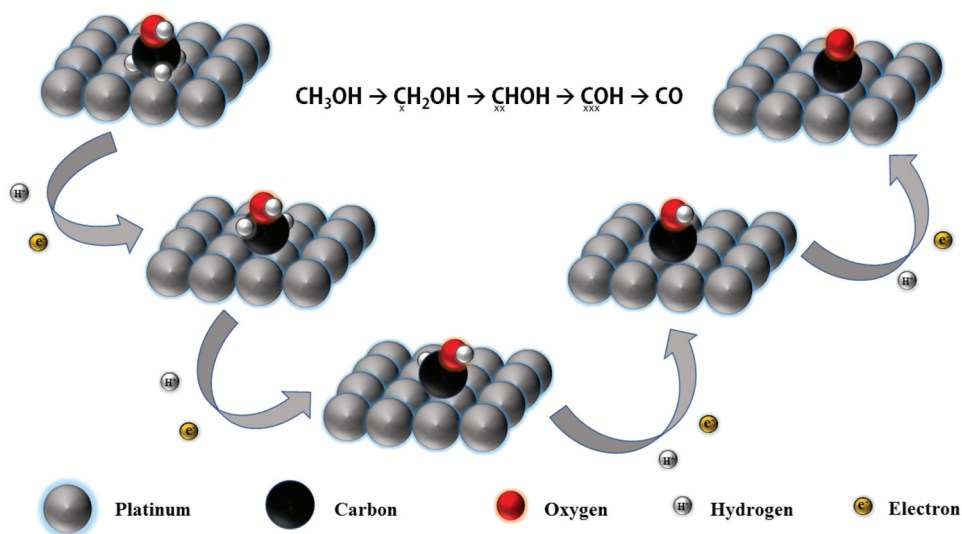


Figure 2. An illustration of the successive stripping of hydrogen atoms during methanol oxidation.

leads to OH group being formed. The OH group then combines with the carbonaceous species that causes di-oxygenated species (e.g. dihydroxycarbene ($\text{C}(\text{OH})_2$) or formic acid (HCOOH) to be produced. Dehydrogenation then follows the OH addition to form either carboxyl (COOH) or formate (HCOO), that lead to the production of CO_2 after subsequent dehydrogenation. CO_2 production can also occur through an alternative direct pathway. Through this pathway a proton/electron pair is stripped off of water and the hydroxyl that is formed is added to formaldehyde to produce H_2COOH . This intermediate can then become formic acid or dioxymethylene (H_2COO) as it gets dehydrogenated. Further dehydrogenation of dioxymethylene produces formate that also undergoes the same reaction to ultimately form CO_2 .

A possibility of removing carbon monoxide from the catalyst surface can be accomplished by oxidizing this intermediate with species such as water (or OH^- ions) containing oxygen which can get adsorbed onto the surface of the catalyst. Water gets dissociated separately to produce OH on the surface. The two surface species can then react together to produce carbon dioxide in a similar way to that of water-gas-shift reaction.^[21,22] Hence, many studies have been carried out with other metals or by incorporating those along with platinum to create catalysts that do not only enhance catalyst activity, but that are also not susceptible to carbon monoxide poisoning.^[23–25]

It is also vital to understand the kinetics and the thermodynamics involved in modeling DMFC in which MOR occurs. Several tools exist that should be considered to evaluate the overall performance of a cell and to comprehend the kinetics involved in MOR, and they are described in the following sections.

2.1. Polarization curve

This curve is a plot of cell voltage against current density. In this curve both the cathode and anode losses are summed together and the information related to each half-cell is lost. Common data regarding the performance of the cell and the different losses occurring in the system are identified using the polarization curve.

The various losses that can be determined from a polarization curve are mass transport, ohmic, and activation losses, which are illustrated in [Figure 3](#). Mass transport loss occurs due to the lack of reactants present near the catalyst sites. The loss is remarkably notable at high values of current density where high demand for reactants at the catalyst sites cannot be achieved. Observing [Figure 3](#), the value of the limiting current density is at 600 A m^{-2} at which the concentration of either methanol at the anode catalyst layer (ACL) or oxygen at the cathode catalyst layer (CCL) are markedly reduced. The loss in mass transport becomes the leading cause of voltage loss near the point where limiting current density is reached. Ohmic losses involve the loss of potential due to resistance in the flow of electric charges (ions or electrons) as they move through a medium. In direct methanol fuel cells, this type of loss mostly originates from the ionic (H^+) transport in the membrane layers and the

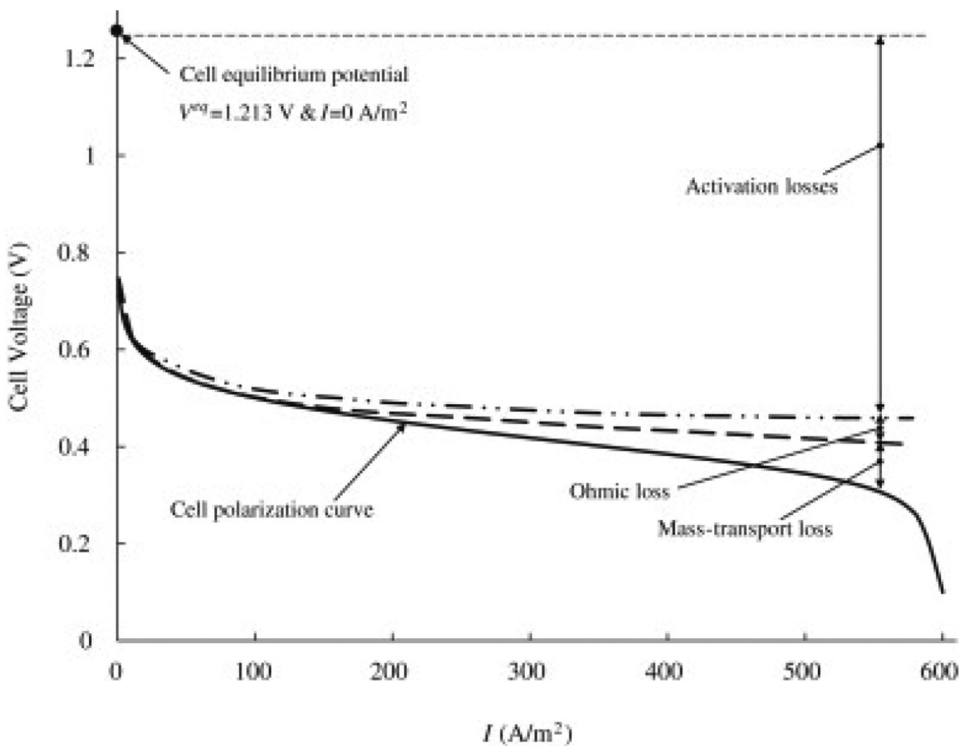


Figure 3. A schematic representation of a polarization curve. Reproduced with permission from Elsevier ^[26]

catalyst. The gas diffusion layer has an electron conductivity of $O(1000 \Omega^{-1} \text{ m}^{-1})$ that is almost 2 order of magnitude larger than the membrane's proton conductivity, $O(10 \Omega^{-1} \text{ m}^{-1})$. Hence, an ohmic loss that is due to the transport of electron is generally neglected. The third type of loss in direct methanol fuel cells is the activation loss which is the primary contributor to the loss of cell voltage at lower values of current density. It is the potential that is needed to shift the reaction from the equilibrium conditions. The anode activation loss might be a little bit greater than that of the oxygen reduction because of the slow kinetics of methanol oxidation.^[27]

2.2. Kinetics

This term describes the rates of electrochemical reaction for nonequilibrium conditions. In DMFC, two common approaches exist, the Butler-Volmer equation and the Tafel assumption. These are the very basic models used to describe electrochemical kinetics. There is also the non-Tafel kinetics which will also be described subsequently.

2.3. Butler-volmer model of kinetics

This model can be used to explain the kinetics of reactions taking place in both the cathode and anode electrodes. For a generic equilibrium electrochemical reaction of the form



Arrhenius equation may be used to display the backward or forward reaction rate constant (k , $\text{m}^2 \text{ s}^{-1}$):

$$k = A \cdot \exp\left(\frac{-E_A}{R_u T}\right) \quad (3)$$

Where,

A = frequency factor, $\text{m}^2 \text{ s}^{-1}$

T = temperature, K

R_u = universal gas constant, $\text{J K}^{-1} \text{ mol}^{-1}$

E_A = activation energy, J mol^{-1}

When the basic concept of activation overpotentials is applied into the Arrhenius equation and the mass transport limit is neglected,^[28] the kinetics of Equation 2 can be presented by the Butler-Volmer relation as follows:

$$J = aJ_o \left[\exp\left(-\frac{\alpha_c F}{R_u T} \eta\right) - \exp\left(-\frac{\alpha_a F}{R_u T} \eta\right) \right] \quad (4)$$

Where,

a = electrochemically active area per unit catalyst volume, m^{-1}

J = reaction rate, A m^{-3}

J_o = exchange current density, A m^{-2}

η = overpotential, V

α = transfer coefficient

Subscripted 'a' = anodic reaction (backward, $\eta > 0$)

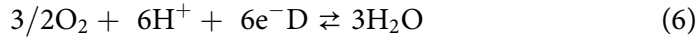
Subscripted 'c' = cathodic reaction (forward, $\eta < 0$)

In Equation 4:

$$\alpha_a + \alpha_c = 1 \quad (5a)$$

$$\eta = V - V^{\text{eq}} \quad (5b)$$

Tafel kinetics refers to the situation in which the reaction in Equation 2 shifts in a preferential direction so that one of the terms on the right hand section of Equation 4 is way smaller than that the other. For the oxygen reduction reaction, the Tafel kinetics is attained by incorporating the mass-transport considerations [28] as well as assuming insignificant oxidation (backward) reaction of the equilibrium half-cell reaction in the cathode catalyst layer that has the equation:



The Tafel kinetics obtained is then as follows:

$$J_{\text{O}_2} = \alpha J_{o,\text{O}_2} \cdot \left(\frac{C_{\text{O}_2}}{C_{\text{O}_2}^{\text{ref}}} \right) \cdot \exp\left(-\frac{\alpha_c F}{R_u T} \eta_c \right) \quad (7)$$

Where,

C = concentration at the reaction sites, mol m^{-3}

Superscripted 'ref' = reference value

Aside from the continuous usage of Tafel kinetics for MOR, [29–38] it is not a suitable assumption for the sluggish methanol oxidation reaction. For MOR, the Tafel kinetics is obtained in a similar way to that of Equation 7 and it is as follows:

$$J_{\text{MeOH}} = \alpha J_{o,\text{MeOH}} \cdot \left(\frac{C_{\text{MeOH}}}{C_{\text{MeOH}}^{\text{ref}}} \right) \cdot \exp\left(\frac{\alpha_a F}{R_u T} \eta \right) \quad (8)$$

Although a negativity in anodic reaction rate is observed in Equation 4, from the mass transport modeling point of view, the absolute value of the rate is what matters.

It is essential to understand the relation between the phase potentials and the overpotential (η) before moving on to the non-Tafel kinetics for

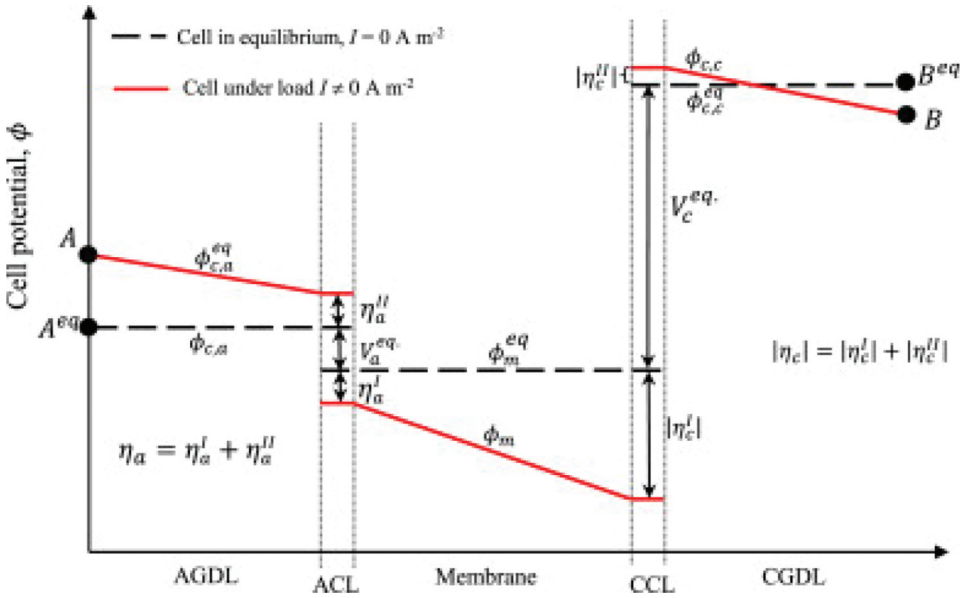


Figure 4. A schematic representation of potential distributions for a direct methanol fuel cell in nonequilibrium ($I \neq 0 \text{ A m}^{-2}$) and equilibrium ($I = 0 \text{ A m}^{-2}$) conditions. Reproduced with permission from Elsevier ^[26]

methanol oxidation reaction. In Figure 4, a conceptual illustration of the overpotential is presented by differentiating the local potential distributions for the nonequilibrium ($I \neq 0 \text{ A m}^{-2}$) and equilibrium ($I = 0 \text{ A m}^{-2}$) conditions. In the same figure the membrane potential is denoted by ϕ_m and the electrode potential is represented by ϕ_c . An assumption is also made that there is no methanol crossing through the membrane. All of the potential lines are horizontal when the cell is at equilibrium. This means that there is no voltage loss and is represented by dashed lines in Figure 4. The difference in electrode potential (ϕ_c) between the 2 ends of the cell, which is between points A and B in Figure 4, is termed as the overall cell equilibrium voltage. It has the equation:

$$V_{cell}^{eq} = \phi_{c,c}|_{B^{eq}} - \phi_{c,a}|_{A^{eq}} = V_c^{eq} - V_a^{eq} \quad (9)$$

Based on the fundamental thermodynamics principles, the equilibrium half-cell potentials of both the anode (V_a^{eq}) and cathode (V_c^{eq}) at standard temperature (25 °C) and pressure (1 atm) can be achieved according to the change in standard Gibbs free energy (\bar{G}) for the corresponding half-cell reaction as follows:

$$V_a^{eq} = \frac{-\Delta\bar{G}_a}{6F} = 0.016V \quad \& \quad V_c^{eq} = \frac{-\Delta\bar{G}_c}{6F} = 1.229V \quad (10)$$

Where,

F = Faraday constant

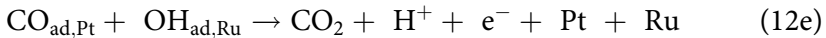
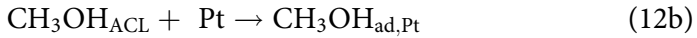
Hence, the value of the equilibrium cell voltage ($V_{\text{cell}}^{\text{eq}}$) is 1.213 V. During situations in which the cell is under a load, ($I \neq 0 \text{ A m}^{-2}$), losses are experienced by the potential as the protons and electrons flow through the corresponding transport medium (represented by continuous lines in Figure 4). The overpotentials of the cathode and anode in the layers of the catalyst are interpreted as follows:

$$\eta_c = -\left(\phi_{c,c} - \phi_m - V_c^{\text{eq}}\right) \quad (11a)$$

$$\eta_a = -\left(\phi_{c,a} - \phi_m - V_a^{\text{eq}}\right) \quad (11b)$$

2.4. Non-Tafel kinetics for methanol oxidation

This type of kinetics is generally used for studying a reaction as a collection of multistep reactions. The Butler-Volmer kinetic model previously described is still utilized for each individual step. Different sets of multistep reaction of methanol oxidation reaction have been reported.^[39–41] Non-Tafel kinetic for methanol oxidation reaction that is most common is attained by taking into account the elementary and intermediate reactions that are as follows^[41]:



Where,

Subscripted ‘ad’ = adsorption to the corresponding catalyst surface

When the Butler-Volmer relation is used for each step while assuming a methanol solution that is dilute and carrying out some mathematical modifications, the extensively implemented non-Tafel kinetics of the methanol oxidation reaction is obtained as follows^[41]:

$$J_{\text{MeOH}} = \alpha J_{o,\text{MeOH}} \frac{C_{\text{MeOH}}}{C_{\text{MeOH}} + \Gamma \exp\left(\frac{\alpha_a F}{R_u T} \eta\right)} \exp\left(\frac{\alpha_a F}{R_u T} \eta\right) \quad (13a)$$

Where the symbol ‘ Γ ’ is the kinetic constant and has the following equation ^[41]:

$$\Gamma = K \exp\left(\frac{\alpha_a F}{R_u T} V_a\right) \quad (13b)$$

The constant ‘ K ’ is calculated according to the reaction rate constant found in Equations 12c and 12e.

When the Tafel and non-Tafel kinetics of Equations 8 and 13a are compared the non-Tafel kinetics is exhibited to give a significant concentration dependency for the kinetics of MOR that is $C_{\text{MeOH}}/(C_{\text{MeOH}} + \Gamma \exp(\alpha_a F \eta / R_u T))$. Tafel kinetics linearly links the rate of reaction and the concentration of methanol by providing a reference value, $C_{\text{MeOH}}^{\text{ref}}$, that must be fitted using experimental data.

3. Types of catalyst for MOR

One of the most important factors that contribute to the reliability of DMFC is the electro-catalyst used to enhance its performance. The motivation to search for an effective and efficient cathodic or anodic catalyst has presently become predominant amongst researchers seeking alternative materials that bring about more attractive features to replace the generally used noble metal-based catalysts (e.g. platinum-based). New catalysts that are relatively cheaper and easier to synthesize, which possesses a highly superior activity, anti-CO ability, and durability are more favorable for catalyzing reactions such as methanol oxidation. Hence, catalysts containing lesser amount of Pt noble metal and more non-noble metals that may be supported or not, are widely studied and developed for operation in DMFC and a number of them will be examined in the following paragraphs. The types of catalysts discussed are categorized into those containing noble metals, such as platinum (in pure, alloyed, or supported form), rhodium (in pure and supported form), palladium (in supported form), and non-noble metals that include nickel (as nickel oxides and in supported form), cobalt, and copper. Their performance are analyzed based on the methanol oxidation peak (or current density) at a given onset potential that is generally identified using cyclic voltammetry and based on catalytic stability commonly studied using chronoamperometry. Other useful parameters such as mass specific current densities and peak area will also be stated to assist with comparison between different catalysts. In addition, characteristic parameters playing important role in determining the electrochemical performance, for example, morphology, composition, thermal stability, durability, electrochemical active surface area, and endurance toward poisoning species (e.g. CO) are also presented from different studies.

3.1. Catalysts based on noble metals

3.1.1. Platinum and alloys of platinum

Catalysts synthesis research incorporating minimum quantity of platinum have also considered exploring and optimizing structures at nanoscales as an effective way to increase the available surface area, such as mesoporous platinum^[15,42-46] and as well to maintain this area for an extended time period.^[47-49]

The type of morphology that is suitable to maintain long-term stability is known to be the self-supported one-dimensional architecture.^[13,50-52] With this structure it is possible to avoid the problem of catalytic activity loss commonly faced by platinum catalysts due to oxidation/dissolution process. This issue is also largely found in materials such as carbon-supported platinum.^[53,54] In addition, the structure also promotes smooth transfer of electron and prevents damage to the catalyst structure.^[55,56] Li *et al* have earlier invented a novel “electrochemical micelle assembly” soft-template method to produce a mesoporous platinum of controlled pore size, and to better control the type of shape for platinum-based materials, such as one-dimensional nanowires and two-dimensional films.^[13,57-59] Implementing a mesoporous design can improve the electrochemically active area and build a concave surface to provide more active sites for reactions to take place. They then expanded the micelle assembly method to prepare different mesoporous platinum nanowires of varying lengths and diameters. This was made possible by activating the extension of mesoporous platinum within polycarbonate membrane channels. The various types of mesoporous platinum nanowires synthesized possess ideal design of a catalyst with large surface area and good facile mass transportation via the mesoporous structures present in the nanowires. The one-dimensional mesoporous platinum nanowires displayed great durability, largely due to the self-assembled one-dimensional morphology that allows the presence of a large electrochemically active surfaces suitable for methanol oxidation.^[60]

3.1.1.1. Pure platinum. Jiang’s research group utilized a different approach to produce mono-dispersed mesoporous architectures and, for the first time, employed a synthetic route that incorporates a slow reduction reaction with a surfactant (one-pot method).^[12] The mesoporous platinum are produced in the form of nanospheres that also have a large number of active sites being created by the selective adsorption of bromide ions [Figure 5a](#). In addition to the high-quality electrochemical performance of the mesoporous platinum nanospheres (MPNs) as a catalyst for methanol oxidation, it also demonstrates tremendous structural thermostability. This characteristic is an extremely important element related to the practical use of the catalyst as the performance is determined by their potential to

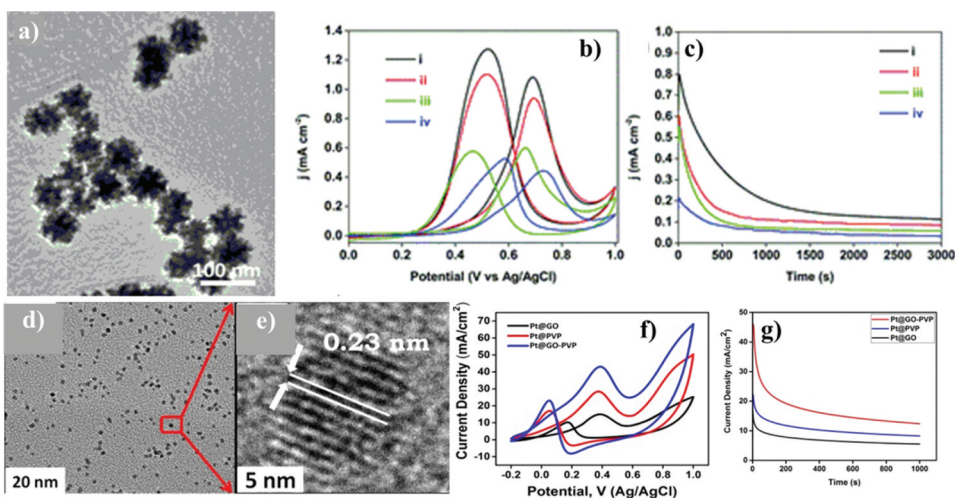


Figure 5. (a) Low-magnification TEM image of mesoporous Pt nanospheres. (b) CV curves (at 50 mV s^{-1} scan rate) and (c) CA curves (at 0.6 V) for (i) MPNs with interconnected mesopores, (ii) DPNs, (iii) PtCarbon-20% and (iv) PtBlack catalysts in $0.5 \text{ M H}_2\text{SO}_4 + 0.5 \text{ M CH}_3\text{OH}$. (d) TEM and (e) HRTEM images of Pt@GO-PVP NPs. (f) CV curves of Pt@GO NPs, Pt@PVP NPs and Pt@GO-PVP NPs at a scan rate of 50 mV s^{-1} (in $0.5 \text{ M H}_2\text{SO}_4 + 0.5 \text{ M}$ methanol nitrogen-saturated solution). (g) CA curves of Pt@GO-PVP NPs, Pt@PVP NPs and Pt@GO NPs at 0.39 V potential (in $0.5 \text{ M H}_2\text{SO}_4 + 0.5 \text{ M CH}_3\text{OH}$ nitrogen-saturated solution). Reproduced with permission from Royal Society of Chemistry ^[12], Reproduced with permission from Elsevier ^[61]

achieve and retain their initial structure and shape. To test this result, Jiang *et al* treated the MPNs, dendritic platinum nanoparticles (DPNs), PtCarbon-20% and PtBlack at $250 \text{ }^\circ\text{C}$ or $350 \text{ }^\circ\text{C}$ for 3 hours. ^[12] Plots of their cyclic voltammetry were obtained after calcination (at a scanning rate of 50 mV s^{-1} , in $0.5 \text{ M H}_2\text{SO}_4$ solution) and their relative platinum electrochemical active surface area (ECSA) values were calculated **Figure 5b**. Comparison have shown that MPNs managed to preserve 97% of their original ECSA even when exposed to $350 \text{ }^\circ\text{C}$, while for DPNs, PtCarbon-20%, and PtBlack their values were 82%, 38%, and 23%, respectively. The reason for this distinct characteristic of MPNs is due to the resistivity of the mesoporous structure toward particle aggregation. Such behavior is not observed in DPNs as their stability is impaired at high temperature when their structure wither. ^[43,62] PtCarbon-20% and PtBlack, on the other hand, suffer an enormous drop in their ECSA values that can be explained by the aggregation of nanoparticles and carbon support disintegration at high temperatures.

3.1.1.2. Platinum alloy. Recent studies have also involved platinum and its alloys with other metals to optimize the activity of catalysts for methanol oxidation reaction. Metals with which platinum were combined include ruthenium, bismuth, copper, cobalt, and nickel prepared through various

synthesis methods to obtain a highly satisfactory bimetallic catalytic activity in comparison to those of catalysts present commercially.^[63–68]

A study performed by Taylor *et al.* covered the preparation of a series of Ru-Pt bimetallic catalysts (Ru on commercial monometallic Pt/C catalyst), using electroless deposition technique, in which their activities were analyzed according to their surface composition.^[63] With electroless deposition, the surface composition could be accurately controlled and is a less costly method to deal with the sensitivity of activity toward the surface coverage. It was observed that a maximum activity occurred at about 50% monodisperse ruthenium surface coverage (or 0.51 monodisperse coverage θ_{Ru} (on platinum)) of 20 wt% platinum and 1.1 wt% ruthenium and this activity, based on a mass of platinum, was 7 times greater than that of a pure platinum. Moreover, in comparison to the commercial bimetallic catalysts consisting of a bulk 1:1 atomic ratio of ruthenium to platinum, the maximum activity was 3.5 times more and the quantity of ruthenium metal present in the catalyst is reduced as a result of the single-layer coverage of ruthenium on platinum.

Lu and coworkers published a study that focused on the creation of bimetallic platinum-based nanodendrites to make use of their large surface areas and low densities.^[64] Ruthenium was again the accompanying metal used alongside platinum and the resulting catalyst was synthesized using coreduction of platinum and ruthenium precursors in oleylamine by H_2 (one-pot synthesis). The catalytic activity and durability of PtRu nanodendrites for methanol oxidation was also compared with nanocrystals of PtRu, of platinum, and commercial platinum/carbon catalyst and was proved to be far more superior. This is to a certain degree due to the enhanced electrochemical active surface area (ECSA), as a result of the dendritic shape. Furthermore, the catalyst's morphology, such as the presence of multiatomic corners, multiple branched arms, and surface cavities plays an important role in providing adequate catalytic sites for methanol molecules. Another point to consider is that when compared with the platinum nanoparticles in Pt/C the nanodendrites of PtRu are slightly resistant toward dissolution and aggregation. In terms of the bimetallic composition, alloying platinum with ruthenium modifies the electronic configuration of platinum that assists in breaking the bond between carbon and hydrogen in methanol molecules at lower potential. Simultaneously, the existence of a lattice mismatch between platinum and ruthenium atoms creates a strain effect that reduces the binding energies of intermediates such as carbon monoxide, hence increasing the catalyst's tolerance toward such intermediates. Ruthenium also has the capacity to efficiently oxidize carbon monoxide by delivering species carrying oxygen at lower potential.^[69–72]

3.1.1.3. Supported platinum. Platinum may also be combined with certain supporting materials to enhance its catalytic performance and resistivity

toward deactivating species. Using Graphene oxide (GO), for example, introduces electrochemical stability, and provides greater surface area, conductivity, and elasticity. Another material called Polyvinylpyrrolidone (PVP) is also assumed to have a good potential as a support as it possesses nontoxicity and chemical durability as well as very good solubility in several polar solvents.^[73–79] A hybrid of GO and PVP may then be able to further magnify the electrocatalytic activity of catalysts when they are used as a support. To support this view, Daşdelen *et al* synthesized shape-controlled platinum nanoparticles supported by GO and PVP hybrid, to serve as DMFCs' anode materials, through an eco-friendly method that combines sonochemical and Dimethylamine-borane (DMAB) reduction methods.^[61] During their studies the effect that the hybrid has on activity and durability was compared with that of Platinum@GO (metal-carbon) and Platinum@PVP (metal-polymer) catalysts. In comparison to these catalysts, it was observed that there is an increased adsorption rate of methanol molecules due to relatively more active surface area being present on the hybrid catalyst. In addition to larger surface area, the hybrid support assisted in minimizing electrocatalytic reduction in the methanol oxidation reaction. For these reasons, the hybrid supported catalyst functioned with greater catalytic activity than the other individual catalysts synthesized. Cyclic voltammetry experiment in an acidic medium (0.5 M H₂SO₄) showed 2 distinct high oxidation peaks in both forward and backward potential scans (50 mV s⁻¹ scan rate) **Figure 5f**. The methanol oxidation peak in the forward scan is approximately 0.38 V that has a peak current density of 43 mA/cm². The oxidation current then dropped when about 0.59 V is reached, and this is due to the production of platinum oxides. In the backward scan, an oxidation peak at about 0.05 V is observed as the oxidized carbonaceous species produced in the forward scan is removed and as methanol is oxidized. The activity performance of the hybrid-supported catalyst during comparison were found to be about 2.87 times more than Platinum@GO nanoparticles and about 1.53 times more than Platinum@PVP nanoparticles. In addition, chronoamperometry displayed a better catalytic stability and efficiency through a higher current value for the hybrid-supported catalyst when experimented for 1000 cycles (at 0.39 V) **Figure 5g**. Moreover, other detailed studies on catalysts based on platinum have also been performed to analyze their performance on the oxidation of methanol. They include catalysts such as Pt-Ru-Ni/C,^[80] Pt-Sn,^[81] Pt-WC/C,^[25] and Pt-MoO₃/C.^[24]

3.1.2. Rhodium

Fuel cells comprising of alkaline media, such as alkaline direct methanol fuel cells, have lately been analyzed because of their potential to boast enhanced reaction kinetics for both methanol oxidation and oxygen

reduction reactions. In addition, there is a broader usage of nonprecious metals, such as carbon and perovskite-type oxides as cathode electrocatalysts in alkaline medium. This helps substitute expensive platinum-based materials as catalysts and reduce the cost of commercializing DMFCs. Furthermore, the issue of managing water system in DMFCs previously mentioned can also be tackled and simplified using an alkaline medium.^[82–85]

3.1.2.1. Pure rhodium. Rhodium-based electrocatalyst that are relatively cheaper than Pt have recently been synthesized by Kang's team to study its catalytic activity toward methanol oxidation reaction in an alkaline medium.^[86] They demonstrated the controlled synthesis of rhodium nanodendrites with nanosheet subunits, using an effective and facile diethylene glycol reduction method in presence of polyethyleneimine (PEI, a surfactant and a complex-forming agent) **Figure 6(c – k)**. The specific nanodendrite morphology selected displayed an unexpectedly fine stability and catalytic activity characteristic when exposed to an alkaline medium. To support the findings, the catalyst was tested alongside the commercial electrocatalysts, and rhodium nanoaggregates that are formed when the rhodium nanocrystals vastly aggregate in the absence of PEI. The chronoamperometry results obtained for both rhodium nanodendrites and rhodium nanoaggregates showed that the current on rhodium nanodendrites sustained a value of nearly 20.5 times greater than that of rhodium nanoaggregates, even after

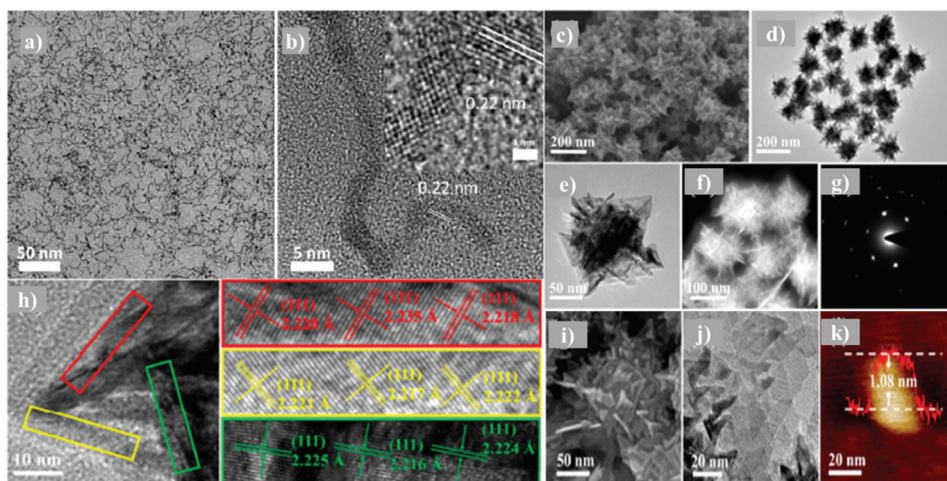


Figure 6. (a) TEM and (b) HRTEM images of ultrathin rhodium wavy nanowires. Rhodium nanodendrites' images obtained using (c) SEM, (d) TEM, (e) HRTEM, (f) HAADF-STEM and their (g) SAED pattern. (h) Rhodium nanocrystal subunits' HRTEM image along with the magnified version of different sections. (i) SEM image of rhodium nanodendrite (magnified). Images of strongly ultrasonic-treated rhodium nanodendrites obtained using (j) HRTEM and (k) AFM. Reproduced with permission from Springer Nature^[86,87]

6000 seconds. This means that rhodium nanodendrites possess a reduced decay rate (great stability) and fairly higher oxidation current (highly active) in comparison to rhodium nanoaggregates for methanol oxidation reaction. The finer characteristic can also be due to the effect of area and the two-dimensional ultrathin nanosheet structure. Furthermore, tests data obtained from cyclic voltammetry and chronoamperometry of commercial rhodium black, palladium black, and platinum black still indicate that the catalytic activity of rhodium nanodendrites are far better.

Generally, electrocatalysts based on rhodium have low values of ECSA. For instance, mesoporous rhodium NPs and nanodendritic rhodium possess ECSA values of $50 \text{ m}^2 \text{ g}^{-1}$ and $\sim 43 \text{ m}^2 \text{ g}^{-1}$, respectively.^[86,88] The employment of ultrafine nanostructures is a possible way of enlarging ECSA to enhance the activity of catalysts. However, with this morphology achieving stability in harsh operating conditions is difficult because of the occurrence of Oswald ripening processes as well as due to aggregation. A number of research work has been performed in past to study the capabilities of rhodium in the form of ultrathin wavy nanowires by Huang *et al* and Fu *et al* for various reactions.^[87,89] Ultrathin wavy rhodium nanowires showed an outstanding performance for catalytic oxidation of benzyl alcohol to benzaldehyde.^[89] In another study ultrafine wavy rhodium nanowires, with 2 to 3 nm diameters, were synthesized to effectively catalyze MOR in alkaline media [Figure 6\(a, b\)](#).^[87] The ultrathin wavy rhodium nanowires displayed significantly higher mass activity of 722 mA mg^{-1} (at 0.61 V potential vs. RHE) that is greater by more than 2.5 times the values obtained for other rhodium nanomaterials previously tested.^[86,88,90] The rhodium-based nanowire catalyst also demonstrated an ultrahigh ECSA_{CO} value of $144.2 \text{ m}^2 \text{ g}^{-1}$. This enhancement may be explained by the presence of large specific surface area and rich surface defects that could serve to improve catalytic performance by demonstrating a higher mass activity.^[89] In addition, there is also the advantage of the one-dimensional nanowire geometry in promoting charge transport.

3.1.2.2. Supported rhodium. Kang and coworkers introduced a hybrid electrocatalyst of rhodium nanosheets on reduced graphene oxide (RGO) via a one-pot hydrothermal method [Figure 7\(a – g\)](#).^[90] Its behavior for methanol oxidation reaction in alkaline media, in terms of electrocatalytic activity, prevailed over single-component rhodium nanoparticles and rhodium nanoparticles/RGO hybrids. The enhancement is due to the presence of the two-dimensional structure of rhodium nanosheets as well as the outstanding chemical/physical property of the reduced graphene oxide. Experimental measurements using cyclic voltammetry and chronoamperometry have confirmed that the hybrid catalysts function more actively than the commercial

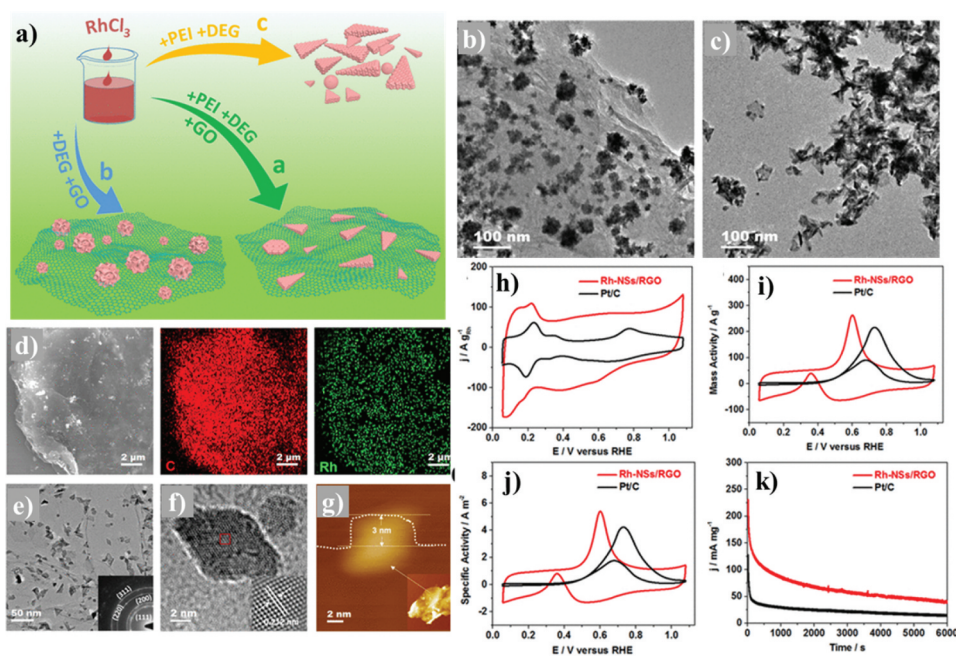


Figure 7. (a) Schematic representation of the synthesis of (arrow a) Rh-Ns/RGO hybrids, (arrow b) Rh-NPs/RGO hybrids and (arrow c) Rh-NPs. Images of (b) Rh-NPs/RGO hybrids and (c) Rh-NPs acquired via TEM. (d) Rh-Ns/RGO hybrids' SEM image along with their SEM-EDX elemental mapping (carbon mapping (red) and rhodium mapping (green)). (e) Rh-Ns/RGO hybrids' TEM image and its SAED pattern (inset image). (f) Image of Rh-Ns/RGO hybrids obtained using HRTEM along with the magnified version of a region in red square (inset image). (g) Image of Rh-Ns/RGO hybrids acquired using AFM. (h) Cyclic voltammograms of Rh-Ns/RGO hybrids and Pt/C catalyst at 50 mV s^{-1} scan rate (in 1 M KOH solution). (i) Metal mass-normalized and (j) ECSA-normalized cyclic voltammograms of Rh-Ns/RGO hybrids and Pt/C catalyst at 50 mV s^{-1} scan rate (in $1 \text{ M KOH} + 1 \text{ M CH}_3\text{OH}$ solution). (k) Chronoamperometry data of Rh-Ns/RGO hybrids and Pt/C catalyst at 0.61 V potential (in $1 \text{ M KOH} + 1 \text{ M CH}_3\text{OH}$ solution). Reproduced with permission from American Chemical Society^[90]

PtCarbon electrocatalyst. Although records from cyclic voltammetry showed that the hybrids have slightly lower ECSA value ($48.66 \text{ m}^2 \text{ g}^{-1}_{\text{Rh}}$) than that of commercial PtCarbon (which was $51.04 \text{ m}^2 \text{ g}^{-1}_{\text{Pt}}$), however a negative shift of around 120 mV in the onset potential of rhodium nanosheets/RGO hybrid was observed in comparison to the commercial PtCarbon for methanol oxidation. The current value for the hybrids was also 3.6 times greater than the value for commercial PtCarbon electrocatalyst at a potential of 0.61 V ($264 \text{ A g}^{-1}_{\text{Rh}}$ and $73 \text{ A g}^{-1}_{\text{Pt}}$ for rhodium nanosheets/RGO and PtCarbon, respectively) **Figure 7i**. Besides, chronoamperometry experiments showed a higher current value for the hybrids relative to PtCarbon that decays very slowly within 6000 seconds **Figure 7k**. This further provides a strong evidence that not only the synthesized hybrids have higher activity for an extended time period, but also stability that makes it invulnerable to poisonous carbonaceous species such as carbon monoxide.

3.1.3. Palladium

Palladium as a catalyst has also recently been used as an alternative to platinum. Its nanostructural form that has greater number of active centers and specific surface area has attracted the attention of researchers with interest in exploring their electrochemical reaction behaviors for industrial applications. The synthesis of various palladium structures made up of nanowires,^[91] nanoplate arrays,^[92] nanoflowers,^[93] nanoparticles,^[94] and nanotrees^[95] by research teams in the past have discovered that their electrocatalytic activities for both methanol and ethanol oxidations are predominantly excellent. With regards to palladium having nanoporous structures that are expected to show an incredible performance compared to other palladium structures previously mentioned, not enough research has been performed. In addition to their bicontinuous, three-dimensional, interpenetrating nanosized ligament-channel arrangement they also contain increased surface area, open porosity, and structural durability with no agglomeration that can be utilized to better advance various reactions. Nevertheless, the difficulty or complexity of operation such as the time-taking dealloying process and the great dealloying driving force required are some of the downsides faced by previous studies that needs to be overcome.

3.1.3.1. Supported palladium. Wang's group managed to develop nanoporous palladium (NP Pd) rods electrocatalyst through a simplified method of dealloying a binary $\text{Al}_{80}\text{Pd}_{20}$ alloy in a solution of 5 wt% hydrochloric acid solution under free corrosion conditions.^[96] These nanoporous rods, when observed under scanning electron microscopy and transmission electron microscopy, were revealed to have the standard bicontinuous, three-dimensional, interpenetrating ligament-channel system that are 15 to 20 nm in length. These newly synthesized materials were further mixed with Vulcan XC-72 Carbon powder to form NP Pd/C catalyst for the testing of methanol oxidation reaction in alkaline media. 1 M KOH and 0.5 M methanol solution were used with Hg/HgO reference electrode (MMO) and the cyclic voltammetry data showed that the catalyst activity depends on the metal loading on the glassy Carbon (GC) electrode. Metal loading values of 0.2, 0.4, 0.6, 0.8, 1.0, and 1.2 mg cm^{-2} were used on the GC electrode and a loading 0.4 mg cm^{-2} displayed the best catalytic performance for MOR. Under this loading, the onset potential (E_{op}) was -401 mV, the forward scan oxidation peak current density (J_p) was 223.52 mA mg^{-1} (oxidation peak potential (E_p) of -42 mV), and the backward scan oxidation peak current density (J_p) was 146.18 mA mg^{-1} (oxidation peak potential (E_p) of -123 mV) (10 mV s^{-1} potential scan rate). On the contrary, testing with methanol concentration of more than 2 M in the KOH solution results in a decrease in the oxidation current density because of the increased competition in adsorbing hydroxyl (OH_{ads}) and methoxyl ($(\text{CH}_3\text{O})_{\text{ads}}$) intermediates.^[96] Overall, the catalytic

activity of NP Pd/C catalyst for MOR is a diffusion-controlled reaction and in comparison, to other palladium nanostructures it is a promising electrocatalyst that can be implemented industrially such as in direct methanol fuel cells.

Zhao's research team synthesized a palladium-based electrocatalyst that is supported by multiwalled carbon nanotubes modified by Mn_3O_4 ($\text{Pd-Mn}_3\text{O}_4/\text{MWCNTs}$) via a wet impregnation method **Figure 8(a – e)**.^[97] The electrochemical performance of the resulting catalyst for MOR was analyzed using CV, LSV, and CA. It was determined that the composites have better endurance toward poisoning CO_{ads} species and possess the greatest active surface area compared to Pd/MWCNTs and Pd/XC-72 catalysts. Based on the CV results of the 3 different types of catalyst toward MOR the onset potential of

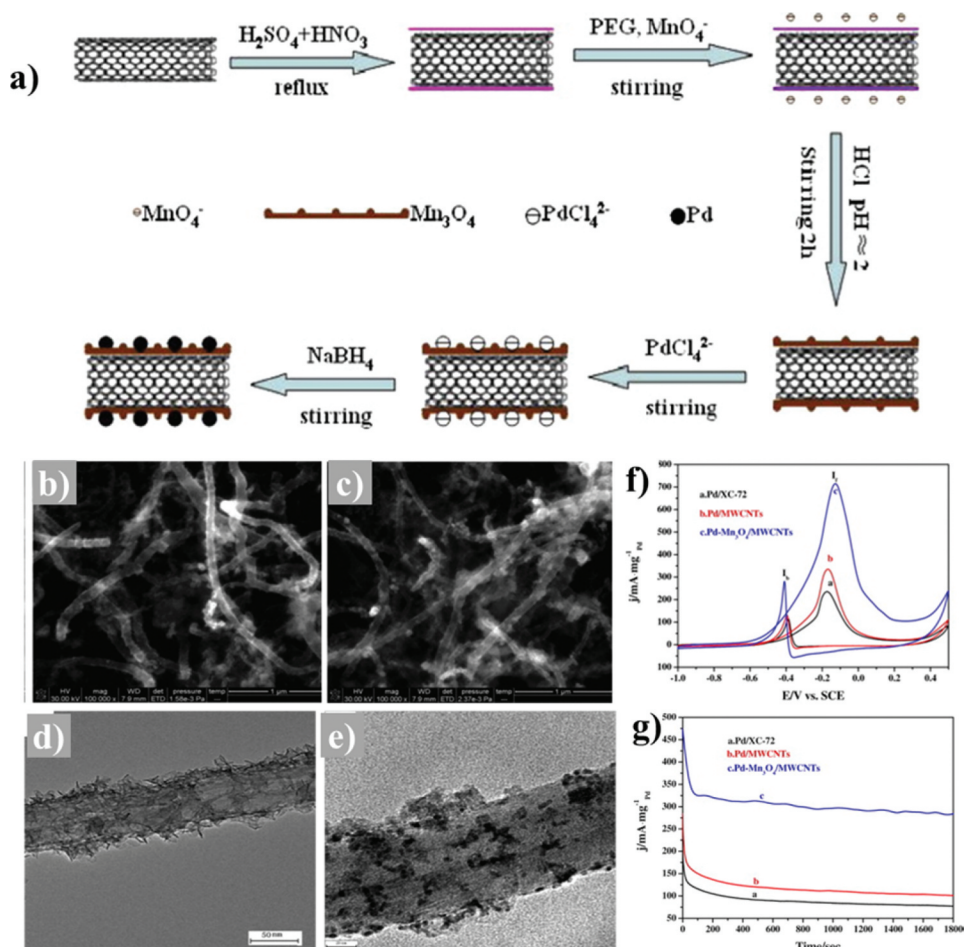


Figure 8. (a) A diagram representing the steps involved in the preparation of $\text{Pd-Mn}_3\text{O}_4/\text{MWCNT}$ composites. Images of (b) $\text{Mn}_3\text{O}_4/\text{MWCNTs}$ and (b) $\text{Pd-Mn}_3\text{O}_4/\text{MWCNTs}$ acquired through SEM. (d) $\text{Mn}_3\text{O}_4/\text{MWCNT}$ and (e) $\text{Pd-Mn}_3\text{O}_4/\text{MWCNT}$ TEM images. (f) CV curves (at 50 mV s^{-1} scan rate) and (g) CA curves of Pd/XC-72 , Pd/MWCNTs , and $\text{Pd-Mn}_3\text{O}_4/\text{MWCNTs}$ catalysts in $0.5 \text{ M NaOH} + 1 \text{ M CH}_3\text{OH}$ nitrogen-saturated solution. Reproduced with permission from Elsevier^[97]].

Pd-Mn₃O₄/MWCNTs' methanol oxidation peak shifted negatively by more than 160 mV relative to the value for Pd/MWCNTs. In addition, for a given oxidation current density, the potential value of Pd-Mn₃O₄/MWCNTs is comparatively lower. This signifies the relatively greater catalytic performance of Pd-Mn₃O₄/MWCNTs toward MOR at all the values of potentials used (i.e. potentials of -1.0 V until -0.2 V) **Figure 8f**.^[98] The recorded values of the methanol forward oxidation mass specific peak current for Pd-Mn₃O₄/MWCNTs, Pd/MWCNTs, and Pd/XC-72 were 715.8 mA mg⁻¹_{Pd}, 332.4 mA mg⁻¹_{Pd}, and 236.1 mA mg⁻¹_{Pd}, respectively. The high value exhibited by Pd-Mn₃O₄/MWCNTs is most probably due to the behavior of Mn₃O₄ nanoparticles as a catalytic-activity-modifier and as a promoter of the appropriate condition to form Pd nanoparticles^[99] and of methanol oxidation. Relative to the other catalysts, Pd-Mn₃O₄/MWCNTs displayed the most stable characteristic as well as the best tolerance toward poisoning. Chronoamperometric analysis for 1800 seconds (in 0.5 M NaOH + 1.0 M CH₃OH) was implemented to prove these points when it recorded a current density of 284.14 mA mg⁻¹_{Pd} for Pd-Mn₃O₄/MWCNTs, 101.03 mA mg⁻¹_{Pd} for Pd/MWCNT, and 77.25 mA mg⁻¹_{Pd} for Pd/XC-72 **Figure 8g**.

A multifunctional catalyst in which palladium NPs are supported by nitrogen and sulfur-doped graphene (Pd/NS-G) was produced by Zhang *et al* in their study.^[100] The production steps involved a thermal treatment process to integrate both nitrogen and sulfur atoms into graphene. In addition, a solvothermal approach was performed to allow the controlled growth of palladium NPs onto the support. These combinations resulted in a catalyst possessing fine synergistic effects in addition to its unique structure that allows it to be used to oxidize both methanol and formic acid. Improvement in performance, compared to Pd/Vulcan XC-72 R and Pd/undoped graphene catalysts, included relatively high anodic peak current and greater stability. CV analysis in 0.5 M NaOH and 0.5 M methanol displayed a weak cathodic peak, but a strong anodic peak by all the catalysts. The former can be due to the removal of the intermediate carbonaceous species, while the latter is the result of the oxidation of chemisorbed methanol.^[101,102] Amongst the 3 catalysts analyzed, Pd/NS-G achieved the highest specific activity value of 11.3 mA cm⁻² and a mass activity value of 399.3 mA mg⁻¹. The high mass activity exhibited by Pd/NS-G can be explained by increased utilization efficiency of palladium in the hybrid catalyst. LSV data also showed that Pd/NS-G performs better compared to the other catalysts and showed lower potential for a given oxidation current density. The long-term stability of the catalysts was studied using CA and the slowest decline in current was demonstrated by Pd/NS-G for MOR.

Other potential catalysts for MOR, that comprises of palladium, have also been explored by researchers in the past and their examples include PdNPs/PVP-graphene,^[103] NPPd,^[104] Pd/TiO₂-C,^[105] and Pd/CNF.^[106]

Summary: To conclude, several synthesis methods have been utilized to incorporate noble metals as anode catalysts. A morphology of self-supported one-dimensional architecture can assist in preventing catalytic activity loss in carbon-supported platinum while enhancing the transport of electrons as well as improving the long-term stability. Employing a mesoporous design through the novel “electrochemical micelle assembly” soft-template method could help in increasing the electrochemically active area by providing concave surface. Some authors also reported enhanced durability for platinum nanowires possessing one-dimension mesoporous architecture that also has larger active surfaces. A great structural thermal stability along with improved electrochemical performance was demonstrated by mesoporous platinum nanospheres designed through a slow reduction reaction in presence of shape directing surfactants. MPNs could retain 97% of their original ECSA when subjected to a temperature of 350 °C as a result of their resistivity against particle aggregation. Alloying commercial monometallic Pt/C with ruthenium through an electroless deposition method allows maximum activity to be achieved at approximately 50% monodisperse ruthenium surface coverage. In comparison to pure platinum the activity was sevenfold higher. Nanodendrites of platinum and ruthenium alloy, synthesized through co-reduction of the metals in oleylamine by hydrogen, can assist in obtaining improved ECSA in the form of multiatomic corners, branched arms, and cavities for better oxidation of methanol molecules. In addition to resistivity toward dissolution and aggregation, combining ruthenium with platinum adjusts the electronic configuration of platinum for easy bond breaking between hydrogen and carbon and creates a strain effect that decreases intermediates’ binding energies. Supporting platinum with a hybrid of graphene oxide and polyvinylpyrrolidone enhances methanol adsorption rate and minimizes electrocatalytic reduction in MOR. Relative to platinum@GO and platinum@PVP nanoparticles the performance of the hybrid-supported catalyst were approximately 2.87 times and 1.53 times, respectively.

Rhodium, one of the cheaper alternatives to platinum, with nanodendritic morphology could demonstrate great activity and reduced decay rate in alkaline medium. Its performance has been demonstrated to be far superior relative to platinum black and palladium black. Implementing ultrafine nanostructures could prevent low ECSA characteristic generally found in rhodium-based electrocatalysts. An ultrathin wavy rhodium nanowire could display a high mass activity and in turn better catalytic performance that may be due to the availability of rich surface defects and large specific surface area. A difficulty is, however, faced in maintaining stability due to Oswald ripening and aggregation under extreme operating circumstances. Introducing RGO as a support for rhodium nanosheets could help promote enhanced chemical/physical properties that allow it to perform better than rhodium NPs/RGO

hybrids and single-component rhodium NPs toward MOR. It could also demonstrate a very slow decay in comparison to commercial Pt/Carbon when analyzed through CA experiments. This proves that the hybrid structure is not only capable of maintaining fine activity for long durations, but it also could endure the poisoning effect of carbonaceous compounds.

Palladium nanostructures, as a noble metal, possess many active centers and large specific surface area. Those with nanoscale porous structures show bicontinuous, three-dimensional, interpenetrating ligament-channel system with large surface area, open porosity, and structural stability to be suitable for improving different reactions. Introducing composites to a support, as demonstrated by MWCNT supports modified by Mn_3O_4 to support palladium, could promote better endurance toward poisoning CO compounds and enhance active surface area. The improved characteristics enable Pd- Mn_3O_4 /MWCNTs to perform better than Pd/MWCNTs and Pd/XC-72 catalysts by displaying higher methanol forward oxidation mass specific current and high current density during CA analysis of 1800 seconds. Combining palladium NPs with sulfur and nitrogen-doped graphene could generate fine synergistic effects in the resulting catalyst and assist in oxidizing both formic acid and methanol. Relative to Pd/Vulcan XC-72 R and Pd/undoped graphene catalysts, Pd/NS-G possesses the highest mass activity that could be due to the improvement in usage efficiency of palladium.

3.2. Catalysts based on non-noble metals

3.2.1. Nickel

Previously, it has been noticed that one of the advantages of alkaline DMFC is the capability of utilizing electrocatalysts based on non-noble metals. This possibility has, in recent years, motivated researchers to find alternative materials belonging to the category of non-noble metals to avoid the high-cost and, in some cases, the decaying activity of noble metals as anode catalysts. Transition metal oxides are the type of non-noble metal based materials where many attempts have been made. Transition metal oxide such as nickel oxide (NiO) has received a number of recognitions and has been used as lithium ion batteries, ^[107] supercapacitors, ^[108] and catalysts ^[109–111]; and reported to perform well electrochemically.

3.2.1.1. Nickel oxide. Sponges that are available commercially consists of uniform-sized macro-pores and have hierarchical macro-porous nature that can behave as a template to yield extraordinary electrodes.^[112] However, because of the lack of commercial sponge being utilized as a template to synthesize nickel oxide nanostructures, Tong's team developed a novel catalyst of NiO nanoparticle/nanoflake grown on a tube of Ni-P alloy via a sponge template method [Figure 9a](#).^[113] With this method amorphous Ni-P undergoes

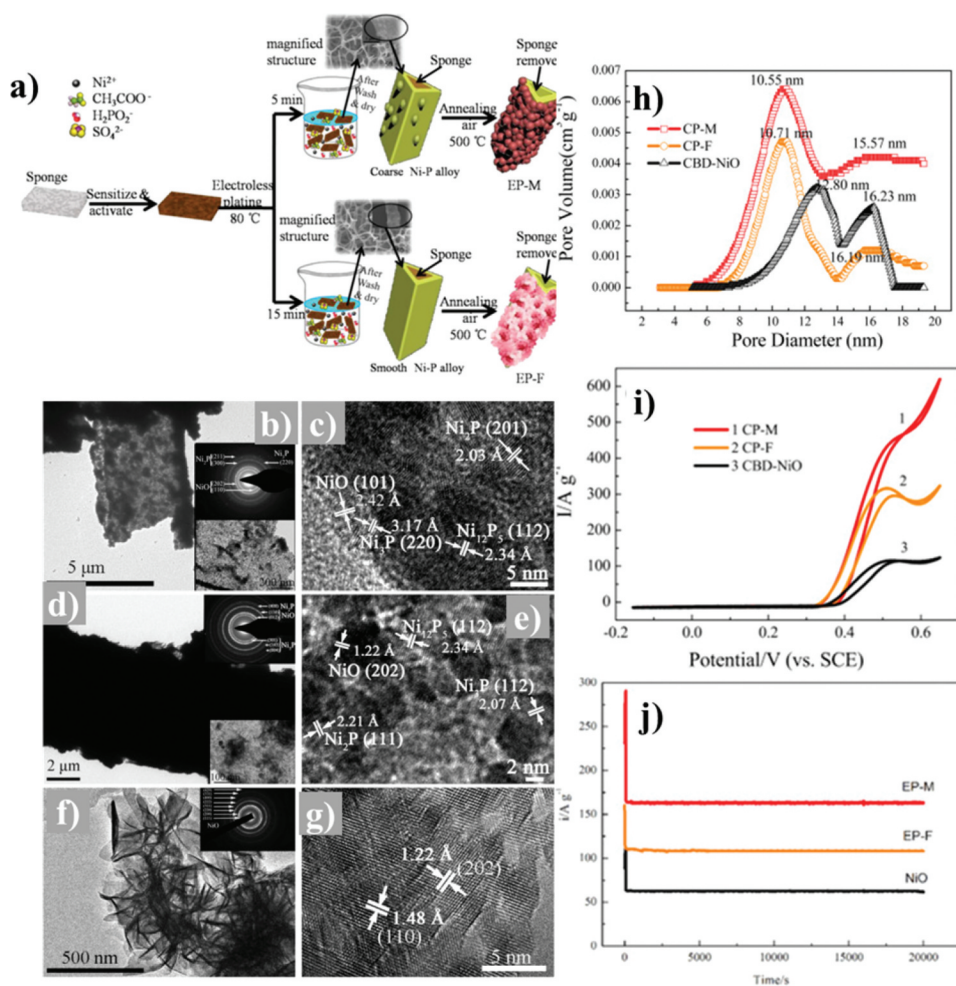


Figure 9. (a) Schematic representation of the synthesis of microspherical NiO (EP-M) and nanoflake NiO (EP-F). (b, c) EP-M, (d, e) EP-F and (f, g) CBD-NiO TEM and HRTEM images (inset images are the magnified images and the SAED patterns). (h) The pore size distributions of EP-M, EP-F, and CBD-NiO from nitrogen adsorption-desorption method at a temperature of 77 K. (i) CV curves (at 50 mV s^{-1} scan rate) and (j) CA curves (at 0.5 V and 20,000 s) of EP-M, EP-F, and CBD-NiO in 0.5 KOH + 1 M methanol. Reproduced with permission from Elsevier^[113]

electroless plating on sponge and an annealing process occurs in air at 500 °C. The purpose of the annealing is to remove the templates, allow Ni-P to crystallize, and produce nanostructures of NiO on the external surface of Ni-P tubes. Microspherical NiO (EP-M) or nanoflake NiO (EP-F) decorates the surface of the tubular Ni-P system and any of the two NiO structures can be generated depending on the electroless plating time Figure 9(b – g). Comparison of their functions as electrocatalysts for methanol oxidation (in alkaline solution) was also performed with porous NiO nanoflakes produced via the chemical bath deposition (CBD-NiO). Hence, three types of NiO-based

catalysts are created, and their surface areas and porous structures were analyzed through nitrogen adsorption-desorption method (at 77 K temperature) **Figure 9h**. Amongst the samples EP-M (containing 16.2 wt% Ni-P and 83.8 wt% NiO) displays the largest specific surface area value of $210.03 \text{ m}^2 \text{ g}^{-1}$. Cyclic voltammetry result of EP-M for MOR in alkaline solution (0.5 M KOH and 1.0 M CH_3OH at 50 mV s^{-1} scanning rate) recorded a relatively greater current density of about 467 Ag^{-1} (or 28.56 mA cm^{-2}) **Figure 9i**. Simultaneously, the newfound catalyst demonstrated a long stability duration (more than 20,000 seconds) when tested with chronoamperometry **Figure 9j**. These incredible characteristics of EP-M suggest that it can perform better than many other modern catalysts possessing NiO, such as GC/ $\text{MnO}_x/\text{NiO}_x$ (8.21 mA cm^{-2} , in 0.5 M NaOH + 0.5 M CH_3OH at 50 mV s^{-1}) and GC/ NiO_x (5.38 mA cm^{-2} , in 0.5 M NaOH + 0.5 M CH_3OH at 50 mV s^{-1}).^[114] Other reason for its superiority can be due to the powerful electronic interaction of both Ni-P and NiO toward each other. Al-Enizi and coworkers have developed a nickel oxide (NiO) catalyst supported by carbon nanofibers that are uniform and highly doped with nitrogen (N-CNFs).^[115] The N-CNFs support was generated through a method that involves the electrospinning of solution mixture comprising of polyaniline, polyacrylonitrile, and graphene. Annealing was then performed at a temperature of $1200 \text{ }^\circ\text{C}$. The loading of nickel oxide onto N-CNFs, to form NiO/N-CNFs hybrid, was done via chemical precipitation of $\text{Ni}(\text{OH})_2$ and treatment at $400 \text{ }^\circ\text{C}$ temperature. Results obtained from CV and CA investigations have shown that NiO/N-CNFs catalyst is capable of outperforming other nickel-based catalysts. It displayed greater mass and specific activities for MOR along with a less positive shift in the methanol oxidation potential. The observed improvement can be due to the existence of mesoporosity, high contribution of nitrogen functionality, and the fine interaction between both NiO catalyst and CNFs support.

3.2.1.2. Supported nickel. Das *et al* published a work that involved catalyst supporting matrices used alongside nickel metals.^[116] They experimented with 3 types of supports that included partially sulfonated polyaniline (SPANi), polyaniline (PAni), and Vulcan Carbon for methanol oxidation. Ni catalyst nanoparticles supported by SPAni (Ni/SPANi) proved to be the best for dispersion, deposition, utilization, and distribution that promoted high mass specific current densities and output area. Characterization of Ni/SPANi included using cyclic voltammetry (CV) (potential ranges of 0 V to +0.8 V) and linear sweep voltammetry (LSV) (potential ranges of 0 V to +2.0 V) in a solution of 2 M CH_3OH and 0.05 M H_2SO_4 (with a scanning rate of 100 mV s^{-1}). Data from CV generated mass specific current densities and forward peak area of 6.1 mA g^{-1} and $306 \text{ } \mu\text{A cm}^{-2}$, respectively. The CV current records for Ni/SPANi are much higher than that for Platinum-Ruthenium/C, with mass

specific current densities of 0.6 mA g^{-1} and forward peak area of $25.6 \mu\text{A cm}^{-2}$. The enhancement in value can be explained by the presence of $-\text{SO}_3\text{H}$ groups on the PANi matrix that intensifies nickel catalysts' efficiency and decreased the reverse peak current density. In comparison to Ni/PANi, furthermore, Ni/SPANi's mass specific current densities and forward peak area values were greater by 1.61 mA g^{-1} and $85.2 \mu\text{A cm}^{-2}$, respectively. In addition, LSV plots provided more evidence for Ni/SPANi's improved efficiency when it generated a higher maximum current density by 0.65 mA cm^{-2} compared to Ni/PANi and by 0.37 mA cm^{-2} compared to Pt-Ru/C at $+0.2 \text{ V}$. The plots of chronoamperometric analysis were also reported and the test occurred within the same solution at an anodic potential of $+0.4 \text{ V}$. After an initial drop in the current density, LSV shows a steady decay where Ni/SPANi demonstrated a relatively greater stability with a current density of $121 \mu\text{A cm}^{-2}$ (after 700 seconds) compared to other types of catalyst experimented with. This value is even almost double than that of the commercial Pt-Ru/C catalyst, with a value of $62 \mu\text{A cm}^{-2}$. This is possibly because of the enhanced proton uptake capacity of the catalyst support promoted by $-\text{SO}_3\text{H}$ groups that enhances the anti-poisoning effect on the catalyst. The results determined from this study provided sufficient data that the use of Pt-Ru can be substituted by nickel and suitable support matrices such as partially sulfonated polyaniline can facilitate in creating an effective catalyst as an anode for DMFCs systems in oxidizing methanol.^[117] Wang's group has also prepared a supported-nickel catalyst in the form of ordered mesoporous Ni/ Al_2O_3 .^[118] A solvent evaporation induced self-assembly (EISA) method was implemented for preparation and the performance for MOR was analyzed via CV and CA. An enhancement in the electrocatalytic activity of the synthesized catalyst was observed for MOR in alkaline electrolytes. The reason for the improved performance can be explained by the synergetic effects generated by high nickel dispersion and ordered mesoporous structure that promotes methanol and product diffusion

3.2.2. Cobalt

Cobalt and cobalt oxides (Co_3O_4 and CoO) have been used as an emerging catalyst owing to their exceptional intrinsic characteristics such as excellent structural flexibility, tunable chemical properties and higher activity. The outstanding catalytic performance of cobalt oxide is attributed to the abundant electroactive surface sites and tailored electronic structure that can be achieved through cost-effective synthesis methods. Subsequently, cobalt has been reported as a primary catalyst and also as a cocatalyst in many methanol oxidation reactions so far.

Jafarian and coworkers prepared cobalt hydroxide modified glassy carbon electrodes using anodic deposition and tested its activity for electro-catalytic methanol oxidation reaction. The proposed mechanism showed the presence of cobalt in multiple valence state where Co(IV) was found to be the most

active site for methanol oxidation reaction.^[119] Xia's group fabricated three-dimensional (3D) ordered mesoporous cubic Co_3O_4 using KIT-6- and SBA-16-templating strategies. 3D ordered mesoporous Co_3O_4 possessed much higher activity than nonporous Co_3O_4 due to the presence of high surface adsorption species concentration, larger surface area (118–121 m^2/g) and lower reducibility temperature.^[120] Zafeiratos conducted a simple study on the geometrical structure effect of spinel (Co_3O_4) and rocksalt (CoO) oxides, in which the former one had more mobile lattice oxygen that favors the partial oxidation of methanol to formaldehyde.^[121] In order to improve the catalytic activity and stability of cobalt, various techniques have been employed including functionalization, incorporation of hetero atoms and carbon-based materials. Thamer *et al* introduced co incorporated nitrogen doped carbon nanofibers using electrospinning technique as a functional electrocatalyst with excellent adsorption capacity and smaller electron transfer resistance. The effect of nitrogen content in the catalyst was studied by varying the amount of urea (0, 1, 2, 3, 4, and 5 %). It was evident that there was enhanced activity for Co/N(4%)-CNFs with maximum current density of 100.84 mA cm^{-2} , that is much higher than undoped sample (63.56 mA cm^{-2}).^[122] Shahid and his group, reported the hydrothermal technique for the synthesis of Co_3O_4 nanocubes incorporated over reduced graphene oxide (rGO- Co_3O_4) and it showed enhanced current density of methanol oxidation when compared to rGO, Co_3O_4 nanocube and bare Pt particles. The rGO content was optimized to 2%, with a maximum oxidation peak current of 362 mA cm^{-2} during the forward scan, along with a better reversibility with retention current of 108% and excellent stability for methanol oxidation.^[123]

Shenashen's group reported the fabrication of heterogeneous mesoarchitectures of N- Co_3O_4 @C unit blocks oriented axially on basic nanoscale structures such as nanorod pellets (NRPs), nanoneedles (NNs), and crossed-X nanosheets (X-NSs) with the exposure of highly active {112} crystal facets and functional mesoporous surface topography to ensure rapid electron transfer. The as-prepared nanostructures exhibit specific surface areas in the increasing order of NNs (54.7 $\text{m}^2 \text{g}^{-1}$) < X-NSs (65.1 $\text{m}^2 \text{g}^{-1}$) < NRP (82.5 $\text{m}^2 \text{g}^{-1}$) as shown in Figure 10. Among the three nanoscale architecture, nanorod pellets (NRPs) have densely exposed {112} crystal facets for the faster adsorption and diffusion of charge carriers toward methanol oxidation.^[124]

Recently, more development on cobalt based materials triggered the search for improving the chemical and physical features of the cobalt, through replacing some atoms of Co with new ternary atoms. Nickel, copper, cadmium, tungsten, etc. are the most used metals for the replacement. Asgari and coworkers worked on the coating of Ni-Co alloy on glassy carbon electrode as an anomalous process. Their results showed that methanol oxidation over Ni-Co/GCE was catalyzed through the redox couples Ni(II)/Ni(III) and Co(II)/

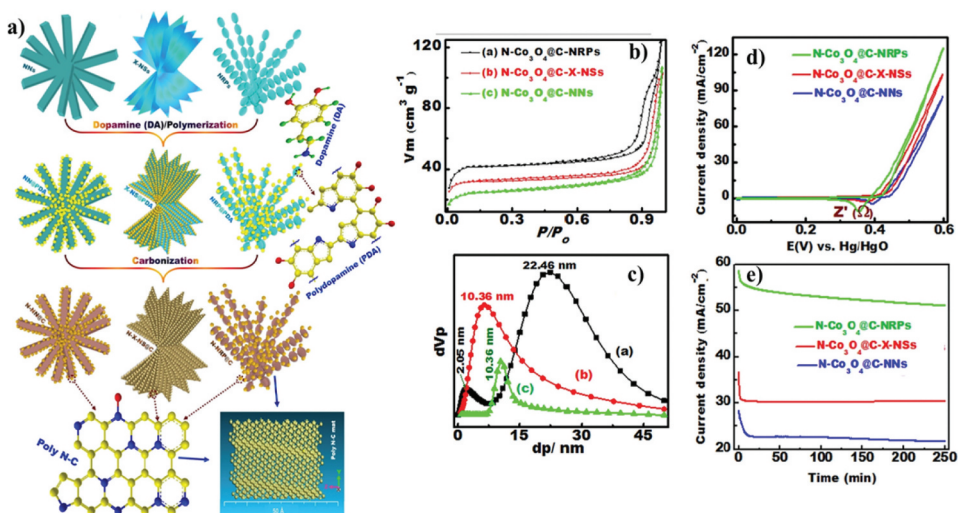


Figure 10. (a) Schematics on the design of one-pot-simple hydrothermal process to prepare mesoporous $\text{N-Co}_3\text{O}_4@\text{C}$ catalysts with controlled surface morphologies and hierarchical architectures of nanorod pellets (NRPs), nanoneedles (NNs), and crossed-X nanosheets (X-NSs) (b) N_2 -adsorption/desorption isotherms for specific surface area and (c) the corresponding pore size distribution analyzed by using nonlocal density functional theory (NLDFT) of nanorod pellets (NRPs), nanoneedles (NNs), and crossed-X nanosheets (X-NSs) measured at 77 K. (d) Cyclic voltammogram of mesoporous $\text{N-Co}_3\text{O}_4@\text{C}$ catalysts recorded in 1.5 M methanol. (e) Chronoamperometric current-time profile of the catalysts measured in 1.5 M methanol at a fixed potential of 0.52 V (vs. Hg/HgO) for 250 min. Reproduced with permission from Elsevier^[124]

Co(IV) over the catalysts layer within the pH layer of 10 to 12 and follows a first order kinetics on methanol oxidation.^[125] Mengqi *et al* followed a one-pot additive free solvent thermal decomposition route coupled with a post calcination treatment for the successful preparation of coral-like nickel cobalt oxides with hierarchical pores. CV results revealed that coral-like NiCo_2O_4 exhibited much higher current density than moss-like NiCo_2O_4 . The chronoamperometry results showed that the current density decayed to $7.140 \text{ mA}\cdot\text{cm}^{-2}$ from its initial $9.844 \text{ mA}\cdot\text{cm}^{-2}$ (72.53% retention) for coral-like NiCo_2O_4 , whereas the initial current density drops to $0.105 \text{ mA}\cdot\text{cm}^{-2}$ from $7.166 \text{ mA}\cdot\text{cm}^{-2}$ (1.47% retention) for moss-like NiCo_2O_4 , which could be due to the amorphous nature of moss like NiCo_2O_4 .^[126] Sun and Xu studied the composition dependence in Ni-Co hydroxide and oxides by adjusting the ratio of precursor solution. They found that the oxidation reaction in Ni-Co hydroxide increases with increase in Ni content, and in case of Ni-Co oxide it followed a volcano profile with Ni 46% showing the highest activity, lowest charge transfer resistance, lowest onset potential, and smallest Tafel slope.^[127] A binder free direct growth of Co_3O_4 with different morphology on Ni foam using simple hydrothermal method followed by calcination was studied in detail by Rajeshkhanna and Rao.^[128] Microflowers, microspheres and nano-grass morphologies of Co_3O_4 were prepared by varying the anion precursors

to chloride, sulfate and acetate salts of cobalt, respectively. Based on CV and CA results, all the three catalysts show low onset potential, but the oxidation current increases in the order of $28 \text{ A g}^{-1} < 34.9 \text{ A g}^{-1} < 36.2 \text{ A g}^{-1}$ for micro flower, nanoglass and microsphere respectively. Wang *et al* highlighted the study on NiCo_2O_4 nanosheets and nanocloth arrays supported over Ni foam prepared using a mild hydrothermal method. NiCo_2O_4 /nanocloth exhibits excellent performance, including high current density (134 mA cm^{-2}), lower onset potential and stability with 88% of current retention after 100 cycles.^[129]

Tae-Hoon *et al* reported a facile synthesis of NiCo_2O_4 with average size of $6 \pm 2 \text{ nm}$ homogeneously decorated over MWCNTs to form a core/shell like morphology. NiCo_2O_4 /MWCNTs exhibited a high current density of 327 mA cm^{-2} and a low onset potential (0.128 V). They displayed excellent stability by retaining a current density of 76% even after 250 cycles^[130]. Tonga and coworkers proposed a new series of Ni-Co-P-O compound prepared using one-pot solvothermal technique for methanol oxidation in alkaline environment. The final chemical composition, crystallographic structure and morphology of the Ni-Co-P-O composite were highly influenced by the molar ratio of $\text{Co}^{2+}/\text{Ni}^{2+}$. They conducted a detailed study on optimization and found that $\text{Co}^{2+}/\text{Ni}^{2+}$ of 0.81 (NiCoPO-2) exhibits larger surface area ($540.5 \text{ m}^2 \text{ g}^{-1}$) and bimodal pore distribution that contributed to the highest oxidation current density of 1567 A g^{-1} with excellent stability over more than 20000s. They noticed the presence of electron tunneling junctions between the metal phosphides and phosphates that triggers the fast transport of methanol and its products in and out of the catalysts.^[131] In the same year, Vernickaite and team studied the effect of composition and structure of cobalt-tungsten composite prepared through electrodeposition technique toward the methanol oxidation reaction in acidic medium. While varying the tungsten content from 3 and 18 atomic % to 30 atomic %, the structure of Co-W changed from crystalline to amorphous nature. They found that Co-W with 3 and 18% of W content was inactive for methanol oxidation due to the dissolution of Co-W alloy in acidic medium, while Co-W with 30% of W showed catalytic performance by coating the active surface with W that avoids the dissolution of alloyed particles.^[132] Barakat and coworkers developed Cd-doped cobalt nanoparticles decorated over graphite shell using simple sol-gel technique. The prepared catalyst showed considerably high current density (70 mA cm^{-2}), lower onset potential ($\sim 600 \text{ mV vs. NHE}$) and good stability due to the graphite sheathing.^[133] Other similar examples of cobalt-based electrocatalyst using different precursors and supporting materials have been also reported and shows satisfactory performance in methanol oxidation.^[134–138]

3.2.3. Copper

Copper is another class of electrocatalyst that received wide attention due to excellent reactivity, low cost, low to moderate stability and ease of synthesis.

Cu shows much lower selectivity for carbon monoxide (CO) than any other well-known metal catalysts such as Pt, Pd, Ru, and Rh.^[139,140] This is beneficial for the long-term stability run, where CO is formed as possible intermediate products that generally poison or deactivate the active sites of the catalyst and thereby reduces the activity of the catalyst in long-term runs. Some of the selected Cu-based catalyst for methanol oxidation reaction is discussed in the following section. Cu alone as a catalyst shows low activity; however, Carugno and coworkers developed some simple treatment method such as electro corrosion and electrodeposition that generate some micro- and nano-structure to enhance the methanol oxidation reaction. The pretreatment helps in the increase of effective surface area and the exposure of more active sites toward the reaction^[141].

Han and his group reported a seed mediated approach for the preparation of bimetallic CuPt alloy with different morphologies and proved that morphology and electronic coupling effect greatly influences the electrochemical properties. While varying the Cu/Pt ratio during synthesis, it causes a rapid inter diffusion of Cu and Pt which results in the formation of three different morphologies of polyhedral, stellated, or dendritic bimetallic CuPt. Dendritic CuPt shows highest activity for methanol oxidation owing to its abundant atomic steps, edges, and corner atoms on the surface, while polyhedral CuPt shows the best CO tolerance owing to a strong coupling between Cu and Pt that is capable of promoting better electron transfer mechanism.^[142] Ren *et al* synthesized Pd particles with a thickness of ~50 nm that are uniformly decorated over ultra-long copper nanowires with an average diameter of 100 ± 20 nm and thickness of 35 ± 5 nm through a facile hydrometallurgy technique. The developed binary shell-core structured Pd-Cu exhibited higher activity and stability when compared with Pd-Cu, and also the Tafel analysis shows that the first charge transfer is the rate determining mechanism for methanol oxidation.^[143] In 2015, Duhong's group synthesized star-like PtCu for the first time using copper (II) chloride dehydrate as the precursor instead of copper (II) acetylacetonate. The mean sizes of platinum particles were also calculated using the Scherrer equation as well as the diffraction peak of Pt (111) that was determined from XRD analysis. The calculated mean sizes were found to be in the range of 14.3 nm for PtCu/rGO. The star-like PtCu supported over reduced graphene oxide (PtCu/rGO) revealed excellent catalytic activity and durability (2.3 times) than PtCu/XC72 and Pt/rGO. They proposed the reasons for the higher activity for star-like PtCu as: (a) Special star-like structure provide a strong synergetic effect between Pt and Cu, (b) the unique electronic property and metal interaction with rGO enhances the electrocatalytic effect, (c) choosing Cu as the second doping element in the Pt alloy influences the activity through providing oxygen-containing species for the oxidation of CO at lower potentials than Pt and translating the electronic properties of Pt for the adsorption of CO as well as for

dissociative adsorption of methanol.^[144] In order to maximize the activity of PdCu, Xu *et al* added TiO₂ as a supportive material in which more oxygen-containing group can be generated on its surface that could enhance the catalytic activity and reduce the CO poisoning. The surface morphology shows that TiO₂ nanoneedles are distributed randomly and densely over the surface of the nanoporous PdCu. The oxidation current for PdCu/TiO₂ was measured to be 381 mA mg⁻¹, which is 7.04 times higher than pure nanoporous Pd and 1.41 times higher than nanoporous PdCu.^[145] Vertically grown reduced graphene oxide decorated with PdCu nanoparticles with average particle size of 8.7 nm shows a significant activity improvement by taking advantage of the orientation of reduced graphene particles. The electrochemical characterization shows that the overall performance is dependent on Cu content, with an optimized atomic ratio between Cu and Pd to be 1:4.42, in order to balance the Pd and Cu active sites to enable an optimal electrocatalytic performance and stability. For pure Pd, incompletely oxidized CO gets adsorbed onto the active sites of Pd atom and causes poisoning of the Pd atoms, thus reducing the activity and stability. While doping Cu into Pd, the intermediate CO gets more attached to Cu than Pd, because Cu is much more active for Cu oxidation than Pd. Moreover, alloying Cu and Pd modify the electronic structure of Pd through shifting the d-band center upward to the Fermi level, thus increasing the reactivity. Nevertheless, the presence of excess Cu atoms in the catalyst reduced the activity through blocking the active sites of Pd for adsorption-activation-dissociation of methanol molecules.^[146] Later in 2017, Subramanian *et al* conducted a similar study on optimizing the ratio of PdCu nanoalloy, by employing different stoichiometric ratios of PdCu of 1:1, 1:3, and 3:1 using simple coreduction technique. Cyclic voltammetry and chronoamperometric result of PdCu with optimized ratio of 3:1 showed better current density of 778.98 mA mg⁻¹ and are 1.95, 22.4, and 3.64 times higher than that of 1:1, 1:3, and Pt/C respectively.^[147] The reason for much lower activity for 1:3 was due to the presence of more Cu that masks the active site of Pd as explained by Yang *et al*.^[146]

Chang *et al* developed ternary tip-cracked PtPdCu nanodendrites (NDs) with tailored morphology. Cylindrical PtPdCu nanowires (NWs) array was first electrodeposited inside aluminum anodic oxide (AAO) channel and followed by the wet chemical modification of NWs into NDs with cracked tips with the effect of Cu on the galvanic cell reaction as intermediates. They marked Cu as an intermediate for NW to ND transformation, along with the tailoring of the tip cracking morphology. The enhanced methanol oxidation is benefited from the synergetic effect between porous tip-cracked morphologies and Pd dopants, and the specific and mass activity of methanol oxidation reaction was found to be ~2.14 and ~1.78 times higher than commercial Pt/C.^[148] In the same year, Xiaoqin *et al* reported another CuPtPd dendrites prepared through the direct reduction of metal ions and proved that ternary

catalyst shows better catalytic and anti-poisoning activity when compared to Pt/C and Pd/C.^[149] Zheng's group used copper wire as a template for the preparation of platinum–ruthenium-coated copper nanowires using galvanic displacement reaction. XPS analysis showed that more electron transfer from Cu or Ru to Pt leads to lowering its d band center and weakened the binding with the adsorbate (CO). Moreover, the presence of Cu in PtRu/Cu NW altered the optimum ratio of PtRu, due to the electronic effect induced by Cu on Pt.^[150] Recently, Liu and his group developed a 3D urchin-like titanium copper nitride as a Pt support that demonstrated impressive mass and specific activity of $0.84 \text{ A mg}^{-1}_{\text{Pt}}$ and 1.46 mA cm^{-2} , respectively, which were approximately 3 times higher than commercial Pt/C. The TEM image shows that a Pt nanoparticle with an average size of 3.3 nm was well dispersed over $\text{Ti}_{0.7}\text{Cu}_{0.3}\text{N}$. HRTEM analysis confirms the presence of fcc-Pt (111) facet and TiN (111) plane with a d-spacing of 0.227 nm and 0.249 nm, respectively **Figure 11**.^[151] More than bi and tri-metallic catalyst, researchers took effort in developing more active multimetallic catalyst such as PtCuCoNi,^[152] PtRuCuOsIr,^[153] PtRuCuW,^[154] in order to improve the activity, stability and durability toward methanol oxidation reaction.^[152]

Few works were recently reported on the Pt-free Cu-based catalyst for methanol oxidation. Ali Doner's group successfully fabricated alkaline leached CuZn/Cu electrode using electrodeposition method. CuZn/Cu delivers an oxidation current of $297.14 \text{ mA cm}^{-2}$ that was higher than Cu/Cu electrode ($235.65 \text{ mA cm}^{-2}$). The reason for that was claimed to be due to the presence of greater surface area, higher surface porosity and strong electronic interaction between Cu and Zn.^[155] Yue and coworkers

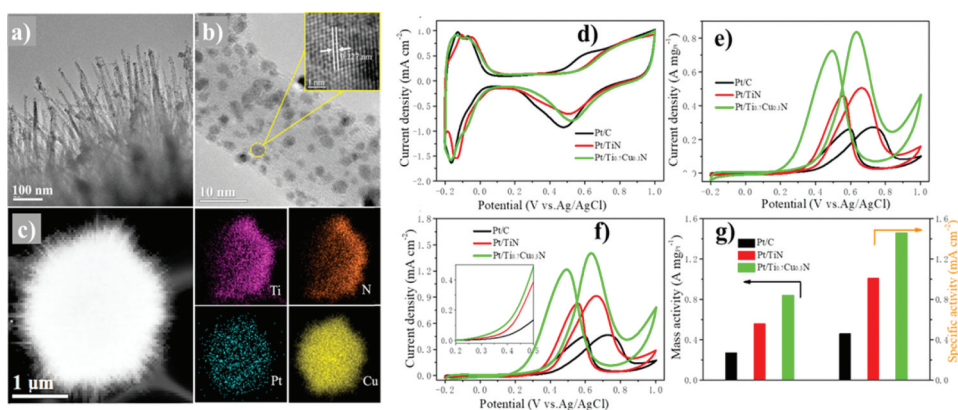


Figure 11. (a) Low and (b) high magnification TEM image of Pt/Ti_{0.7}Cu_{0.3}N (inset – HRTEM of the yellow circle portion) (c) HAADF – STEM image of the Pt/Ti_{0.7}Cu_{0.3}N and the corresponding elemental mapping of Ti, N, Cu, and Pt. (d) Cyclic voltammogram of three catalyst in N₂-saturated 0.1 M HClO₄ solution. (e) Mass activities, (f) specific activities in 0.1 M HClO₄ + 0.5 M CH₃OH solution (inset – selected area with a potential range of 0.2e0.5 V), and (g) Overall performance of the three catalysts represented in bar plot. Reproduced with permission from Elsevier^[151]

fabricated Cu trapped in CoO_x cage on a carbon layer that has specific activity and mass activity of $150.41 \text{ mA cm}^{-2}$ and $467.94 \text{ mA mg}^{-1}$, respectively, and which possesses the highest MOR activity so far reported for noble metal free catalyst. *In-situ* X-ray absorption spectroscopy (XAS) was used to understand the reaction mechanism as the CoO_x cage can provide Co^{4+} as an active site that can easily oxidize methanol, while Cu can act as a methanol adsorption center. The overall methanol oxidation can be performed by a synergetic capturing-catalyzing reaction on core-cage morphology.^[156] Izabela's group reported an activity loss in the hybrid material due to the incorporation of Cu. They synthesized Ni, Cu, and Cu-Ni nanoparticles using simple coprecipitation method and embedded it over ultrathin two-dimensional C_3N_4 . Ni/ C_3N_4 shows the highest activity and they recommended the reason for sluggish kinetics of Cu-Ni as the irreversible reaction of Cu^+ to Cu^0 and Cu^{2+} , that resulted in the segregation of CuO and increase in the redox potential of MOR. In addition to the above discussion, several other groups also reported Cu-based catalysts that show excellent ultrahigh performance toward methanol oxidation.^[157-162]

Summary: In conclusion, the availability of non-noble metals to serve as catalysts for MOR creates a great possibility to avoid the use of expensive noble metals as well as take advantage of the stability of non-noble metals as anode catalysts. Reports indicate nickel oxide with micro-spherical structure demonstrates a large specific surface area compared to NiO nanoflake and porous nanoflakes structures. Synthesizing the micro-sphere catalyst through growth on a Ni-P alloy tube (via sponge template method) results in a powerful electronic interaction between NiO and Ni-P that improves performance toward MOR with incredible stability. Supporting NiO on nitrogen doped carbon nanofibers enables the achievement of high mass and specific activities for MOR. A more negative change in the methanol oxidation potential could be observed in presence of a good interaction between NiO and the support, with high meso-porosity, and addition of nitrogen functionality. Partially sulfonated polyaniline (SPANi) is another promising support in enhancing the properties of nickel as anode catalysts for MOR. The combination could help achieve a high dispersion of active sites required to attain high mass specific current densities. Furthermore, CV analysis have shown that Ni/SPANi displays significantly better mass specific current densities and forward peak area relative to carbon supported platinum-ruthenium catalyst.

Cobalt is another potential option as a catalyst material to achieve outstanding MOR catalytic performance. Methods such as functionalization, hetero-atoms integration, and carbon-based material incorporation could be implemented to improve both the catalytic activity and stability

of cobalt. Introducing cobalt into nitrogen doped carbon nanofibers is appropriate for attaining less resistance for electron transfer and remarkable adsorption capacity. Oxides of cobalt alloyed with nickel could be fabricated to have hierarchical pores and coral-like structures that have been demonstrated using a one-pot additive free solvent thermal decomposition method along with a post calcination treatment. The electrochemical behavior of the synthesized catalyst could surpass the current density and current stability recorded using other structures of nickel-cobalt alloys. As reported by some authors, combining nickel-cobalt oxide and nano-cloth or CNTs could also generate a catalyst with high current density, low onset potential, and long-term stable performance. NiCo_2O_4 supported over MWCNTs has exhibited a high current density of 327 mA cm^{-2} in addition to low onset potential. The percentage of current density retained by this catalyst after 250 cycles is 76%. A compound of Ni-Co-P-O is reported to contain electron tunneling junctions between the phosphates and metal phosphides resulting in quick transfer of both methanol and its products in and out of the catalysts.

Copper could also be considered as an appropriate non-noble metal substitute that is best for achieving long-term stability with low selectivity toward carbon monoxide compared to noble metals such as palladium, ruthenium, rhodium, and platinum. Copper by itself is less active as a catalyst and certain modifications (by alloying as well as by changes in the nanostructure) could be employed to improve its behavior toward MOR. Copper alloyed with platinum with dendritic morphology demonstrates the better activity toward MOR relative to those with polyhedral or stellated structure. This fine performance could be due to the presence of many atomic steps, edges, and corner atoms on its surface. The catalyst with polyhedral morphology, however, displays the best endurance toward CO due to the better electron transfer promoted by the strong coupling between copper and platinum. Palladium could also be alloyed with copper and adding TiO_2 as a support material to the combination can generate additional oxygen-containing group to minimize CO poisoning and improve catalytic activity. Alloying copper with zinc, to form CuZn/Cu , could also create MOR catalyst with large surface area, high surface porosity, and strong electronic interaction between the two metals that contribute to an oxidation current density. Copper trapped in CoO_x cage on a carbon layer is reported to have the highest activity, in non-noble metal electrodes, with specific activity of $150.41 \text{ mA cm}^{-2}$ and mass activity of $467.94 \text{ mA mg}^{-1}$. This is due to the presence of Co^{4+} being provided by the CoO_x cage that serves as an active site for easier methanol oxidation. Copper, on the other hand, acts as a center for methanol adsorption.

4. Effects of various parameters on methanol oxidation reaction

4.1. Shape and size

Based on the research findings described in the previous sections majority of the catalysts synthesized that produced superior performance are those possessing nanostructured systems. For instance, compared to the bulky arrangements, porous nanostructures of rightly controlled pore size, embedded into platinum-based materials, can enhance both mass transfer surface area and electron mobility in the solid ligaments. Porous materials having mesoporous arrangements, furthermore, introduces a concave surface that increases the active sites available for methanol oxidation reactions. As previously mentioned, combining such structures into platinum nanowires with a one-dimensional morphology improves not only the activity of the catalyst, but also its durability. The same improvement in performance can also be observed when mesoporous systems are implemented on platinum nanospheres. The unique characteristic generated from the resulting catalyst is the stability toward high temperatures as a result of the structure's ability to withstand particle aggregation.

Tang and coworkers published a work in 2013 that specifically focused on investigating the effect of size and shape of electrocatalysts on MOR and oxygen reduction reaction (ORR).^[163] They applied a robust chemical-tethering approach for the purpose of immobilizing gold (Au) nanoparticles onto surfaces of transparent indium tin oxide (ITO). Three types of Au nanostructures were tethered onto the ITO and they were 20 nm × 63 nm nanorods (NRs), 45 nm nanospheres (NS45s), and monodisperse 20 nm nanospheres (NS20s). Although the resulting electrodes displayed a great electrocatalytic performance toward both MOR and ORR, there is still a dependency of their mass current densities on the particles' shapes and sizes. From the study performed on MOR it was determined that for particles that have the same shape, such as NS20s and NS45s, the parameter that distinguishes their performances in terms of mass current densities is their sizes. Hence, NS20s (with peak position at 11.00 mA mg⁻¹) perform better than NS45s (with peak position at 5.59 mA mg⁻¹) and the reason is that the smaller the size of the particle the larger the catalytic current densities per unit mass due to larger surface-to-volume ratio. On the other hand, when particles exhibit different sizes, it was their crystalline structure or shape that dictated their electrocatalytic performance. Experimental data recorded that the mass current density of NRs (with peak position at 0.91 mA mg⁻¹) was lower than that of NS45 because the dominant (111) facets in NS45 were exposed. Generally, it can then be deduced that both shape and size play an important role in affecting the performance on MOR of different electrocatalytic electrodes.

4.2. Type of electrolyte (acidic and alkaline media)

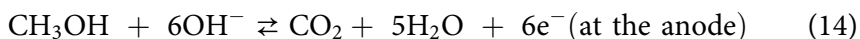
Methanol oxidation by electrocatalysts can also be affected by the type of electrolyte where the reaction takes place. The effectiveness of electrodes containing platinum, for example, is improved in alkaline medium due to the weak binding of the products on the surface of the catalyst. Such situation is not observed in acidic medium, where a strong binding of the products on the catalytic surface causes the anodic potential to be relatively higher. In an alkaline medium, hydroxide ions are also present that can easily get absorbed to cause methanol oxidation even at lower potential.^[164–168] To further take the advantages of alkaline media, the use of alkaline membranes in place of alkaline solutions should be considered. There are also many potential advantages of alkaline membrane that have been previously reported in literatures.^[169–174] The first advantage is that there more possibilities to obtain appropriate anodic catalysts for use in alkaline media than in acidic media. Secondly, the kinetics of the cathode reaction (i.e. oxygen reduction) is well known to be more fitting in alkaline media in comparison to acidic media. The third advantage is that the charge carrier in membrane in an alkaline membrane direct methanol fuel cell is cation and it flows to the anode from the cathode during the operation of the fuel cell. This is opposite to the flow of the proton in acidic membrane.

A study previously performed by Tripković *et al* on MOR by platinum and Pt/Ru catalyst (with different metal loadings), have similarly deduced that the platinum-based catalysts performed better in alkaline medium (0.1 NaOH) compared to acidic medium (0.5 M H₂SO₄).^[175] For instance, at 295 K platinum catalyst of 47.5 wt% exhibited a mass-specific current density value of 1.3 mA mg⁻¹_{Pt} in the acidic medium, whereas it displayed a value of 17.6 mA mg⁻¹_{Pt} in the alkaline medium at the same temperature. This can occur as a result of the competitive adsorption of OH_{ad} against bisulfate anions with varying pH. Temperature also contributed to the improved performance in alkaline medium as the mass-specific current densities in alkaline solution at 333 K had a value of 78.6 mA mg⁻¹_{Pt} for Platinum and a value of 84.1 mA mg⁻¹_{Pt} for Pt₂Ru₃ (at 0.5 V_{RHE}). These values are much higher than those determined at a lower temperature of 295 K in the same alkaline medium for both platinum and Pt₂Ru₃ catalysts with values of 17.6 mA mg⁻¹_{Pt} and 14.8 mA mg⁻¹_{Pt}, respectively.

Yang published a study that analyzed the catalytic capabilities of a nanoparticle-type of catalyst comprising of platinum and bismuth in both acidic and alkaline media.^[65] The catalyst was produced via a simple potentiostatic deposition, and characterization was performed using cyclic voltammetry and chronoamperometry. It was determined that methanol electrooxidation using PtBi catalyst has lower onset potentials (reaction

starting point) than platinum itself in the two different media. However, through the experiments performed it was also deduced that the acidic medium triggered a contradictory effect on methanol electrooxidation kinetics at higher overpotentials with both PtBi and platinum. The activity of platinum was observed to be more satisfactory than PtBi above 0.460 V (vs reversible hydrogen electrode (RHE)) in acidic medium, which is due to there being only a small number of continuous platinum sites available on PtBi for adsorption and dehydrogenation of methanol molecules. Alkaline medium, on the other hand, generates a different result in which the oxidation current on PtBi are significantly greater than that on platinum for overpotentials above 0.768 V (vs RHE). A reason for this can be attributed to the presence of Bi₂O₅ sites on the surface of PtBi where OH_{ad} is adsorbed and platinum sites remain vacant for methanol dehydrogenation. From the recorded data, PtBi nanoparticles seem more favorable to be utilized as a catalyst for MOR than platinum nanoparticles in alkaline conditions.

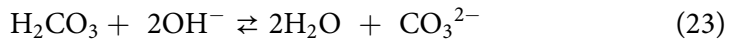
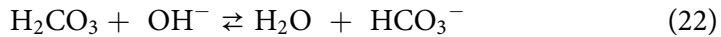
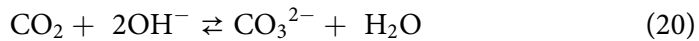
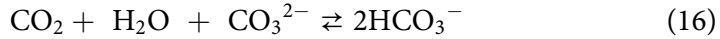
A DMFC operating with alkaline aqueous solutions is unstable as these solutions could also give rise to drawbacks such as carbonation. During the initial development of DMFCs, liquid alkaline electrolytes were preferred, however they have practical limitations that include the formation of sodium or potassium carbonate and their precipitation in the catalyst pores. A regular regeneration of the electrolyte is required for maintaining the DMFCs performance that adversely affects the catalysts membrane assembly leading to leakage of the liquid electrolyte through the electrode. These disadvantages add up to major drawbacks for proton-conducting electrolyte-based DMFCs such as fuel crossover and slow reaction kinetics. Some of the challenges related to the performance of alkaline electrolytes in fuel cells can be avoided by implementing more robust anion exchange membranes. Wang *et al.* performed a study that looked at the disadvantages of direct methanol fuel cell operating with an alkaline media.^[176] The drawbacks arise from the pH changes that occur in anodic region due to carbonation that will thermodynamically cause a voltage loss to the fuel cell. The pH difference occurs due to the following reactions that are expected to take place in an alkaline medium methanol fuel cell that utilized OH⁻ from anion-exchange membrane:



The OH⁻ anions produced at the cathode are transported to the anode through the membrane. The hydroxide ions originally present in the anode section may form CO₃²⁻/HCO₃⁻ due to their reaction with CO₂ being produced at the anode. Therefore, during the steady state operation of the fuel cell the anions electrostatically neutralizing the charge present in the anode section will mostly be a mixture of HCO₃⁻ and CO₃²⁻. The cathode section, on the

other hand, will have constant production of hydroxide ions. Thus, a difference in pH will develop between the anode and cathode sections during the operation that will thermodynamically lead to a reduction in voltage.

The same group performed a theoretical estimation of pH difference across the membrane in an alkaline membrane direct methanol fuel cell using equilibrium reactions that are linked to anode section's pH value as a starting point. The equilibrium reactions are as follows:



Out of the eight reactions above only three are independent reactions that govern the pH in the anode section. These reactions are those in [Equations 16–18](#) and are used to calculate the pH in the anode region at steady state. [Figure 12](#) illustrates the calculated difference in pH across the membrane (curve 1) and the potential loss due to the difference (curve 2) as functions of temperature, with an assumption of 1 atm. of carbon dioxide pressure, and accounting for the temperature dependence of equilibrium constants. The anions concentration in the alkaline membrane was assumed to be 1 mol/L or 0.1 mol/L during the analysis and both gave the same results as presented in [Figure 12](#). A large pH difference of 6.1 was observed at a low temperature of 20°C, which corresponds to a thermodynamic potential loss of around 360 mV. It was also noticed that as the temperature increases the difference in pH and voltage losses decrease.

This shows that the operation of an alkaline membrane direct methanol fuel cell is favorable at high temperatures. This requirement however is not practical as high temperature is not suitable for the structural stability of membranes.^[177]

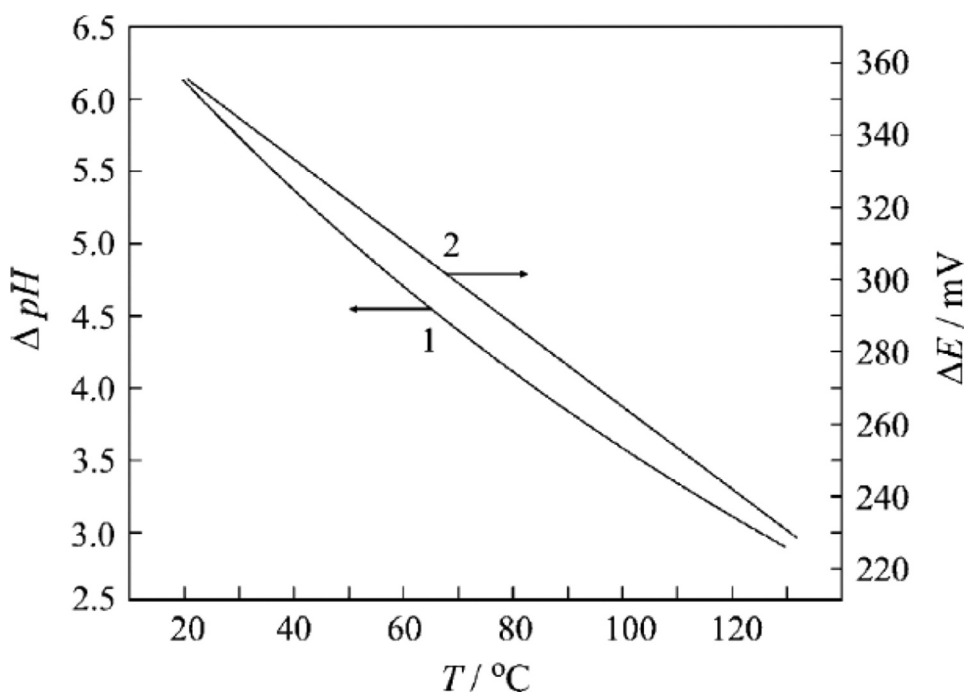


Figure 12. A graph representing pH difference $\Delta\text{pH} = \text{pH}_{\text{cathode}} - \text{pH}_{\text{anode}}$ (curve 1) and the appropriate potential loss ΔE (curve 2) as functions of temperature. Reproduced with permission from Elsevier^[176]

4.3. Support

The type of support being used for electrocatalysts can influence the stability, morphology, and dispersion of the metal nanoparticles being placed upon them. A number of materials possessing a characteristic of a high surface area and strong interaction with the loaded metal NPs are necessary provide a wider dispersion that is also stable. In addition, there is the need for high electrical conductivity to assist with the transfer of electrons when the reaction occurs on the electrode. Another important support property is to hold the composites' structural integrity (stability) to withstand severe electrochemical conditions. In addition to the properties previously mentioned, porosity, morphology, corrosion resistance, and hydrophobicity should also be considered to provide a good support for the catalyst being synthesized. Materials with such characteristics have been experimented in the past and they are discovered to be capable of magnifying the performance of catalysts significantly. An appreciable number of these studies are concentrated toward carbon as well as noncarbon materials and some of their results will be reviewed in this section. The different catalyst supports discussed in this section are classified into conductive polymer supports, carbon-based

supports (e.g. carbon black, carbon nanofiber, mesoporous carbon, carbon nanotubes, and graphene), and mesoporous silicas (e.g. Santa Barbara Amorphous 16 (SBA-16) and Mobil Crystalline Material (MCM-41). Various characteristics possessed by the support materials that contribute in determining the overall catalyst performance are also discussed. These characteristics include the surface area, interaction with the support, electrical conductivity, porosity, morphology, CO resistivity, and environmental and thermal stability. Furthermore, main parameters such, as methanol oxidation peak (or current density) at a given onset potential, stability current, and power density, that are vital in determining the electrochemical performance are discussed.

4.3.1. Conductive polymer supports

The exploitation of conductive polymer supports such as polyaniline (PAni) was previously studied by Kim *et al* ^[178] and Choi *et al* ^[179] to support PtRu-based catalysts. With this type of support a similar methanol oxidation current as carbon-supported PtRu catalyst can be achieved. Furthermore, catalytic tests performed by Kim's group on PtRu/PAni and PtRu/Carbon catalysts provided the reasons for the improved catalytic performance of the PAni-supported catalyst.^[178] They include, (i) the presence of larger electrochemical surface area, (ii) enhanced diffusion of ions, and (iii) the support's high electrical conductivity property. A combination of carbon and PAni as a support for PtSn was synthesized by Amani *et al* via the impregnation method.^[180] Different Pt:Sn atomic ratios were used in the study and the C-PAni-supported catalyst with Pt:Sn ratio of 30:70 performed relatively better for MOR. When compared to Pt/C-PAni catalyst the current density was around 50% greater, while in comparison to PtRu/C catalyst it was around 40% higher. Additional advantages promoted by the newly synthesized catalyst also included enhanced stability and CO resistivity as well as reduced methanol crossover. A modified form of PAni in the form of partially sulfonated polyaniline (SPANi) was synthesized by Das *et al* as a supporting matrix that paved the way for developing new type of catalysts.^[116] SPAni is an aromatic conductive polymer (ACP)-based matrix created by partial sulfonation of polyaniline with chlorosulfonic acid (CSA) that could have properties, such as high surface area and electronic conductivity, low weight, better interaction of their heteroatoms with catalyst particles, and environmental and thermal stability.^[181–186] With nickel nanoparticles as the metal being supported, the catalyst exhibited high mass specific current densities due to enhanced dispersion of active sites. Improved stability was also observed for Ni/SPANi catalyst that could be described by the presence of -SO₃H groups that increased the support's proton uptake capacity to further aid the catalyst against poisonous species.

Another type of polymer, known as polypyrrole (PPy), have also been used by Selvaraj and Alagar as a support material to synthesize a catalyst comprising of

Pt-Ru nanoparticles.^[187] During the synthesis, PPy was combined with multi-walled carbon nanotubes using the in situ polymerization of PPy on CNTs that involved ammonium peroxydisulphate $(\text{NH}_4)_2\text{S}_2\text{O}_8$ as an oxidizing agent (with 0 to 5 °C temperature range). To better study the performance of the produced PtRu/PPy-CNT catalyst another PPy-CNT-supported catalyst was loaded with platinum to form Pt/PPy-CNT via a chemical reduction technique. Results from the study have shown that PtRu/PPy-CNT catalysts demonstrated greater stability and finer catalytic activity for MOR relative to Pt/PPy-CNT catalyst.

4.3.2. Carbon-based supports

Catalysts made of platinum or platinum-based alloy are generally supported on carbon black, such as Vulcan XC-72 R, when used in fuel cells. The frequency of their use as a support is due to certain beneficial properties they possess including high specific surface area (BET surface area of $\sim 250 \text{ m}^2 \text{ g}^{-1}$), greater stability in alkaline or acidic media, and good electric conductivity (2.77 S cm^{-1}), etc..^[188] The latter is necessary to reduce the resistance of electrode as well as to prevent oxidation.^[189] The carbon materials that support the catalysts in fuel cells will largely determine performance parameters (metal nanoparticle stability, electronic conductivity of catalyst layer, mass transport, and surface area) during operations.^[190] Wide variety of carbonaceous nanomaterials such as carbon nanofiber (CNF), carbon nanocoil (CNC), nano carbon black (CB), single/multiwalled carbon nanotubes (SWCNT/MWCNTs), carbon mesoporous (CMS) and graphene/graphene oxides (G/GOs) with several nanometers are the possible choice for enhancing the electrocatalytic activity. Various carbon-based electrocatalyst that demonstrated exceptional electrocatalytic performance for methanol electrooxidation reaction are systematically explained in this section.

4.3.2.1. Carbon black. Carbon black is a widely used electrocatalyst carbon support owing to its low cost, large surface area, high electrical conductivity, high availability, surface functionality, large and stable pore volume where Vulcan XC-72, Ketjen Black, acetylene black, etc., are the commonly used ones. Out of these, Vulcan XC-72 has a relatively satisfactory electronic conductivity and greater specific surface area when compared to others. Carbon black is a promising supportive agent for NPs with controllable size and shape.

Performance evaluation of Pt–Ru supported over different carbon materials for direct methanol fuel cell was conducted by Salgado and coworkers.^[191] The carbon black functionalized with HNO_3 provides the highest power density due to the presence of oxygenated group in carbon black. Abdel and Sherif reduced Ni nanoparticles with different weight percentage (10, 20, 30, 40, and 60%) over Vulcan XC-72 R carbon black using microwave irradiation.^[192] Ni/C-30 showed the higher electrocatalytic activity, approximately 5.2 times

higher than Ni/C-10. The physiochemical characterization shows that spherical carbon black particles with average diameter of 45 nm have lower metal loading of Ni 10% and there is a formation of a dense deposition of particle if the weight percentage increases to higher value (Ni 60%). Ni 30% is found to be an optimum loading of Ni particles to uniformly deposit over the carbon black. Wang *et al* designed a hybrid Pd/g-C₃N₄/carbon black using low-temperature heating treatment followed by a wet chemistry route.^[193] Due to the synergetic effect of the individual components, Pd/g-C₃N₄/carbon black exhibits an exceptional forward peak current density of 1720 mA mg⁻¹_{Pd} for methanol oxidation and shows an outstanding performance. In effect, Pd/g-C₃N₄/carbon black with exceptional activity and stability was reported as the best choice for the practical application in high-performance portable fuel cell systems. Yabei *et al* prepared Sn-doped TiO₂ mixed with carbon black (Ti_xSn_{1-x}O₂-C) as a hybrid Pt support that was used as a promising candidate for methanol oxidation.^[194] An optimization study was conducted to identify the best ratio for Ti_xSn_{1-x}O₂ to carbon ratio and Sn doping content to obtain high performance. Pt nanoparticles supported over Ti_{0.9}Sn_{0.1}O₂-C exhibited the highest activity when compared to Pt/TiO₂-C and commercial Pt/C catalysts. Pt nanoparticles in the range of 2 to 3 nm size were mostly deposited on the edge of the Ti_xSn_{1-x}O₂-C and they cause the formation of special triple junction that improves the overall ECSA. Moreover, the high content of OH group on Ti_xSn_{1-x}O₂-C strengthened the metal-supports interactions that is expected to have immense scope of higher electrocatalytic activity. Amin *et al.* tested the electrocatalytic methanol oxidation of Ni and Pd-Ni loaded over Vulcan XC-72 R carbon black prepared via impregnation method with NaBH₄ as a reducing agent in alkaline medium.^[195] Pd-Ni/C electrocatalyst reported in their work shows improved performance when compared to other Pt-Ni based catalyst. Xiaoqing and coworkers synthesized hollow PtCu nanostructure deposited on commercial carbon black that shows specific and mass activity of 1.77 mA cm⁻² and 0.889 A mg⁻¹_{Pt}, respectively, which are far better than solid PtCu/C.^[196]

4.3.2.2. Carbon nanofiber (CNF). Although carbon black support can contribute in improving the electrical conductivity of fuel cell electrodes,^[197] it still offers relatively unsatisfactory performance in terms of reduced utilization of the deposited metal and weak durability.^[198] CNFs are cylindrical graphene layered nanostructure with an average diameter of 80 to 200 nm and 50–200 μm length with a specific surface area between 10 and 200 m² g⁻¹ and are usually in the shape of a cup, ribbon, platelets, tubes, and herring bones to provide a higher surface area. HyeLan and coworkers synthesized octahedral Co₃O₄/carbon nanofibers composite-supported Pt catalysts sequentially using electrospinning, hydrothermal, and chemical reduction technique with three different ratios of Co precursors (0.05, 0.1, and 0.2 M)

to the solution.^[199] Co precursor with 0.1 M concentration exhibited a higher electrocatalytic activity ($\sim 415.6 \text{ mA mg}_{\text{Pt}}^{-1}$) and excellent stability when compared to commercial Pt/C and Pt/conventional CNF due to optimal size octahedral Co_3O_4 growth in CNF support that maximizes the dispersion of Pt nanoparticle. Yudai and coworkers demonstrated ultrahigh performance of TiO_2 embedded on carbon nanofiber (TECNF) as an excellent support of PtRu catalyst toward methanol oxidation.^[200] The mass activity of PtRu/TECNF with optimal Ti/C ratio is found to be 4 folds higher than PtRu/C. Moreover PtRu/TECNF with $\frac{1}{4}$ PtRu loading delivered two times higher power, when compared to commercial PtRu/C. The obtained excellent performance can be attributed to the superior support to metal interaction between TiO_2 /CNF and PtRu nanoparticles. Bimetallic Pt@Ni supported over CNF shows superior specific and mass activities for methanol oxidation. They studied the effect of weight ratio of nickel precursors to polyacrylonitrile (PAN) as 1:10, 3:10, and 5:10 in the overall performance. The specific surface area ($234.1 \text{ m}^2 \text{ g}^{-1}$) and total pore volume ($0.157 \text{ cm}^3 \text{ g}^{-1}$) is higher in Ni_{50} /CNFs, that facilitate the high dispersion of larger number of Pt nanoparticle in the average size of 3.8 nm than compared to other catalyst as shown in Figure 13. Subsequently, Ni_{50}

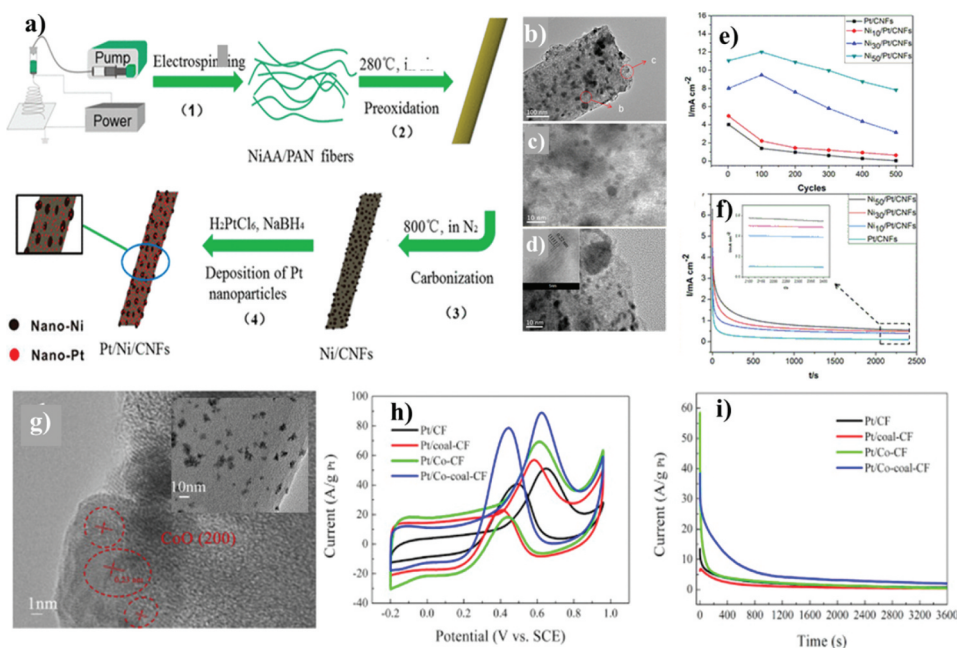


Figure 13. (a) Illustration of the synthesis process of Pt/Ni/CNFs (b) TEM and (c and d) HRTEM of Ni_{50} /Pt/CNFs, (e) anodic peak current densities of at different scan cycles of methanol oxidation, (f) chronoamperometric analysis of Pt-Ni-CNF catalyst at 0.45 V vs Ag/AgCl in 0.5 M H_2SO_4 + 1 M CH_3OH acidic solution, and (g) HRTEM and TEM (inset) of Co-coal-CF (h) cyclic voltammogram and chronoamperometric profile of Pt/CF, Pt/coal-CF, Pt/Co-CF, and Pt/Co-coal-CF for methanol oxidation. Reproduced with permission from American Chemical Society^[201], Reproduced with permission from Elsevier^[202]

/Pt/CNFs showed an excellent electrocatalytic performance with a maximum current density of 10.9 mA cm^{-1} , with slightly slower current decay over time and higher CO poisoning-tolerance.^[201] Xue *et al* proposed the fabrication of Co embedded coal-based carbon nanofiber as a promising support of Pt nanoparticles for electro-oxidation of methanol.^[202] Novel well-dispersed Pt/Co-coal-CF shows excellent catalytic activity and stability, and the mass activity of Pt/Co-coal-CF ($78.5 \text{ A g}^{-1} \text{ Pt}$) is almost 50% higher than Pt/CF ($46.0 \text{ A g}^{-1} \text{ Pt}$), Pt/Co-CF ($49.0 \text{ A g}^{-1} \text{ Pt}$), and Pt/coal-CF ($40.8 \text{ A g}^{-1} \text{ Pt}$). Pt/Co-coal-CF provides a well-dispersed smallest-Pt size distribution on highly graphitized CNF support due to the presence of more nucleation sites that provides homogeneous deposition of Pt nanoparticles when compared to Pt/Co-CF as shown in Figure 13. Dempsey *et al* proposed a new strategy to improve the utility by allowing an effective dispersion and excellent decoration of Pt nanoparticle inside and outside the functionalized carbon nanofibers. The proposed idea thereby shows an excellent response toward methanol oxidation and causes strong resistance to the poisoning species during electrocatalytic reactions.^[203]

Barakat and his team synthesized Co/Cu-decorated carbon nanofibers in which the CNF were prepared from the graphitization of high carbon-containing poly(vinyl alcohol) that shows excellent activity and stability.^[204] The physiochemical properties showed that metallic Co nanoparticles are shielded with the highly crystalline thin layer of graphite that enhances the adsorption property of the carbon and enhances the active catalyst surface area. Zafar Khan *et al* introduced Co/SrCO₃ nanorods-decorated carbon nanofibers prepared using sol-gel technique as novel promising catalysts for electro-oxidation of methanol in alkaline medium.^[205] They studied the effect of methanol oxidation and presented that the current density increases with increase in methanol concentration; moreover the introduced catalyst shows the lowest onset potential among the other reported non-precious catalysts at that time. Same group reported a study on Co/CeO₂ decorated carbon nanofibers as an effective electro-catalyst for methanol oxidation.^[206] Recently, Miloud and his group worked on the facile and rapid synthesis of Ni nanoparticles supported over the CNF/poly(paraphenylenediamine) (PpPD) using simple electrochemical methods.^[207] The electrochemical result shows that the synergetic effect of each component leads to a high methanol oxidation reaction with ultrahigh durability and stability.

4.3.2.3. Mesoporous carbon. While considering the electrochemical reactions with the molecule diffusion and ion transportation, micropores of less than 2 nm are extremely small to access the active ions and macropores of greater than 50 nm are much larger that reduces the specific surface area, and to balance both it is better to take the benefit of mesoporous materials.

Highly ordered mesoporous carbon with high surface area, tunable porosity (2–50 nm), narrow pore size distribution and interconnected channels for the absorption and diffusion of electroactive species have been widely used for many electrochemical applications.^[208–210]

Tianbao *et al* prepared mesoporous carbon support with large specific surface area and high pore size diameter by carbonizing soybean and used it as an active medium for the fine dispersion of Pt nanoparticle.^[211] The prepared Pt supported mesoporous shows significantly high activity and durability when compared to Pt/Vulcan carbon XC-72, owing to the supportive effect and better dispersion of Pt(0) nanoparticles with unique morphology in mesoporous support. Similarly, Jing and coworkers developed graphitic mesoporous carbons (GMC) with two different carbon precursors (resorcinol and formaldehyde) and varied the pore size and surface area by adjusting the amount of iron nitrate as the graphitization catalyst.^[212] PtRu-GMC-2, where GMC-2 with larger amount of pore of 20 nm facilitates a smooth transfer of reactants and products between the catalyst layers, exhibits a high power density that is 26% higher than commercial PtRu-XC. Wang *et al* successfully synthesized 2D hexagonally ordered mesoporous carbon-tungsten carbide (OMC/WC) nanocomposite with high surface area using soft-template method for the first time.^[213] Pt loaded ordered mesoporous self-supported metal carbides offered a specific mass activity of 3.2 times (per mg metal) and 2.4 times (per mg Pt) higher than commercial PtRu@C. The enhancement in the activity was not only because of synergetic effect between OMC/WC and Pt, but also due to the highly ordered nanostructure with larger surface area that enhances the utilization efficiency of well-dispersed Pt nanoparticle with desirable product and reactant transfer. Chengwei *et al* successfully fabricated 3D ordered mesoporous carbon sphere array (OMCS) supported Pt nanoparticles, where Pt with mean size of 1.6 nm was finely dispersed over the walls of mesoporous carbon sphere as in [Figure 14](#).^[214] Pt/OMCS possesses higher electrochemical surface area (ECSA), activity and durability than Pt/Vulcan carbon and commercial Pt/C. They found that the hierarchical structure with ordered mesopores and macropores can facilitate the mass transport and improve the dispersion of Pt nanoparticles

Gui-fa and coworkers used nitrogen-doped ordered mesoporous carbon supported (NOMC) with Pt to study the effect of carbon size and metal loading.^[215] They found that the size of mesoporous carbon support has considerable effect on the narrow and uniform distribution of fine Pt particles. The size of Pt nanoparticle formed was smaller over 2D-NOMC than 3D-NOMC, with a 10% of metal loading. XRD and XPS data revealed that there existed a strong interaction between the Pt and support, which is strong enough to form Pt-N bond on the surface. These strong coupling favored the electrochemical reaction and demonstrated a surprisingly high

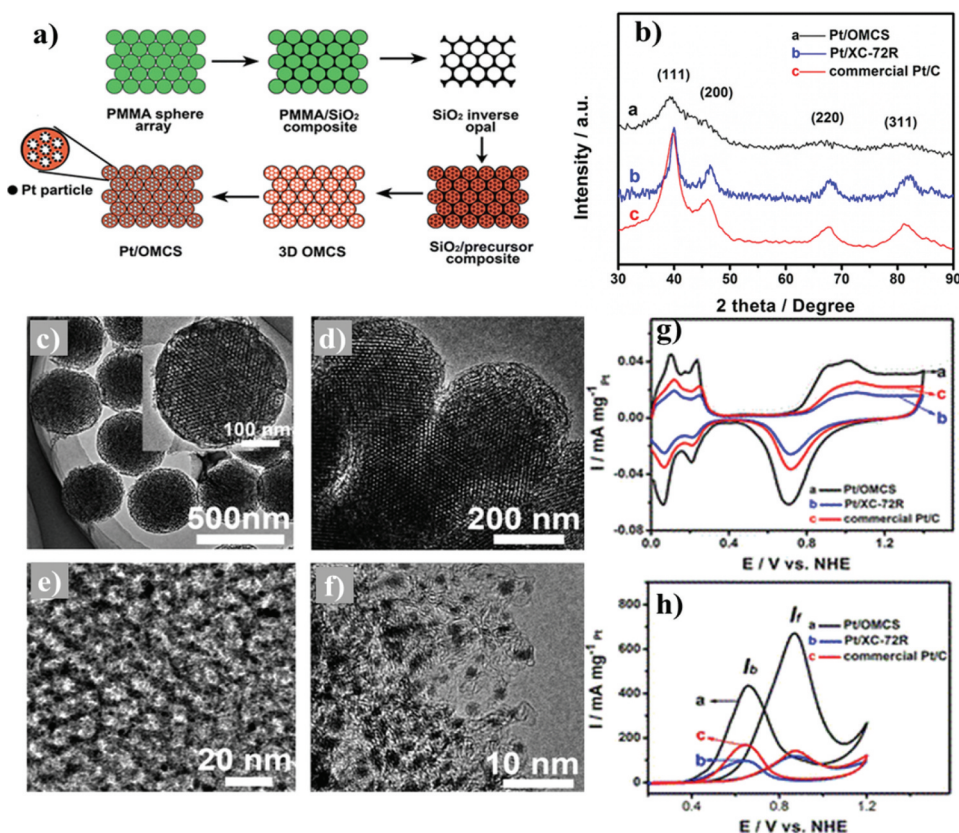


Figure 14. (a) Schematic illustration on the synthesis of Pt/OMCS catalysts. (b) XRD profile of the Pt/OMCS, Pt/XC-72 R, and commercial Pt/C. (c) TEM image of the OMCS. Inset: Higher magnification image of single mesoporous carbon spheres, (d) TEM and (e) higher magnification TEM image of the Pt/OMCS, and (f) HR-TEM image of the Pt particles on the mesoporous carbon spheres and (g) cyclic voltammograms (CVs) of the catalysts in Ar-saturated 0.5 M H_2SO_4 ; (h) Ar-saturated 0.5 M H_2SO_4 and 1 M CH_3OH . Reproduced with permission from American Chemical Society^[214]

activity and stability when compared to commercial Pt/XC-72. In order to provide better facility for the oxidation of CO species and reduce poisoning, oxygen containing support was also impregnated with Pt and other precious metals particles, and recently, Qiang's group reported the MOR of highly dispersed Pd-CeO₂ catalyst supported over N-doped core-shell mesoporous carbon sphere (NMCS) support with excellent activity, CO resistance, and stability in alkaline medium.^[216] They studied the significance of the atomic ratio of Pd/CeO₂ in catalytic activity and optimized it to 20:20 (Pt_(20%):CeO_{2(20%)}/NMCS) that exhibits ~6 times higher peak current density than commercial PtRu/C. Density functional theory calculations were also performed showing a strong electronic interactions between palladium and the surrounding CeO₂ and the N₂ dopants existing in supports significantly decreases the adsorption energy of the carbon monoxide at the surface of palladium. This, therefore, improves the tolerance of Pd-CeO₂/NMCS

catalyst toward CO and further enhances the activity of methanol oxidation reaction. Moreover these, there were more detailed studies reported on the mesoporous carbon structure such as PtFe/OMC, ^[217] PtRu-CMK3, ^[218] Pt/BLC, ^[219] Co-N-OMC ^[220] etc., for the methanol oxidation reaction.

4.3.2.4. Carbon nanotubes. Carbon nanotubes are made of single sheets of carbon atoms that are arranged hexagonally and that are rolled to produce a two-dimensional cylindrical nanostructure. In addition to their mechanical, electronic, and magnetic properties they are also capable of capturing atoms belonging to other elements in their molecular structure.^[221] The two categories into which carbon nanotubes are usually distributed are single-walled carbon nanotubes (SWCNTs), cylindrical structures of diameters as small as 0.4 nm; and multiwalled carbon nanotubes (MWCNTs), tubes nested into a concentric set. MWCNTs offer greater conductivity while SWCNTs provide higher surface area.

A number of studies implementing carbon nanotubes as supporting materials have been reported. One of them was the synthesis of activated MWCNTs by Wang's team that utilized an activating agent of solid potassium hydroxide in an alkali treatment.^[222] Palladium is then loaded onto chitosan (CS)-functionalized aCNTs along with La₂O₃ via a reduction reaction that involves NaBH₄. A high catalytic activity was observed in the resulting Pd-La₂O₃/C catalyst that can be attributed to the better dispersion of metal particles by CS and greater presence of palladium. Another research carried out by Jha's group also involved the production of MWNTs that employed chemical vapor deposition.^[17] The prepared support material was then loaded with platinum and platinum-ruthenium via chemical reduction method to synthesize Pt/MWNT and Pt-Ru/MWNT, respectively. Data recorded regarding the performances of the synthesized catalysts demonstrated a temperature dependency of power density. At 80 °C, the power density displayed a maximum value of 39.3 mW cm⁻² with a current density of 130 mA cm⁻². The high values attained can be explained by the accessibility and enhanced scattering of both Pt-Ru and MWNT in the electrocatalyst. Based on the studies performed on CNTs it can be seen that they are capable of improving electrocatalytic activity when used as a support, however their production method still faces cost restrictions and is not suitable for large scale.

Yang *et al* fabricated Pd-Pt nanoparticles with an average size of 3.4 ± 0.5 nm that were uniformly deposited over side walls of the CNTs using ultrasonic assisted method that exhibits higher activity toward methanol oxidation.^[223] The results show that the catalytic activity of Pd-Pt nanostructure is highly influenced by the Pt content, where PdPt₃/CNTs gives the highest activity with a maximum mass current of 1.0 A mg⁻¹ that could be attributed to the synergetic interaction of well-alloyed Pd-Pt nanoparticles with the CNTs. High quality nanohybrid Pt/CeO₂/CNTs with smaller particles and fine

dispersion was synthesized by Lou's research group via layer-by-layer assembly.^[224] The presence of CeO₂ in the nanocomposite effectively reduces the aggregation of Pt nanoparticle and the oxophilic nature of CeO₂ helps in the elimination of CO_{ads} poisoning from the active Pt site by donating the OH bond from the CeO₂-OH, thereby oxidizing the CO-like species at lower potential. However, Pt/CeO₂/CNTs exhibited a higher activity and stability when compared to commercial catalyst. Zhan and coworkers developed a hybrid CNTs@TiCoN support with tunable composition for the deposition of small-sized well-dispersed Pt nanoparticle.^[225] CNTs@TiCoN utilized the advantage of high conductivity of CNTs and good corrosion resistance of external TiCoN coating and it shows superior activity and stability as compared to commercial Pt/C. Pd nanoparticles decorated over the carboxyl-functionalized MWCNTs using one-pot thermal decomposition method was demonstrated by Yiran and his team.^[226] The carboxylic group effectively disperses the Pd nanoparticle by anchoring it to the CNTs, which was attributed to the highest current density toward methanol oxidation reaction. The presence of COOH group in Pd-MWCNT (Pd-MWCNT-COOH) enhanced the mass current value by two folds higher than normal Pd-MWCNT and it demonstrated the significance of functionalizing CNTs with carboxyl group which gives the uniform distribution of Pd and that promised a strong interaction between the nanoparticle and support.^[226] Xiang *et al* exploited the use of hemin as a binder for Pt nanoparticles deposited on carbon nanotubes.^[227] Hemin acted as a catalyst as well as a binding agent that enhances the activity of the nanohybrids used for methanol oxidation. Pt/Hemin-MWCNT displayed higher current density (425.0 mA mg⁻¹) and electrochemical surface area (67.46 m² g⁻¹) than Pt-MWCNT in the absence of hemin. Lizhen *et al* described the in-situ growth of 3D tungsten carbide-CNTs with W₁₈O₄₉ as a starting agent at different holding temperature set at 700, 800, 900, and 1000 °C, in which W₁₈O₄₉ not only acts as a source of tungsten, but also as nucleation sites for CNT formation.^[228] The resultant WC-CNTs acts as a support for the deposition of Pt and was tested for its electrochemical activity toward methanol oxidation that gives a maximum peak current density of 1350 mA mg⁻¹ Pt for optimized Pt/WC-CNT-900 sample. MWCNTs decorated with MoS₂ and Ti₃C₂T_x quantum dots (MoS₂QDs@Ti₃C₂T_xQDs@MMWCNTs) was reported as an excellent Pt-free bifunctional catalyst for oxygen reduction reaction and methanol oxidation reaction. MoS₂QDs@Ti₃C₂T_xQDs@MMWCNTs provides a maximum methanol oxidation current density of 160 A g⁻¹ at 2.2 V and are comparable with commercial Pt/C.^[229]

The catalytic activity of the CNTs was further improved by applying some doping strategies. Some of them are acid oxidation and side wall functionalization, which is complex and may, impair the mechanical properties of CNTs and also cause the addition of some unwanted species

that can adversely affect the catalytic activity. However, doping the CNT surface with some heteroatoms such as boron, nitrogen, phosphorous and sulfur can effectively enhance the physical and chemical properties of CNT.^[230,231] Li-Mei *et al* used nitrogen-doped carbon nanotubes (CN_x-NTs) as a supportive medium for the effective dispersion of Pt nanoparticle.^[232] They studied the effect of pyrolysis temperature (600, 700, 800, or 900°C) on the particle characteristics and in turn its influence toward methanol oxidation reaction and reported that Pt/CN_x-NTs-800 exhibits the highest activity owing to the morphology of nanotube and high nitrogen content. High nitrogen content creates an environment for better dispersion and anchoring of nanoparticle, where the nanotube morphology forms a flexible open network bound to the catalyst for the smoother pathway for mass transfer. Apart from these results, many other works have also been reported with CNTs including Pt-Ru/c-MWCNT,^[233] PtCo/MWCNT,^[234] Co@Pt/MWCNTs,^[235] PtNi/MWCNT,^[236] PdSnNi/CNT,^[237] and Pd_{20-x}Ag_x/CNT^[238] as promising carbon-supported catalysts.

4.3.2.5. Graphene. Graphene have recently been used as well to act as a support to take advantage of its good chemical stability, structural flexibility, high surface-to-volume ratio, electrical conductivity, ultrathin appearance, and the presence of distinctive porous systems.^[239–241] In addition, it is a material that is highly resistant toward poisonous species. A study conducted by Liu *et al* involved a preparation of three-dimensional graphene aerogel (3DGA) through an efficient and facile hydrothermal technique in absence of palladium NP catalyst template and surfactant.^[242] Merging both palladium and DGA generates Pd/3DGA nanocomposites having a high surface area that could produce an ECSA of 425 m² g⁻¹ that is 3.4 times greater than that obtained for commercial Pd/C.

Functional groups containing either boron or nitrogen can also be doped onto graphene to finely adjust the size of particles and distribution of loaded materials to enhance the performance of supported catalysts on MOR. Doping graphene with nitrogen, for example, can finely alter the physical and chemical characteristics of carbon-based materials when used for MOR. This is because the doped nitrogen atoms are capable of promoting better electrical conductivity via partial structure recovery. In addition, there will be more efficient anchor sites made available for the greater dispersion of metallic NPs over the carbon support.^[243] Graphene-doping modification was at one time performed by Lu *et al* to support PtRu that employed a single-step heat treatment approach.^[244] CV results obtained from the study showed that, at a scan rate of 50 mV s⁻¹, PtRu/NG (Nitrogen-doped) has a peak current density of 328.1 A g⁻¹ at a potential of approximately 0.7 V. This value is higher than that of commercial PtRu-

C-HS catalyst on MOR, with a value of 307.8 A g^{-1} .^[245,246] Nonetheless, PtRu/BG (Boron-doped) exhibited a relatively higher forward current density on CV in comparison to both PtRu-C-HS and PtRu/NG catalysts.

Graphene doped with nitrogen and loaded with platinum was synthesized by Zhao's group through a facile single-step technique.^[239] Using this approach, graphene oxide is simultaneously reduced to graphene which is functionally doped further with nitrogen. Platinum nanoparticles are then loaded onto the doped graphene with the help of ethylene glycol and *N*-methyl-2-pyrrolidone mixture. In comparison to the catalyst in which the graphene support is not doped, there is a narrower distribution of particle size in addition to the enhanced performance of the synthesized catalyst. Moreover, test data of Pt/*N*-graphene catalyst obtained using CV showed peak current densities (platinum mass normalized) that are two times greater than Pt/undoped graphene catalyst for MOR. Tests using CA in an electrolyte solution of 0.5 M H₂SO₄ and 1 M methanol (at 0.6 V potential) also provided further proof for the superiority of Pt/NG catalysts. It displayed a slower rate of decay and a steady-state limiting current that is nearly 2 times the value for Pt/G catalyst.

Zhao and coworkers implemented a solution dip-coating method to synthesize three-dimensional hierarchical nitrogen-doped graphene frameworks (3D-NG).^[247] The method utilizes commercial sponges as the initial template, and this prevents the restacking of graphene plates during the annealing process. Furthermore, a polyol reduction technique was employed to fabricate the final Pt/3D-NG catalyst. Relative to Pt/G, the newly produced catalyst demonstrated a catalytic activity that is 2.3 times greater with an improved stability property by 10% for MOR. The reason for this enhancement can be explained by the presence of large pore volume, great specific surface area, high level of nitrogen doping, and platinum NPs that are homogeneously dispersed.

Zhao *et al* also synthesized frameworks of nitrogen-doped three-dimensional porous graphene (NGAs) via a supramolecular assembly-assisted method that utilized graphene oxide as the building block.^[241] Supramolecular aggregate of self-assembled melamine and cyanuric acid was also adopted to reduce graphene nanosheets from restacking, as a self-sacrificial pore-forming agent, and a source of nitrogen to promote simultaneous doping of nitrogen. The function of supramolecular aggregates is to form free-stacking and loose porous structure and to direct the fabrication of a special three-dimensional structure. When the resultant Pt/NGA catalyst was used to catalyze MOR it exhibited an excellent behavior, both in terms of stability and catalytic activity. CV experiments performed in 0.5 M H₂SO₄ and 0.5 M methanol provided an oxidation current density value of 507.5 mA mg^{-1} for Pt/NGA. This value is actually 1.5 times greater than the value exhibited by commercial Pt/C (336.8 mA mg^{-1}). CA analysis (at 0.6 V potential), on the other hand, showed

that Pt/NGA has greater stability and the catalyst displayed a low decay in current throughout the CA experiment with a final value that is about 3 times greater than that of commercial Pt/C.

The hybrid support of graphene oxide and Polyvinylpyrrolidone produced by Daşdelen's research group, as a support for platinum nanoparticles, facilitated in reducing the electrocatalytic reduction in MOR.^[61] Also, in comparison to platinum supported individually by GO and PVP supports (Pt@GO and Pt@PVP, respectively) there was an enhanced methanol molecules adsorption rate provided by the larger active surface area present on the catalyst.

Although previous studies have shown that graphene can be a suitable support material to promote improved electrocatalytic oxidation of methanol there are still challenges facing with its utilization. Issues include severe accumulation of platinum nanoparticles on the surface of graphene and the restacking of graphene layers because of Van der Waal forces.^[247] In addition, due to the inert nature of graphene and its insolubility in aqueous solutions or organic solvents it is still difficult to deposit metals on graphene surfaces.

4.3.2.6. Other carbon-based supports. Supported catalysts have also included the use of carbon in other unconventional forms. One of these types is the carbon paper (CP) that was used by Amini's research team in their study to support an alloy of platinum and gold.^[248] The synthesis method implemented was the repeated copper underpotential deposition (UPD) redox replacement process which involve loading different quantity of platinum onto the support. Amongst the various platinum coverage utilized PtAu/CP catalyst possessing an almost similar thickness to a monatomic platinum layer exhibited the best Pt utilization efficiency toward the oxidation of methanol. Another type of nonmainstream carbon-based support is the carbon aerogel (CA) and it was previously exploited by Wei *et al* to synthesize a new form of supported catalyst.^[249] Carbon aerogel of different pore structures was analyzed to obtain a uniform dispersion of platinum. In addition, Pt/CA demonstrated the highest mass specific current value for MOR in comparison to E-TEK 20% Pt/C catalyst (118.4 mA mg⁻¹) by showing a value of 395.3 mA mg⁻¹. Zhang's group has also, in the past, produced a platinum-loaded catalyst supported by a carbon material consisting of a single-crystalline C₆₀.^[250] By modifying the reaction variables, they managed to selectively synthesize various C₆₀ nanostructures that included nanoplates, hollow nanobowls, nanorings, nanowires, and nanorods. Experimental results obtained during the MOR study have shown that Pt/C₆₀ nanobowls generated a less positive onset potential of 0.10 V (vs. SCE) compared to Pt/C₆₀-solid-nanoball catalyst (0.29 V vs. SCE). This finer phenomenon can be explained by the availability of high surface area to volume ratio posed by the C₆₀ hollow nanobowl. Carbon materials of nanospherical morphology are also useful in providing improved

properties when used as supports such as fine chemical durability and electro-
nic conductivity, proper mass transport porosity, and high surface area. Liu
and coworkers utilized carbon nanosphere (CS) in their investigation to
support platinum and observed the performance of the resulting electrocata-
lyst to that of commercial Pt/C containing Vulcan XC-72 R Carbon.^[251]
Experimental data from their research showed that the newly synthesized
catalysts exhibited a wider active surface area of $56 \text{ m}^2 \text{ g}^{-1}$ relative to com-
mercial Pt/C that has a value of $28 \text{ m}^2 \text{ g}^{-1}$. As a result, the peak current density
gave a higher reading by 2.6 times at a lower potential with a difference of
100 mV compared to commercial Pt/C catalyst. Another CS-based catalyst
with an active surface area of $89.2 \text{ m}^2 \text{ g}^{-1}$ was synthesized by Zhang *et al* that
possessed a honeycomb-like mesoporous structure and that was also doped
with nitrogen.^[252] This special support was once again loaded with platinum
to form Pt/MNCS and the combination demonstrated a stronger durability
and an extremely high catalytic activity for MOR valued at 1007 mA mg^{-1} peak
current density. A suitable reasoning for such enhancement could be a positive
alteration in the electronic structure, growth behavior, platinum nucleation as
well as the fine binding between both the metal catalyst and support by the
honeycomb-like mesoporous arrangement and nitrogen doping. Xie *et al*
fabricated a catalyst supported by carbon spheres embellished with binary
and ternary layered double hydroxide using a one-pot method.^[253] Platinum
nanoparticles (average particle size of $\sim 1.6 \pm 0.2 \text{ nm}$) were deposited on the
carbon spheres via a microwave-assisted polyol process that creates a fine
particle distribution. From the MOR electrochemical analysis implemented in
their study, it was found that the newly fabricated catalyst (Pt/C@NiRu layered
double hydroxide) managed to achieve a mass activity of $2032 \text{ mA mg}^{-1}_{\text{Pt}}$ in
an alkaline solution (1 M KOH + 1 M methanol) and a mass activity of
 $686 \text{ mA mg}^{-1}_{\text{Pt}}$ in an acidic solution (0.5 M H_2SO_4 + 1 M methanol).
Doping with cerium to form Pt/C@NiRuCe layered double hydroxide, how-
ever, generates a much better result than the undoped type of the catalyst. For
instance, in an alkaline solution a mass activity of $2475 \text{ mA mg}^{-1}_{\text{Pt}}$ was
observed by Pt/C@NiRuCe-LDH while in an acidic solution a mass activity
value of $725 \text{ mA mg}^{-1}_{\text{Pt}}$ was exhibited.^[253] The enhancement demonstrated by
the two synthesized catalysts in both acid and alkaline medium shows that they
are capable of performing with better CO resistivity and electrocatalytic
activity compared to home-made Pt/C-H ($665 \text{ mA mg}^{-1}_{\text{Pt}}$ in alkaline medium
and $273 \text{ mA mg}^{-1}_{\text{Pt}}$ in acid medium). One of the factors that could contribute
to the improvement can be due to the provision of many OH species by the
layered double hydroxide to promote the oxidation of poisonous intermediate
species and the strengthening of Pt-support interaction. Furthermore, the
inclusion of cerium accelerates not only the catalytic activity, but also the
transfer of charge. Niu's research team synthesized a catalyst of sulfur-doped
carbon microsphere (S-CMS) that has small palladium NPs encapsulated

inside it and studied its activity and durability for MOR.^[254] The synthesis of Pd NPs inside S-CMS was achievable through a one-pot hydrothermal technique that involved reduced glutathione (r-GSH) to act as a capping and reducing agent. A simple carbonization process was then performed that overall resulted in the fine dispersion of Pd NPs within S-CMS that exhibited an architectural feature similar to the plum pudding model. Analysis performed on the catalyst showed the presence of greater effective surface area (ECSA of $32.09 \text{ m}^2 \text{ g}^{-1}$) toward MOR in comparison to commercial Pd/C catalyst (ECSA of $20.76 \text{ m}^2 \text{ g}^{-1}$). In addition, a higher mass activity value (11.78 mA mg^{-1} from CA) is demonstrated by the catalyst that is 5.9 times greater than that of Pd/C (1.99 mA mg^{-1} from CA), an improvement attributed to the tiny size of Pd NPs along with the great interaction between the heteroatom-modified CMS coating and these Pd particles. Stability is also attained during continuous start-stop operation by the confined Pd NPs that indicate the capability of the new-found catalyst to be a potential anode material for DMFCs. A study that involved the employment of carbon quantum dots to support platinum catalysts was previously reported by Pan *et al.*^[255] The synergistic behavior between the Pt metals and the carbon quantum dots are analogous to that of a bicomponent catalyst (e.g. PtRu). The synthesis of carbon quantum dots derived from Vulcan XC-72 carbon black first involved mixed acid etching. The soaking of carbon black (Vulcan XC-72) in a solution of carbon quantum dots is then followed that occurs for several days (1, 3, 5, and 7 days) in order to generate carbon quantum dots-modified carbon black (XC-72-CQDs). Different XC-72-CQDs supports were produced, depending on the soaking days, and they were XC-72-CQDs1, XC-72-CQDs3, XC-72-CQDs5, and XC-72-CQDs7. The synthesis method is then concluded with a simple chemical reduction method to place Pt catalysts onto the XC-72-CQDs supports. The performance of the resultant Pt/XC-72-CQDs catalysts toward MOR was also evaluated using CV, where XC-72-CQDs were found to be far superior than the commercial PtRu/C (30% Pt + 15% Ru) catalyst. From the analysis, Pt/XC-72-CQDs5 catalyst exhibited a high specific activity value of $1.06 \text{ mA cm}^{-2}_{\text{Pt}}$ as well as a mass activity of $477.6 \text{ mA mg}^{-1}_{\text{Pt}}$. These activity values surpass those that are found for commercial PtRu/C (specific activity of $0.77 \text{ mA cm}^{-2}_{\text{Pt}}$ and mass activity of $280.6 \text{ mA mg}^{-1}_{\text{Pt}}$). Another factor to note that contributed to the improvement of catalytic performance was that CQDs can help enhance the oxidation of chemisorbed CO to CO₂ by providing a swift pathway for the activation of water.^[255]

In addition to the results noted above, many other groups designed other carbon-supported catalysts that displayed enhancement in electrochemical performance which was highly dependent on the unique hierarchical structures. Most of the relevant catalysts reported in the last 4 years are presented in the following [Table 1](#). The listed parameters are

Table 1. List of Various Carbon-based Electrocatalyst and its Electrocatalytic Properties Toward MOR.

Catalysts	Method	Particle size (nm)	Mass activity/current density	ECSA	Medium	Ref
Ni/C-30	Microwave irradiation	6 nm	30 mA/cm ²	-	0.5 M KOH + 0.4 M CH ₃ OH	[192]
Pd/g-C ₃ N ₄ /carbon black	Two-step method	5.2 nm	1720 mA mg ⁻¹ Pd	103.5 m ² g ⁻¹ Pd	1 M NaOH + 1M CH ₃ OH	[193]
PtRu/C-TiN	Microwave-assisted polyol process (MAPP)	1.6–4 nm	0.81 A mg ⁻¹ Pt	115.6 m ² g ⁻¹ Pt	0.5 M H ₂ SO ₄ + 0.5 M CH ₃ OH	[256]
PtRu/C@g-C ₃ N ₄ NS	Microwave-assisted polyol process (MAPP)	2.2–4 nm	1.14 A mg ⁻¹ Pt	96.8 m ² g ⁻¹	0.5 M H ₂ SO ₄ + 0.5 M CH ₃ OH	[257]
Au-Pt/C	Facile and green method	22 nm	5.68 mA/cm ²	29.67 m ² g ⁻¹	1 M NaOH + 0.5 M CH ₃ OH	[258]
Pt@FVC	Ethylene glycol reduction method	3.51 nm	~20 mA/cm ²	78.6 m ² g ⁻¹	0.5 M H ₂ SO ₄ + 0.5 M CH ₃ OH	[259]
Pt/C-OT-4	Ozone Oxidation	1.5–3.5 nm	6.88 mA/cm ²	112 m ² g ⁻¹ Pt	0.5 M H ₂ SO ₄ + 1 M CH ₃ OH	[260]
PtP-NiCo ₂ P _x C	Hydrothermal+ low temperature phosphidation and NaBH ₄ reduction	2.5 nm	1361 mA mg ⁻¹ Pt	-	0.5 M H ₂ SO ₄ + 1 M CH ₃ OH	[261]
PtRu/90 C.10Mn ₃ O	Microwave-assisted polyol process in ethylene glycol	2.6 nm	215 mA mg ⁻¹ PtRu	69.5 m ² g ⁻¹ PtRu	0.5 M H ₂ SO ₄ + 1 M CH ₃ OH	[262]
Pt–Pd/g-C ₃ N ₄ /carbon black	Low-temperature heating + wet chemistry route	4.1 nm	4420 mA mg ⁻¹ metal	84.3 m ² g ⁻¹ metal	-	[263]
10Pt/Ni-MoC _y C	Microwave-assisted deposition/carbonthermal reduction method	2–7 nm	260.5 mA mg ⁻¹	68.4 m ² g ⁻¹	0.5 M H ₂ SO ₄ + 1.0 M CH ₃ OH	[264]
Ni–MnO _x /C	Microwave irradiation	4.5 nm	0.0630 A mg ⁻¹ metal	-	0.4 M methanol + 0.5 M KOH	[265]
Pd–Ni/C 1:2	NaBH ₄ reduction	2.7 ± 0.9	6.77.08 mA mg ⁻¹ metal	0.788 cm ² mg ⁻¹	0.1 M KOH + 1M CH ₃ OH	[266]
Pd-Ni/C	NaBH ₄ reduction	210–250 nm	405.3 mA mg ⁻¹	70.4 m ² g ⁻¹	1 M KOH + 1 M CH ₃ OH	[267]
Pt/C/graphene aerogel	Hydrothermal process.	2 nm	-	-	0.5 M H ₂ SO ₄ + 0.5 M CH ₃ OH	[268]
Pt nanocubes/C	one-pot synthesis	4.3 ± 0.8 nm	1.59 A mg ⁻¹	44.07 m ² g ⁻¹	0.1 M HClO ₄ + 1.0 M CH ₃ OH	[269]
PtSn(70:30)/C-PANI	Impregnation method	Particle size, 3.5–6 nm. Avg. diameter, 5.2 nm	~200 mA cm ⁻² (SA)*	ECSA _{CO} , 74.9 m ² g ⁻¹ Pt	0.5 M H ₂ SO ₄ + 1 M Methanol	[180]
Pt-Co ₃ O ₄ /CNF	Electrospinning, Hydrothermal, and Reduction methods	3–5 nm	415.6 mA mg _{pt} ⁻¹	-	0.5 M H ₂ SO ₄ + 2 M CH ₃ OH	[199]
PtRu/TECNF	Chemical reduction	5 nm	516 mA (mg ⁻¹ PtRu) ⁻¹	427 m ² (g ⁻¹ PtRu) ⁻¹	0.5 M H ₂ SO ₄ + 2 M CH ₃ OH	[200]
Ni ₃₀ Pt/CNFs	Chemical reduction	3.8 nm	10.9 mA cm ⁻²	-	0.5 M H ₂ SO ₄ + 1 M CH ₃ OH.	[201]
Pt/Co-coal-CF	Wet chemical	3.6 nm	78.5 A/g Pt	-	0.5 M H ₂ SO ₄ + 0.5 M CH ₃ OH	[202]
Pt/CNF	Coelectrospinning +reduction method	2.6 nm–4.9	524.09 mA/mgPt	-	0.5 M H ₂ SO ₄ + 2 M CH ₃ OH	[270]
NiO/N-CNF	Chemical precipitation	7–8 nm	1.8 A mg ⁻¹	-	6 M KOH + 1M CH ₃ OH	[115]
Pt-Ru/CNF	Chemical reduction	1.9 and 5.5 nm	6.16 mA·cm ⁻²	28 m ² ·g ⁻¹ Metal	0.5 M H ₂ SO ₄ + 2 M CH ₃ OH	[271]
Nb CNF-Pt	Electrospinning	NiO/N-CNF	783.34 mA mg ⁻¹	94.19 m ² g ⁻¹	0.5 M H ₂ SO ₄ + 1 M CH ₃ OH	[272]

(Continued)



Table 1. (Continued).

Catalysts	Method	Particle size (nm)	Specific/ Mass activity/current density	ECSA	Medium	Ref
Pt/RGO/CF	Liquid phase reduction	2–6 nm	~100 A g ⁻¹		0.5 M H ₂ SO ₄ + 0.5 M CH ₃ OH	[273]
SnO ₂ /NF	Atomic layer deposition	4.2 – 4.8 nm thick	575 mA mgPt ⁻¹		0.5 M H ₂ SO ₄ + 2 M CH ₃ OH	[274]
CoCr ₇ C ₃ -CNFs	electrospinning		65 mA cm ⁻²		1 M KOH +3 M CH ₃ OH	[275]
PdAuCu/rGO-CNT	Electrochemical method	30 nm	1046.72 mA mgPt ⁻¹	155.52 m ² g ⁻¹ Pd	1.0 M KOH + 1.0 M CH ₃ OH	[276]
Pd/NiRGO@NCNTs	One-step electrodeposition	2 nm	95.9 A g ⁻¹	2.75 m ² g ⁻¹	1.0 M KOH + 1.0 M CH ₃ OH	[277]
Pt/CNT/TiO ₂	Sonochemical	2.98 ± 0.28 nm		40 m ² g ⁻¹	0.5 M H ₂ SO ₄ + 0.5 M CH ₃ OH	[278]
Pt/MWCNTs	Microwave-assisted polyol method	2.8 nm	1215 A g ⁻¹	82.8 m ² g ⁻¹	0.5 M H ₂ SO ₄ + 0.5 M CH ₃ OH	[279]
Pt/PIn-MWCNT	In-situ chemical polymerization	3 nm	1013.5 mA mgPt ⁻¹	63.6 m ² g ⁻¹	0.5 M H ₂ SO ₄ + 0.5 M CH ₃ OH	[280]
Pt50%-Ru50%/SWCNT	Chemical reduction method		910 mA cm ⁻²		0.5 M H ₂ SO ₄ + 0.5 M CH ₃ OH	[281]
MWNT/2OH-PBI/Pt	Reduction	2–6 nm	~ 1 A mgPt ⁻¹	47.2 m ² gPt ⁻¹	0.1 M HClO ₄ + 1 M CH ₃ OH	[282]
Pd NFs/ PPy@MWCNT	Electrochemical approach		725 mA mg ⁻¹	1.75 cm ²	1.0 M KOH + 1.0 M CH ₃ OH	[283]
Pt/N-GNR	Hydrothermal selfassembly, freeze-drying, and thermal annealing	1 – 6 nm	111.0 mAcm ⁻²	64.6 m ² g ⁻¹	1 M H ₂ SO ₄ + 2 M CH ₃ OH	[284]
Pt ₇ Fe ₃ /CNT	Coordination complex synthesis	< 4 nm	37.6 mA/cm ²		0.5 M H ₂ SO ₄ + 1 M CH ₃ OH	[285]
Pt-Co-P/CNT	Hypophosphite-assisted one-pot reduction strategy	1.5–2.7 nm	5353 mA mgPt ⁻¹	86.6 m ² gPt ⁻¹	0.5 M H ₂ SO ₄ + 0.5 M CH ₃ OH	[286]
Pd-La ₂ O ₃ /CS-aCNTs	Alkali treatment	Avg. size, 3.393 nm	~0.0025 A cm ⁻² (SA)*	-	1 M KOH + 1 M Methanol	[222]
Ni ₃ Co ₇ C-N/CNT	Direct pyrolysis	100 to 210 nm	212 mA mg ⁻¹		1.0 M NaOH + 1.0 M CH ₃ OH	[287]
Pt/C/TiO ₂	Plasma sputtering	2 nm	315.2 mA mgPt ⁻¹	266 cm ² mgPt ⁻¹	0.5 M H ₂ SO ₄ + 1 M CH ₃ OH	[288]
3D Pt-WN/CNT-rGO	Assembly route	3 nm	702.4 mA·mgPt ⁻¹	85.21 m ² ·gPt ⁻¹	1 M H ₂ SO ₄ + 1 M CH ₃ OH	[289]
MWCNTs@SnO ₂ @Pt	Reduction approach	~ 3 nm	1701.6 A gPt ⁻¹	97.3 m ² ·gPt ⁻¹	0.5 M H ₂ SO ₄ + 0.5 M CH ₃ OH	[290]
Pt/AVCNTs/CFP	Chemical oxidation,microwave irradiation	3–5 nm	660 mA/(cm ² mg)	171.3 m ² /g	0.5 M H ₂ SO ₄ + 1 M CH ₃ OH	[291]
PtCu/3D N-G	Hydrothermal microwave-assisted polyol process	5 ± 0.5 nm	741.2 mA mg ⁻¹ Pt	47.8 m ² g ⁻¹	0.5 M H ₂ SO ₄ + 1 M CH ₃ OH	[292]
Pt-CoOx/MWCNTs.	NaBH ₄ reduction	2 nm	854.7 mA mg ⁻¹ Pt	52.9 mPt ² gPt ⁻¹	0.5 M H ₂ SO ₄ + 1 M CH ₃ OH	[293]
Pt/Ni(OH) ₂ /rGO-4	Hydrothermal	~2-4 nm	0.42 A mg ⁻¹	46.5 m ² g ⁻¹	0.5 M H ₂ SO ₄ + 0.5 M CH ₃ OH	[294]
PtPd/rGO-CNTs	Heat treatment	7–9 nm	~1100 mA mg ⁻¹ Pt	40.10 m ² g ⁻¹	0.1 M HClO ₄ + 1 M CH ₃ OH	[295]
Pt/Ni(OH) ₂ /rGO-4	Two-step method	2 nm	1,236 mA mg ⁻¹ Pt	64.1 m ² g ⁻¹	1.0 M KOH + 1.0 M CH ₃ OH	[296]
Pd-Au-Ag/RGO	Green procedure	4.29 nm	968.9 mA mg ⁻¹ Pd	96.71 m ² g ⁻¹	1.0 M KOH + 1.0 M CH ₃ OH	[297]
Pd Co/NG	Solvothermal method	10 nm	21.33 mA cm ⁻²	44.2 m ² g ⁻¹	1.0 M KOH + 1.0 M CH ₃ OH	[298]

(Continued)

Table 1. (Continued).

Catalysts	Method	Particle size (nm)	Specific/ Mass activity/current density	ECSA	Medium	Ref
PtV ANNs/MWCNT	DES-assisted strategy	~3.8 nm	711.1 mA mg ⁻¹ Pt	46.6 m ² g ⁻¹ Pt	0.5 M H ₂ SO ₄ + 0.5 M CH ₃ OH	[299]
Ni/NiO/MWCNT	Combustion	20–30 nm	49.81 mA mg ⁻¹	–	0.1 M KOH + 0.7 M CH ₃ OH	[300]
Pd ₇₂ Cu ₁₄ Co ₁₄ /RGO	NaBH ₄ reduction	3.7 ± 0.4	~1100 mA mg ⁻¹ Pd	47.1 m ² g ⁻¹	1.0 M KOH + 1.0 M CH ₃ OH	[301]
Pt/rGOAMs	Electrospraying, freeze-casting, and solvothermal	4.72 nm	1098.9 mA mg ⁻¹	44.74 m ² g ⁻¹	0.5 M H ₂ SO ₄ + 1 M CH ₃ OH	[302]
Pt–Pd@ PANI–CSA	Electrochemical deposition	10–30 nm	79.2 mA cm ⁻²	59.46 m ² /g	0.5 M KOH + 1.0 M CH ₃ OH	[303]
Pt/e-RGO-SWCN	Electrodeposition	100 nm	191.71 mA mg ⁻¹ Pt	13.31 m ² g ⁻¹	0.5 M H ₂ SO ₄ + 1 M CH ₃ OH	[304]
(0.6)			1.45 mA cm ⁻²	–		
Ni@3DHPG	Ion exchange/activation method	31.7–103.3 nm	47.108 mA cm ⁻²	–	0.2 M KOH + 1.0 M CH ₃ OH	[305]
Pd/N–P-G	Chemical reduction method	~ 4.59 nm	108.6 mA cm ⁻²	133.5 m ² g ⁻¹	1.0 M KOH + 1.0 M CH ₃ OH	[306]
Pt/SPG	Thermally annealing procedure	2.16 nm	1597 mA mg ⁻¹ Pd	70.21 m ² g ⁻¹	0.5 M H ₂ SO ₄ + 0.5 M CH ₃ OH	[307]
			1.61 mA cm ⁻²	–		
Pd ₁ Pt ₂ NPs/S–NS–GR	Electrodeposition method	20–90 nm	1127 mA mg ⁻¹ Pt	467.72 m ² g ⁻¹	1.0 M NaOH + 0.5 M CH ₃ OH	[308]
			35.13 mA cm ⁻²	–		
			1821.4 mA mg ⁻¹ Pt	–		

known to be the primary factors governing the overall catalytic activity in methanol oxidation reaction, in addition they also give an idea about the active sites and chemical kinetics of the reaction.

4.3.3. Mesoporous silicas

In terms of noncarbon support materials, mesoporous silica nanoparticles (MSNs) are commonly used as inorganic supports for various applications.^[309] Examples of MSNs include Santa Barbara Amorphous 16 (SBA-16), synthesized in acidic media, and Mobil Crystalline Material (MCM-41), synthesized in alkaline media.^[310]

4.3.3.1. SBA-16. SBA-16 possess the most suitable properties to act as a support such as three-dimensional large pores, good thermal stability owing to its thick wall, and normally based on a synthesis method that is economical using cheap silica sources.^[311] Its ideal structure is made up of a spherical body-centered nanocages with cubic arrangement where each sphere is linked to eight other spheres via smaller pore apertures.^[312] Furthermore, its synthesis involves triblock copolymer surfactants Pluronic F127 in acidic medium.^[313] Recently, the preparation of SBA-16 mesostructure of controlled shape and morphology is reported to utilize cetrimonium bromide (CTAB) as a cotemplate.^[314,315] Hydrothermal synthesis of SBA-16 in presence of an acidic medium have also been performed by Azizi's team that employed a gel of SiO/F127/BuOH/HCl/H₂O.^[311] Dispersion in a 0.1 M nickel chloride solution is used to load nickel (II) to produce Ni/SBA-16, which is then further modified into a final Ni/SBA-16CPE catalyst through mixing with carbon paste. The large pore number and increased porosity of SBA-16 in the final structure provides a large surface area of active sites for Ni²⁺ ion, conversion to NiOOH that results in a high activity for MOR. In addition, experiments performed on Ni/SBA-16CPE displayed an enhancement in the anodic oxidation current.

4.3.3.2. MCM-41. Another type of MSNs obtained in alkaline media is Mobil Crystalline Material (MCM-41). It is made of an arranged hexagonal system of cylindrical mesopores whose pore diameter can be adjusted and comprises of a large pore volume and surface area as well as a sharp distribution of pore size.^[316] Its use was undertaken by Hassan's research team whose work covered the preparation of Ni-MCM-41 with 5 wt% nickel through an impregnation technique.^[317] The synthesized catalyst was then mixed with conducting carbon black in a suitable ratio in various NaOH concentrations. Experimental evaluations displayed an increasing current density in Ni-MCM-41 catalyst with an increase in NaOH concentration. CV results signified that MOR begins at a potential of approximately +500 mV (MMO reference electrode), that is accompanied by NiOOH formation. Besides, this

value is the maximum value at the peak potential in the anodic direction. From the result it can be deduced that manipulating Ni-MCM-41 catalysts via Ni^{2+} solution immersion helps improve the catalysis for MOR that is much better than the unmodified electrode. The presence of channels and pores in MCM-41 as well as the large surface area it provides facilitate in enhancing the efficiency of oxidation and the electrolytic diffusion in the electrode.^[317] It should also be known that MCM-41 is also capable of creating an anti-poisoning effect when it is used as a support for nickel.

Summary: Catalyst supports are used to upgrade the properties of the final material, particularly stability and conductivity, under the operational conditions. Properties such as good electrical conductivity can improve electron transfer while large surface area and strong interaction can help attain a wider dispersion and stability, respectively. It is necessary to employ materials that are capable of maintaining stability of the composite to endure the extreme electrochemical environment. Conductive polymer supports such as polyaniline (PAni), for example, could improve catalytic performance by introducing enhanced ion diffusion, greater electrochemical surface area, and high electrical conductivity. Using PAni as a support for PtSn also offers advantages such as reduced methanol crossover and carbon monoxide resistivity. Another conductive polymer support, known as polypyrrole (PPy), could be used to support multiwalled carbon nanotubes and enhance the catalysts overall stability and activity for MOR.

Carbon-based supports such as carbon black have been used as a promising material for nanoparticles possessing controllable shape and size. Functionalizing carbon black with HNO_3 has shown to increase the power density as a result of oxygenated group being present in carbon black. Mixing carbon black with Sn-doped TiO_2 and using them as a support for Pt has also been reported to improve the overall ECSA as a result of the formation of special triple junction. The interaction between metal and support could also be enhanced because of the high content of OH group present on the support. Carbon nanofiber is also another carbon-based support that could be combined with TiO_2 to as a support for metal alloy of PtRu. The mass activity of the resulting catalyst was observed to be four times than that of a PtRu/C, with a twofold power delivery than that of PtRu/C possibly due to improved fine interaction between the support and the metal. Support containing cobalt embedded on coal-based carbon nanofiber could also promote excellent electrochemical performance. A fine dispersion of platinum is seen on highly graphitized carbon nanofiber because of the presence of more nucleation sites that further results in uniform platinum deposition. In addition, a significant improvement in mass activity compared to Pt/CF, Pt/Co-CF, and Pt/coal-CF were reported. Utilizing mesoporous carbon with large pore

size diameter and specific surface area as a support for platinum could positively influence the activity and durability of the whole catalyst. Comparatively better performance than that of Pt/Vulcan carbon XC-72 is observed due to better Pt(0) nanoparticles' dispersion as well as supportive effect. Ordered mesoporous carbon, when doped with nitrogen, creates a strong interaction between the support and the deposited Pt metal.

The synthesis of nano-hybrid catalysts of carbon nanotubes combined with Pt and CeO₂ could have a number of advantages, with the possibility of minimizing Pt nanoparticle aggregation and eliminating poisoning by the adsorbed carbon monoxide that is achieved by the donation of OH bond from the CeO₂-OH for the oxidation of CO-like species at low potential. Multiwalled carbon nanotube can be easily functionalized by carboxyl groups when used to support palladium. This assists in effectively distributing the palladium nanoparticles by anchoring them to the carbon nanotubes that further leads to high current density for MOR. The COOH group could also improve the value of mass current by two times the value obtained for Pd-MWCNT. Doping carbon nanotubes with nitrogen can help attain effective dispersion of metals such as platinum. This is because high nitrogen content can serve as an environment for better distribution and anchoring of nanoparticles. Graphene is another carbon-based support that is useful in obtaining structural flexibility, chemical stability, good electrical conductivity, and poison resistivity. Doping graphene with either nitrogen or boron can enable the adjustment of particle size and finely disperse the loaded materials for improved MOR performance. In addition, the benefit of doping with nitrogen can promote enhanced electrical conductivity that is achieved through a partial structure recovery and introduces more efficient anchor sites for better metal dispersion over the support. Using nitrogen-doped graphene frameworks for supporting platinum could lead to a remarkable enhancement in stability and activity compared to Pt/G. Although graphene could offer several advantages as a support, there are issues that may arise such as difficulty in depositing metals on its surfaces due to its inert nature and insolubility in organic and aqueous solvents.

In terms of noncarbon support materials, mesoporous silica has been used as an alternative support. SBA-16 loaded with nickel (II) and modified by mixing with carbon paste could produce a catalyst with large exposed surfaces and increased porosity. These characteristics introduce a wide and active surface for Ni²⁺ ion conversion to NiOOH to achieve improved activity for MOR. MCM-41, another noncarbon support material combined with nickel could be modified through an immersion in Ni²⁺ solution to enable the improvement of catalysis for MOR. Furthermore, enhanced electrolytic diffusion in the electrode and oxidation efficiency could be obtained due to the large surface area and channels and pores provided by MCM-41. Using MCM-

41 as a nickel support could also help build an anti-poisoning effect necessary for better electrocatalytic performance.

4.4. Synthesis method

To optimize the performance of electrocatalysts for MOR in fuel cells, consideration of the preparation method is vital as it dictates the final surface morphology, particle size, electrocatalytic activity, and composition of the catalyst that can influence the performance of fuel cells.^[318–321] Synthesis methods such as codeposition, electrodeposition, hydrothermal, template, microwave, and impregnation methods are some of the techniques already implemented in the past with each offering different performance levels to catalysts for MOR. This section will discuss the findings of various contemporary researches on MOR electrocatalysts that specifically focus on the effects of different synthesis methods or conditions on the performance of the resulting catalyst products.

Catalysts that are nickel-alloyed or that are purely nickel-based can be prepared by various methods which include codeposition and electrodeposition. These two methods allow the production of thin films on materials such as glassy carbon, polymers, and graphite.^[168,322–328] Techniques also exist that do not rely on solutions in their procedure such as spray pyrolysis^[111] and decomposition of precursors at high temperature.^[329]

4.4.1. Aqueous-phase precipitation method

Simple methods that involve few steps are generally preferable. The aqueous-phase precipitation technique (NaOH- or NH₄OH-induced) is one of the most simplified and frequently used with soluble nickel salts. With this method a variety of nickel-based catalysts possessing different physical properties have been reported.^[329–333] Spinner *et al* have earlier performed a study to observe the performance and physical characteristics of nickel oxide catalysts, produced through different aqueous-phase synthesis techniques, for alkaline media MOR.^[334] Amongst the synthesized catalysts, reflux precipitated reflux-NiO and reflux-Ni(OH)₂ were formed under reflux involving Ni(NO₃)₂·6H₂O and NH₄OH. On the other hand, nickel oxide powders and nickel hydroxide precursors were also prepared via NaOH-induced precipitation at the solution boiling point (~102 °C) and room temperature (~20 °C) that incorporated NaOH pellets and also Ni(NO₃)₂·6H₂O. Hence, through NaOH-induced precipitation four types of catalysts were formed and they were, for simplification, designated as RT-NaOH-NiO and RT-NaOH-Ni(OH)₂ (for room temperature prepared) and BT-NaOH-NiO and BT-NaOH-Ni(OH)₂ (for boiling temperature prepared). The electrolyte for electrocatalytic performance evaluations consisted of either potassium hydroxide or sodium carbonate solution. When

NaOH-precipitated NiO and Ni(OH)₂ synthesized at both room and boiling temperature were analytically compared in CV and EIS (electrochemical impedance spectroscopy) no significant differences in values were observed. However, reflux-precipitated NiO and Ni(OH)₂ demonstrated weaker stability and poor electrocatalytic activity in comparison to RT NaOH-NiO and NaOH-Ni(OH)₂ due to their morphological differences. Between the two room temperature-prepared NaOH-precipitated catalysts, the one comprised of NiO proved to exhibit better electrochemical activity and durability.

The average current density determined in sodium carbonate based electrolyte were relatively greater than in sodium hydroxide electrolyte by about three to four times within the same alkalinity (11.5 pH).^[334] Furthermore, data records from EIS displayed that the charge transfer resistance in carbonate was about 85% lower than that for hydroxide.^[334] Degradation of catalysts can also occur in sodium hydroxide solution due to high pH that can be prevented in the moderate alkalinity of carbonate medium. From this comparison, it can be assumed that electrocatalysis in carbonate electrolyte may be comparatively advantageous than in hydroxide solution to perform MOR.

Synthesis of catalyst particles with nano-sized and well-dispersed characteristics has also been attempted as a means to improve the activity of MOR electrocatalysts. Examples of methods usually employed to obtain well-dispersed nanoparticles include thermal decomposition,^[335,336] electrochemical synthesis,^[337] chemical reduction,^[338–340] vapor deposition,^[341] and the impregnation method.^[342,343] Amongst these techniques, the impregnation method is widely used due to the simple procedures involved.

4.4.2. Impregnation method

Scibio and coworkers implemented impregnation method to synthesize a catalyst for MOR in H₂SO₄ consisting of 40 wt% platinum and 9 wt% CeO₂, which showed better stability and activity than an unmodified Pt/C catalyst.^[344] *Microwave Irradiation Method:* Microwave irradiation method, also known as microwave irradiation, relies on microwave sintering technique that offers fast reaction, high efficiency, uniform heating, and clean energy. Pt/WO₃-C catalysts have been reported to be synthesized by Ye *et al* involving the preparation of WO₃-C hybrid materials via intermittently microwave-pyrolysis and deposition of platinum NPs on WO₃-C by microwave-assisted polyol process.^[345] The resulting catalyst was then calcined at 200 °C and was found to be highly active for carbon monoxide oxidation at a lower potential value by 60 mV in comparison to Pt/WO₃-C and Pt/C that had not been microwave heat-treated.

Amin's group studied the effects of generating Pt-NiO/C electrocatalysts via the microwave and impregnation method for performance comparison on MOR.^[346] The synthesis procedure included supporting NiO on Vulcan XC-

72 R carbon black using the precipitation method and chemically reducing Pt precursor salt with NaBH_4 following microwave heating or simple impregnation without microwave heating. The current density on Pt-NiO/C catalyst with microwave technique showed threefold increase than that produced with impregnation method. However, there was a positive shift in potential by 53 mV relative to the low-performing catalyst. In another study, Amin *et al* utilized copper oxide in place of nickel oxide to observe the effects of synthesis using microwave irradiation and impregnation methods.^[347] Characterization using TEM identified a homogenous distribution of smaller size catalyst particles when microwave method was applied. CV and chronoamperometry analysis were included in the study to investigate the catalysts' oxidation of methanol in an acidic medium (0.5 M H_2SO_4). Based on the test results generated, Pt-CuO/C electrocatalyst from the microwave method displayed an oxidation current density that was double the value of the catalyst synthesized through the impregnation method. Still comparing with the catalyst from the impregnation technique, there was also a negative shift in the potential of the first and second oxidation peak, by 69 mV and 36 mV, respectively, for the catalysts prepared by the microwave irradiation technique. In addition, chronoamperometry analysis of the catalyst produced using the same microwave method provided a proof that the catalyst was capable of withstanding surface poisoning during MOR as it showed a slow fall in current density after 4800 seconds operation. A list of various catalysts discussed above and their corresponding electrochemical performance are summarized in Table 2.

5. Challenges and outlook

Recent progress in DMFCs so far has been targeted toward the search for an efficient catalyst and optimum operating condition to allow them to be used as a reliable alternative source of energy in future. Attention has been given toward the synthesis of an appropriate catalyst as it plays an important role in governing necessary outcomes that include activity, efficiency, stability, and especially the cost. With the appropriate catalyst the kinetics of anodic reactions can be enhanced that will further assist in obtaining the optimum condition for DMFC operations.^[6] A slow reaction kinetics is one of the critical challenges being faced with the use of fuel cells that reduces the reaction rate and consequently a higher catalyst loading is commonly used for Micro-DMFC operating with platinum-based catalyst to counter against the reduction in kinetics for MOR. However, as the catalyst loading increases, problems related to methanol crossover to the cathode section of the cell starts to disappear. However, due to the expensive cost of electrocatalysts based on platinum, a high loading is unfavorable acting as a barrier for micro-DMFC commercialization.



Table 2. Lists of Various Catalysts and their Performance and Property Data.

Catalyst	Synthesis Method	Particle Size	Specific/Mass Activity (SA/MA)	ECSA	Electrolyte	Ref
Mesoporous Pt nanospheres	Controlled chemical reduction reaction (with Pluronic F127 surfactant)	Avg. size, ~70 nm	1.1 mA cm ⁻² (SA)	25.1 m ² g ⁻¹ Pt	0.5 M H ₂ SO ₄ + 0.5 M Methanol	[12]
Dendritic Pt nanoparticles	-	-	0.95 mA cm ⁻² (SA)	17.1 m ² g ⁻¹ Pt	0.5 M H ₂ SO ₄ + 0.5 M Methanol	[12]
Ru-Pt (0.51 monodisperse Ru surface coverage)	Electroless deposition	Avg. size, ~5.16 nm	~720 A g ⁻¹ Pt (MA)*	-	0.5 M H ₂ SO ₄ + 1 M Methanol	[63]
PtRu nanodendrites	Coreduction of Pt and Ru in oleylamine by H ₂	Avg. diameter size, ~21 nm	2.7 mA cm ⁻² (SA), 1.08 mA μg ⁻¹ Pt (MA)	40 m ² g ⁻¹	0.1 M HClO ₄ + 1 M Methanol	[64]
PtRu nanocrystals	-	-	2.1 mA cm ⁻² (SA), 0.61 mA μg ⁻¹ Pt (MA)	29 m ² g ⁻¹	0.1 M HClO ₄ + 1 M Methanol	[64]
Pt nanocrystals	-	-	1 mA cm ⁻² (SA), 0.16 mA μg ⁻¹ Pt (MA)	16 m ² g ⁻¹	0.1 M HClO ₄ + 1 M Methanol	[64]
Pt@GO-PVP nanoparticles	One-pot approach, graphene oxide (modified Hummers method)	Avg. size, ~3.81 nm	43 mA cm ⁻² (SA)	59.82 m ² g ⁻¹	0.5 M H ₂ SO ₄ + 0.5 M Methanol	[61]
Pt@GO nanoparticles	One-pot approach	Avg. size, ~3.76 nm	~14 mA cm ⁻² (SA)*	37.23 m ² g ⁻¹	0.5 M H ₂ SO ₄ + 0.5 M Methanol	[61]
Pt@PVP nanoparticles	One-pot approach	Avg. size, ~3.59 nm	~29 mA cm ⁻² (SA)*	43.67 m ² g ⁻¹	0.5 M H ₂ SO ₄ + 0.5 M Methanol	[61]
Rh nanodendrites (with nanosheet subunits)	Diethylene glycol reduction (with polyethyleneimine surfactant)	Avg. size, ~100 nm	255.6 A g ⁻¹ (MA)	43.35 m ² g ⁻¹	1 M KOH + 1 M Methanol	[86]
Rh nanoaggregates	Diethylene glycol reduction (without polyethyleneimine surfactant)	-	27.5 A g ⁻¹ (MA)	23.09 m ² g ⁻¹	1 M KOH + 1 M Methanol	[86]
Ultrathin wavy Rh nanowires	-	Diameter, 2–3 nm. Length, >200 nm	722 mA mg ⁻¹ (MA)	144.2 m ² g ⁻¹ CO _r 105.3 m ² g ⁻¹ H ₂ upd	1 M KOH + 1 M Methanol	[87]
Rh nanosheets/RGO	One-pot hydrothermal synthesis (with polyethyleneimine surfactant)	Thickness of Rh NS on RGO, ~3 nm	264 A g ⁻¹ Rh (MA)	48.66 m ² g ⁻¹ Rh	1 M KOH + 1 M Methanol	[90]
Rh nanoparticles/RGO	One-pot hydrothermal synthesis (without polyethyleneimine surfactant)	-	171 A g ⁻¹ Rh (MA)	40.09 m ² g ⁻¹ Rh	1 M KOH + 1 M Methanol	[90]
Nanoporous Pd rods	Al ₁₀₀ Pd ₂₀ alloy dealloying in 5 wt% HCl (free corrosion conditions)	Length of ligaments/channels, 15–20 nm	223.52 mA mg ⁻¹ (MA) (with 0.4 mg cm ⁻² metal loading)	-	1 M KOH + 0.5 M Methanol	[96]
Pd-Mn ₃ O ₄ /MWCNTs	Wet impregnation (with NaBH ₄ reducing agent)	Avg. Pd NPs size, ~3.4 nm	715.8 mA mg ⁻¹ Pd (MA)	76.19 m ² g ⁻¹ CO	0.5 M NaOH + 1 M Methanol	[97]
Pd/MWCNTs	Wet impregnation (with NaBH ₄ reducing agent)	Avg. Pd NPs size, ~6.2 nm	332.4 mA mg ⁻¹ Pd (MA)	28.57 m ² g ⁻¹ CO	0.5 M NaOH + 1 M Methanol	[97]

(Continued)

Table 2. (Continued).

Catalyst	Synthesis Method	Particle Size	Specific/Mass Activity (SA/MA)	ECSA	Electrolyte	Ref
Pd/NS-G	Thermal treatment and solvothermal approach	Avg. size, 4.6 nm	11.3 mA cm ⁻² (SA), 399.3 mA mg ⁻¹ (MA)	103.6 m ² g ⁻¹	0.5 M NaOH + 1 M Methanol	[100]
Microspherical NiO/Ni-P composites (EP-M)	Sponge-template method	-	28.56 mA cm ⁻² (SA), 467 A g ⁻¹ (MA)	210.03 m ² g ⁻¹	0.5 M KOH + 1 M Methanol	[113]
Nanoflake NiO/Ni-P composites (EP-F)	Sponge-template method	-	~300 A g ⁻¹ (MA)	106.5 m ² g ⁻¹	0.5 M KOH + 1 M Methanol	[113]
NiO/N-CNFs	Electrospinning, chemical precipitation	N-CNFs avg. diameter, 250 nm, NiO particle size, 7–8 nm	0.3 A cm ⁻² (SA), 1.8 A mg ⁻¹ (MA)	BET SA 31.85 m ² g ⁻¹	6 M KOH + 1 M Methanol	[115]
Ni/Al ₂ O ₃ -2/GC (Al/Ni molar ratio of 2)	Solvent evaporation induced self-assembly (EISA)	Mesopore diameters, 7.7 nm	7.3 mA cm ⁻² (SA)	BET SA 237 m ² g ⁻¹	0.1 M NaOH + 0.1 M Methanol	[118]
Ni/Al ₂ O ₃ -5/GC (Al/Ni molar ratio of 5)	Solvent evaporation induced self-assembly (EISA)	Mesopore diameters, 6.2 nm	11.1 mA cm ⁻² (SA)	BET SA 290 m ² g ⁻¹	0.1 M NaOH + 0.1 M Methanol	[118]
Ni/Al ₂ O ₃ -10/GC (Al/Ni molar ratio of 10)	Solvent evaporation induced self-assembly (EISA)	Mesopore diameters, 6.9 nm	4.2 mA cm ⁻² (SA)	BET SA 304 m ² g ⁻¹	0.1 M NaOH + 0.1 M Methanol	[118]
Ni/SPANi	Ni NPs deposition on matrix by reducing precursor NiCl ₂ ·6H ₂ O (with NaBH ₄ at 80 °C)	Crystallite size, 6.1 nm	306 μA cm ⁻² (SA), 6.1 mA g ⁻¹ (MA)	-	0.05 M H ₂ SO ₄ + 2 M Methanol	[116]
Ni/PAIni	Ni NPs deposition on matrix by reducing precursor NiCl ₂ ·6H ₂ O (with NaBH ₄ at 80 °C)	Crystallite size, 8.6 nm	220.8 μA cm ⁻² (SA), 4.49 mA g ⁻¹ (MA)	-	0.05 M H ₂ SO ₄ + 2 M Methanol	[116]
Co/N(4%) -CNFs	Electrospinning	~23 nm	100.84 mA cm ⁻² (SA)	-	1 M KOH + 3 M Methanol	[122]
Co/undoped-CNFs	Electrospinning	~37 nm	63.56 mA cm ⁻² (SA)	-	1 M KOH + 3 M Methanol	[122]
rGO-Co ₃ O ₄ nanocubes (2 wt% GO content)	Hydrothermal method, Hummer's method	-	362 μA cm ⁻² (SA)	-	0.1 M KOH + 0.1 M Methanol	[123]
N-Co ₃ O ₄ @C-NRP mesoarchitected	Core shell-mediated hydrothermal treatment	-	~122 mA cm ⁻² (SA)*	SSA 82.5 m ² g ⁻¹	0.5 M NaOH + 1.5 M Methanol	[124]
N-Co ₃ O ₄ @C-X-NS mesoarchitected	Core shell-mediated hydrothermal treatment	-	~105 mA cm ⁻² (SA)*	SSA 65.1 m ² g ⁻¹	0.5 M NaOH + 1.5 M Methanol	[124]
N-Co ₃ O ₄ @C-NN mesoarchitected	Core shell-mediated hydrothermal treatment	-	~88 mA cm ⁻² (SA)*	SSA 54.7 m ² g ⁻¹	0.5 M NaOH + 1.5 M Methanol	[124]
GC/Ni-CO	Using deposition bathes with NiSO ₄ ·7H ₂ O and CoSO ₄ ·8H ₂ O	-	2.3 mA cm ⁻² (SA)	-	0.1 NaOH + 0.1 M Methanol	[125]

(Continued)

Table 2. (Continued).

Catalyst	Synthesis Method	Particle Size	Specific/Mass Activity (SA/MA)	ECSA	Electrolyte	Ref
Coral-like NiCo ₂ O ₄ with hierarchical pores	One-pot additive-free solvent thermal decomposition + postcalcination treatment	Pore size, 0–5 nm and 10–40 nm	21 mA cm ⁻² (SA)	BET SA 11.453 m ² g ⁻¹	1 M KOH + 0.5 M Methanol	[126]
Ni-Co hydroxides (100% Ni/(Ni+Co))	Electrochemical deposition on stainless steel mesh (SSM)	-	~200 A g ⁻¹ (MA)	-	1 M KOH + 0.5 M Methanol	[127]
Ni-Co oxides (4g/54 Ni/Co ratio)	Heat treatment on Ni-CO hydroxides	~3.8 nm	~275 A g ⁻¹ (MA)	-	1 M KOH + 0.5 M Methanol	[127]
Microsphere-Co ₃ O ₄ on Ni foam	Hydrothermal method + calcination	5.1 and 19 nm	36.2 A g ⁻¹ (MA)	BET SA 100 m ² g ⁻¹	1 M KOH + 0.5 M Methanol	[128]
Nanogras- Co ₃ O ₄ on Ni foam	Hydrothermal method + calcination	8.3, 22.3, and 53.1 nm	34.9 A g ⁻¹ (MA)	BET SA 65 m ² g ⁻¹	1 M KOH + 0.5 M Methanol	[128]
Microflower- Co ₃ O ₄ on Ni foam	Hydrothermal method + calcination	3.6 and 8.2 nm	28 A g ⁻¹ (MA)	BET SA 53 m ² g ⁻¹	1 M KOH + 0.5 M Methanol	[128]
NiCo ₂ O ₄ nanosheet (Nickel foam supported)	Mild hydrothermal method	9 nm	111 mA cm ⁻² (SA)	SSA 54.2 m ² g ⁻¹	1 M KOH + 0.5 M Methanol	[129]
NiCo ₂ O ₄ nanocloth (Nickel foam supported)	Mild hydrothermal method	~2.2 nm and ~9.1 nm	134 mA cm ⁻² (SA)	SSA 66.9 m ² g ⁻¹	1 M KOH + 0.5 M Methanol	[129]
Core-shell-like NiCo ₂ O ₄ /MWCNTs	Dry synthesis technique	NPs size, 6 ± 2 nm. MWCNT thickness, 48 nm	327.3 mA cm ⁻² (SA)	-	1 M KOH + 5 M Methanol	[130]
NiCoPO-2	One-pot solvothermal method	~3 μm. NW diameter, ~4 nm. NW length, 300 nm	~1567 A g ⁻¹ (MA)	SSA 540.5 m ² g ⁻¹	0.5 M KOH + 1 M Methanol	[131]
Co-W alloys (~30 atm. % W content)	Electrodeposition on stainless steel (type 304)	<5 nm	12.3 mA cm ⁻² (SA)	-	0.1 M H ₂ SO ₄ + 1 M Methanol	[132]
Cd-doped Cobalt NPs (enveloped in Graphite shells)	Sol-gel technique	19 nm	70 mA cm ⁻² (SA)	-	1 M KOH + 2 M Methanol	[133]
Dendritic CuPt alloy NPs (CuPt/C)	Seed-mediated approach	69.2 nm	2.16 mA cm ⁻² (SA)	16.1 m ² g ⁻¹	0.1 M HClO ₄ + 1 M Methanol	[142]
Polyhedral CuPt alloy NPs (CuPt/C)	Seed-mediated approach	27.6 nm	1.76 mA cm ⁻² (SA)	30.0 m ² g ⁻¹	0.1 M HClO ₄ + 1 M Methanol	[142]

(Continued)

Table 2. (Continued).

Catalyst	Synthesis Method	Particle Size	Specific/Mass Activity (SA/MA)	ECSA	Electrolyte	Ref
Stellated CuPt alloy NPs (CuPt/C)	Seed-mediated approach	42.4 nm	0.73 mA cm ⁻² (SA)	42.1 m ² g ⁻¹	0.1 M HClO ₄ + 1 M Methanol	[142]
Pd@CNWs	Hydrometallurgy	Pd shells thickness, 30–50 nm. CNWs avg. diameter, 100 ± 20 nm. CNWs avg. length, 35 ± 5 μm ~15 nm	~12.3 mA mg ⁻¹ Pd (MA)	-	0.1 M KOH + 1 M Methanol	[143]
Star-like PtCu/rGO	Hummers method, Copper (II) chloride dihydrate (CuCl ₂ ·2H ₂ O) as Cu precursor		~670 mA mg ⁻¹ (MA)	45.3 m ² g ⁻¹	0.5 M H ₂ SO ₄ + 1 M Methanol	[144]
Pd/CuO-TiO ₂ (A)	One-pot chemical dealloying (0.25 M HCl)	TiO ₂ needles length, 200 nm, and width, 50 nm	310 mA mg ⁻¹ Pd (MA)	12.7 m ² g ⁻¹	0.5 M NaOH + 1 M Methanol	[145]
Pd/CuO-TiO ₂ (B)	One-pot chemical dealloying (0.75 M HCl)	TiO ₂ needles length, 200 nm, and width, 50 nm	381 mA mg ⁻¹ Pd (MA)	14.4 m ² g ⁻¹	0.5 M NaOH + 1 M Methanol	[145]
Pd/CuO-TiO ₂ (C)	One-pot chemical dealloying (1.25 M HCl)	TiO ₂ needles length, 200 nm, and width, 50 nm	269 mA mg ⁻¹ Pd (MA)	15.8 m ² g ⁻¹	0.5 M NaOH + 1 M Methanol	[145]
PdCu/VrGO	Cyclic voltammetric electrodeposition of GO (with Na ₂ PdCl ₄ and Cu ethylenediamine tetraacetate)	PdCu particle size, 8.66 ± 0.27 nm	762.8 A g ⁻¹ (MA)	0.196 m ² g ⁻¹	1 M KOH + 1 M Methanol	[146]
PdCu nanoalloy (3:1 stoichiometric ratio)	Coreduction process	10–15 nm	2.05 mA cm ⁻² (SA).	40.58 m ² g ⁻¹	1 M KOH + 1 M Methanol	[147]
PtPdCu NDs	Electrodeposition, wet-chemical modification	-	778.98 mA mg ⁻¹ (MA) ~1.154 mA cm ⁻² (SA).	59.6 m ² g ⁻¹ Pt	0.5 M H ₂ SO ₄ + 1 M Methanol	[148]
Cu ₄ Pt ₃ Pd ₂	Direct reduction of metal ions (with hydrazine hydrate)	30 nm	688 mA mg ⁻¹ Pt (MA) 8.45 mA cm ⁻² (SA). 4.296 A mg ⁻¹ (MA)	88.3 m ² g ⁻¹	1 M KOH + 1 M Methanol	[149]
PtRu NTs (Pt/Ru atomic ratio 6:1)	Galvanic displacement reaction	Diameter, ~120 nm. Wall thickness, ~30 nm. Length, 6–10 μm	~0.4 mA cm ⁻² PtRu (SA). ~0.05 mA μg ⁻¹ PtRu (MA)*	9.4 ± 0.9 m ² g ⁻¹ PtRu	0.1 M HClO ₄ + 1 M Methanol	[150]
PtRu/Cu NWs (Pt/Ru atomic ratio 4:1)	Galvanic displacement reaction	Diameter, ~120 nm. Shell thickness, 10–20 nm. Length, ~10 μm	~1.6 mA cm ⁻² PtRu (SA). ~0.45 mA μg ⁻¹ PtRu (MA)*	29 ± 2.4 m ² g ⁻¹ PtRu	0.1 M HClO ₄ + 1 M Methanol	[150]

(Continued)

Table 2. (Continued).

Catalyst	Synthesis Method	Particle Size	Specific/Mass Activity (SA/MA)	ECSA	Electrolyte	Ref
Pt/3D TiN	One-pot reduction approach	Pt NPs avg. grain size, 3.4 ± 0.4 nm	~1 mA cm ⁻² (SA). 0.52 A mg ⁻¹ Pt (MA)	57.5 m ² g ⁻¹ Pt	0.1 M HClO ₄ + 0.5 M Methanol	[151]
Pt/Ti _{0.7} Cu _{0.3} N	One-pot reduction approach	Pt NPs avg. grain size, 3.3 ± 0.4 nm	1.46 mA cm ⁻² (SA). 0.84 A mg ⁻¹ Pt (MA)	60.4 m ² g ⁻¹ Pt	0.1 M HClO ₄ + 0.5 M Methanol	[151]
CuZn/Cu	Electrodeposition	-	297.14 mA cm ⁻² (SA)	-	1 M KOH + 1 M Methanol	[155]
2Cu@Co _x -CLs	Electrochemical method	Particle size on CL, ~60 nm.	150.41 mA cm ⁻² (SA). 467.94 mA mg ⁻¹ (MA)	-	1 M KOH + 1 M Methanol	[156]
NS20s (20 nm nanospheres)	Seed-mediated method and robust chemical-tethering approach	Diameter, 20 nm	11 mA mg ⁻¹ (MA)	-	0.1 M KOH + 10 M Methanol	[163]
NS45s (45 nm nanospheres)	Seed-mediated method and robust chemical-tethering approach	Diameter, 45 nm	5.59 mA mg ⁻¹ (MA)	-	0.1 M KOH + 10 M Methanol	[163]
20 nm x 63 nm nanorods	Seed-mediated method and robust chemical-tethering approach	20 x 60 nm ²	0.91 mA mg ⁻¹ (MA)	-	0.1 M KOH + 10 M Methanol	[163]
Pt (47.5 wt%)	-	Particle size, ca. 4.3 ± 3 nm	78.6 mA mg ⁻¹ Pt (at 333 K) (MA)	-	0.1 M NaOH + 0.5 M Methanol	[175]
Pt ₂ Ru ₃ (54 wt% alloy)	-	Particle size, ca. 4.3 ± 3 nm	84.1 mA mg ⁻¹ Pt (at 333 K) (MA)	-	0.1 M NaOH + 0.5 M Methanol	[175]
PtBi nanoparticles	Electrodeposition	Avg. diameter, 63 ± 20 nm	~1.4 A mg ⁻¹ (MA)*	-	1 M NaOH + 1 M Methanol	[65]

Another commonly encountered challenge is seen with the production of carbon monoxide intermediate that contributes to the degradation of catalysts and needs to be prevented or oxidized. Platinum catalysts in DMFCs, for example, are generally poisoned by such intermediate species when they are adsorbed on the platinum catalyst surface during MOR.^[348] Hence, the utilization of catalysts with great resistivity toward poisoning species such as carbon monoxide is generally desired to increase the catalytic life-cycle in fuel cells. In addition to slow kinetics and carbon monoxide poisoning there are other issues experienced in DMFCs that should be highlighted. The following paragraphs will take a closer look at the types of issues that continue to be a challenge for MOR in DMFCs.

5.1. Lifetime and durability of DMFC

With regards to a fuel cell's operational flexibility to function in wider operating conditions, it is necessary to consider the estimated and specified unexpected conditions during the cell's operating life. Various examples of these conditions are temperature and pressure during operation and of the environment, the composition and flow rate of the reactant, the required peak load and turn-down ratios, humidification levels, the necessary transient responses rate, and duty-cycle characteristics. Although not much information is available on micro-DMFCs' expected lifetime, it is generally known that operating conditions, such as temperature and fuel flow rate, can have an influence on how long cells last.^[349] Micro-DMFC products are still limited in the market, however, prototypes have been displayed by companies such as Motorola and Toshiba to outline its potential for commercialization. There is also a reliance toward the use of pure gold as layers for current collector as it is reported to be capable of achieving long performance life for DMFCs.^[350]

5.2. Assembly of membrane electrode (MEA)

Establishing a proper and effective MEA is necessary in order for a DMFC to be used as a reliable cell to generate electricity. In this section, a number of components of MEA will be examined based on findings from previous research works and they include catalyst loading, membrane thickness, and diffusion layer.

5.3. Catalyst loading

Increasing material loading on a catalyst has its advantages with one of them being a greater active surface area. However, it is practically inconvenient when a thin catalyst layer is desired. Hence, techniques such as decal method, doctor-blade method, and brushing technique cannot be relied

upon to produce a homogenous layer of catalyst on mini-cells such as micro-DMFC. In addition, systematic errors can occur during preparation and this further poses a challenge to catalyst reproduction. It is possible that performance can increase with higher loading, nevertheless there comes a point when increasing the loading will no more enhance the performance of a catalyst. The performance then may either become constant or decline consequently.^[351] Another adverse effect of excess loading is the higher mass transport resistance toward the supply of methanol to the anode as well as toward the removal of CO₂ and other products from the anode.^[352] The consequences of the effects of higher loading was researched in the past by Shimizu *et al* when they experimented with Pt-Ru catalyst (anode) and Pt catalyst (cathode).^[351] Increasing the loading of Pt/Ru and Pt catalyst beyond the optimum (2.5 mg cm⁻²) significantly reduced the performance of the cells.

5.4. Membrane thickness

An increase in membrane thickness can actually reduce the chances of methanol crossing over. However, a consequence arises from the increase in which the power density declines as a result of high ohmic loss.^[353] A study performed by Liu *et al* focused particularly on the influence of membrane thickness on a passive micro-DMFC's performance.^[354] Various series of Nafion having different thicknesses were utilized; such as Nafion 112 (50 μm thickness), 115 (125 μm thickness), and 117 (175 μm thickness). When a cell containing a low methanol concentration of 2 M was tested with the three types of membranes, it was concluded that a good performance was exhibited by the thicker membrane at low current densities. On the other hand, the thinner membrane performed better at higher current densities. Testing with higher concentration of methanol suggested a preference for thicker membranes operating with higher methanol concentration for better cell efficiency with limited methanol crossover.

Another parameter that could be affected by membrane thickness is the operating time. To test this hypothesis Nafion 115 and Nafion 117 was used for comparison and the corresponding results showed that there is an inverse proportionality between operating time and methanol consumption rate. In other words, with increased thickness of the membrane the electric load decreased that is accompanied by an increase in operating duration. Therefore, through this comparison it is evident that thicker membranes are more suitable for micro-DMFC as it does not only promote an increase in efficiency through reduced methanol crossover, but also longer operating duration.

5.5. Diffusion layer

This layer commonly exists to aid with the transfer of electrons to and from the catalyst layer. Effective diffusion of reactants to the layer of the catalyst is also achieved due to its porous characteristic. In addition, the diffusion layer allows water to reach the membrane and be held on it for hydration. Carbon materials such as carbon cloth are usually used as a gas diffusion layer. However, it is being gradually replaced by stainless steel cloth, as better performance is reported, possibly due to the higher conductivity and porous structure. Liu's group performed a study involving implementation of a gas diffusion layer made of sintered stainless steel fiber felt.^[355] Relative to carbon paper a higher performance was observed with the stainless steel-based material because of its high electrical conductivity. Using this metal can also lead to easy supply of methanol due to the possible hydrophilic characteristic of the metal fibers that are present.

5.6. Heat and water management

A passive micro-DMFC has an optimum methanol concentration of approx. 1M, which is considerably greater than that of an active cell. Two factors play a role in promoting the relatively higher concentration; one is the slow characteristic of methanol mass transport rate in a passive cell that is based on natural convection only, and another being an increase in the cell temperature because of methanol oxidation at the cathode as a result of crossover. The higher the concentration of methanol the greater will be the amount to crossover that increases the temperature of the cell and in turn the reaction kinetics at the two electrodes. In addition, out of the total energy available in a micro-DMFC, electricity is produced by only less than 30% of the energy with the remaining given off as heat.^[356] A fast removal of the generated heat is necessary as heat buildup is potentially dangerous for any portable systems.

With regards to the management of water in micro-DMFC, a number of attempts have been made in the past that usually involve wet-proofing the gas diffusion layers of cathode with a PTFE coating. This is done to ensure that pores present on the layer are not clogged with water. The design of a system that implements water recycle from the cathode to the anode have also been achieved by Yao *et al* to assist in reducing the amount of water being supplied externally.^[357] Furthermore, their system had an overall volume of 1 cm³ with up to 10 mW of net output produced (35% energy efficiency) by it. Within the compact fuel cell other features are also present that include micro-pump and passive liquid-gas separator (CO₂ removal unit) as well as layers of hydrophobic-hydrophilic coating.

5.7. Low power density issue

The ideal type of system for micro-DMFC should be a passive one (with unsteady-state operation) that requires the removal of various sections from the design, such as the air blower and fuel pump. Only a built-in fuel reservoir is necessary to supply the methanol-containing fuel to the anode, and hence an external peripheral is not required. Although this design may be simple it can lower the performance of the system as a difficulty is faced when attempting to achieve a continuous supply of fuel to the anode. The bubbles generated from CO₂ production, if not removed due to the absence of a flowing force, can cause a buildup and prevent fuel from being oxidized further at the anode. Furthermore, there is a buildup of water droplet at the cathode that can obstruct the active surface and lower the supply of oxygen.

The optimum concentration of methanol for a passive micro-DMFC was previously reported by Bae's group to be 5 M.^[358] When the concentration of methanol exceeds this value, a decline in performance can occur as a result of rising overpotential at the cathode. A higher concentration can cause a methanol crossover problem that results in a mixed potential and degenerates the neighboring cathode catalyst through poisoning. With 5 M methanol a power density of 45 mW cm⁻² could be achieved. It must also be known that DMFC applications in small or micro-size devices are restricted due to the fact that as a system becomes smaller the energy density will fall dramatically.

5.8. Methanol crossover issue

Methanol crossover results from the high concentration of methanol in the anode that diffuses to the cathode through the electrolyte membranes. These methanol molecules are then directly oxidized by oxygen present on the surface of the cathode catalyst. When there is an increase in the current density the crossover rate will decrease because methanol is being consumed at the anode at an elevated rate. Other factors such as low methanol concentration (or using diluted methanol solutions) in the feed as well as high operating temperatures can also contribute to the reduction in crossover rate. Diluting the methanol solution can, however, significantly decrease the energy density of the DMFC. Hence, the concentration of methanol should be diluted to a suitable level before it get to the anode catalyst layer to prevent severe methanol crossover. There are experiments that have shown that the optimized concentration of methanol is 1 to 2 mol/L (3 to 6 wt%) for active DMFCs and it is approximately 3 mol/L (10 wt%) for passive DMFCs.^[354,359-361] The methanol crossover phenomenon further creates a methanol concentration gradient across the membrane from the anode to the cathode. In addition to the diffusion transport

mechanism, an electro-osmotic transport mechanism also takes place as methanol gets carried by proton (via ion-dipole interaction). There are two practical repercussions from the crossover; an excessive drop in voltage at the cathode and a methanol self-discharge that generates heat. Commercially available polymer electrolyte membranes, including Nafion, are still challenged by both the issues of high electro-osmotic drag coefficient and methanol permeability.^[362] To overcome such challenges, progress has been made in developing new polymer membranes for conducting proton that are suitable for DMFCs. Examples of these polymers are polyphenylquinoxalines, polybenzimidazoles, polyetheretherketones, polyphenylene sulfides, polyether imides, polysulfone, and polyamides.^[363] However, as reported by Schaffer *et al*, these polymers still possess the disadvantage of low ionic conductivity.^[364]

Ren *et al.* performed a study related to the advancement of direct methanol fuel cells that also focused on resolving, to a large extent, the methanol crossover problem through a suitable cell design.^[365] The rate of crossover could be reduced by lowering the concentration gradient of methanol that controls the flux of methanol under steady state operating conditions. Two factors that can significantly lower methanol crossover are lowering the concentration of methanol in the feed and optimizing the cell design. The results of Ren *et al.* shown in Figure 15 illustrate together the performance of DMFC stack (current density at 0.45 V) and fuel usage ((cell current)/(cell current + crossover current)), at a temperature of 60 °C and ambient air pressure of 3 times the stoichiometric flow. Figure 15 displays that the combination of high fuel usage (more than 90%) and high cell performance (near to 0.2 A/cm² at 0.45 V) could be achieved with optimized cell structures even with implementation of rather “leaky” membrane. This also means that remarkable overall energy conversion efficiencies could be achieved in a direct methanol fuel cell, even before employing advanced membranes with way lower methanol permeability and high protonic conductivity.

It is also possible to produce hybrid membranes by combining the various polymers previously mentioned to prevent methanol crossover. For instance, combining both phosphate and zirconium have demonstrated the capability of the inorganic compound to minimize methanol permeability, with the phosphate layer causing water to permeate instead of methanol.^[366] However, utilizing inorganic metals such as tantalum and palladium in the hybrid may cause electrochemical charge transfer over potentials that leads to losses.^[364] The reason is because hydrogen ions mainly transport charges in a fuel cell and a reduction of hydrogen ions can occur on the metallic layer surface facing the anode, which could pass through the metallic layer in the atomic state. Oxidation then takes place on the metallic layer surface at the cathodic section. As a result, instead of a flow of hydrogen there is a diametric cross of an electric compensation

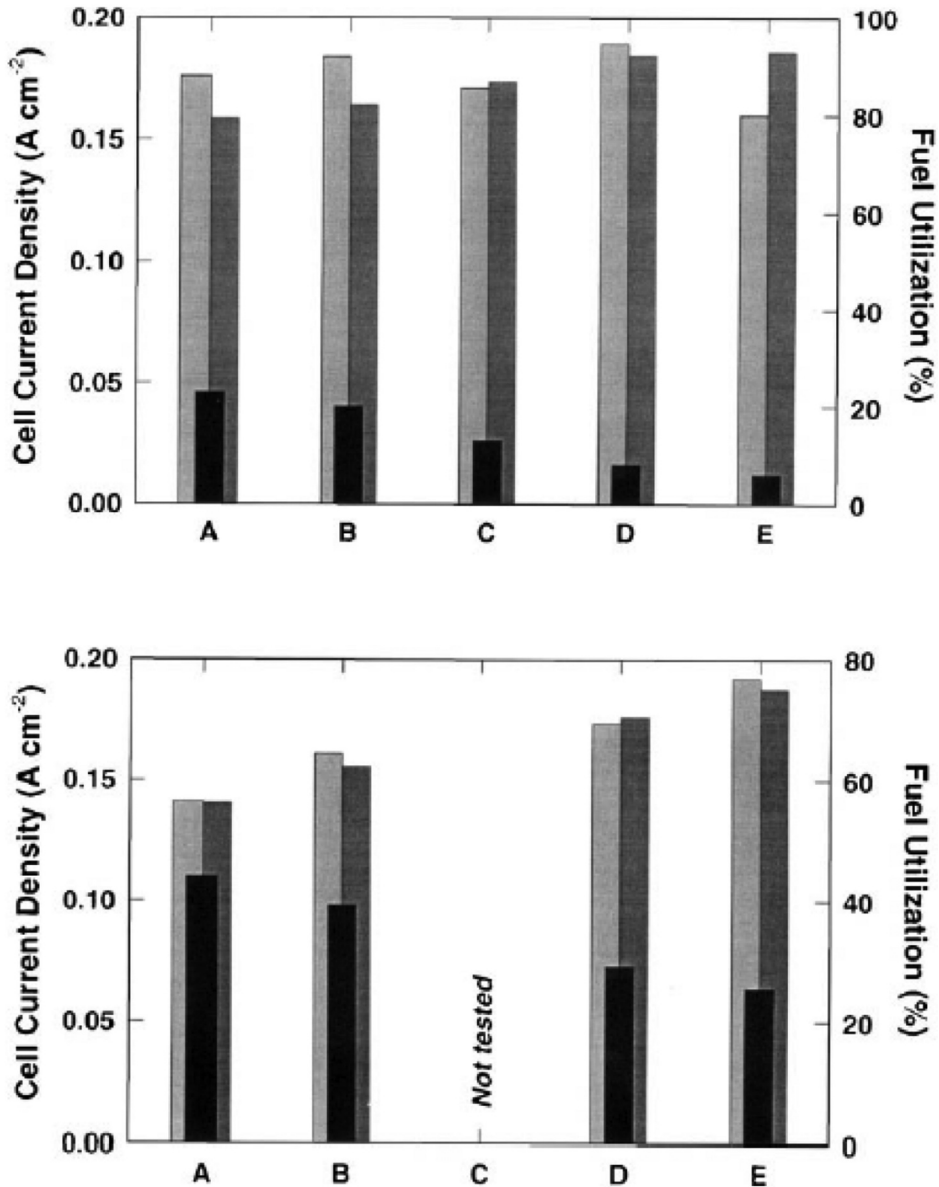


Figure 15. The utilization of combinations of direct methanol/ambient air cell components and operating conditions to obtain both high fuel utilization and cell performance (at 0.45 V and 60 °C cell operation). Examples A–E are five varied cell structures. The top chart illustrates the data for 0.5 M methanol feed stream and the bottom chart is for 1 M methanol feed stream. Bars in light gray correspond to the cell current density at 0.45 V (left axis), the black bars correspond to the rate of crossover in terms of current density (left axis), and the dark gray bars corresponds to fuel usage (right axis). Example D in the top figure represents the best combination that displays 0.18 A/cm² at 0.45 V and >90% fuel utilization data. Reproduced with permission from Elsevier^[365].

current through the metallic layer. Besides, as long as the metallic layer is not defective, methanol present in the electrolyte at the anodic side will not be able to react or cross the metallic surface.

With regards to Nafion, it is possible to prevent methanol crossover by selectively enclosing the water-rich domains, through which methanol diffuses, present on its surface in addition to hydrophobic regions. These water-rich domains are made of -SO_3^- clusters and can be blocked by utilizing palladium nanoparticles without any negative effects on Nafion's proton conductivity. This is because palladium can demonstrate high permeability toward hydrogen and block the proton exchange membrane from methanol. Tang *et al* have previously demonstrated one such combination in their research.^[367] They observed that only about $1.3 \times 10^{-15} \text{ mol cm}^{-2} \text{ s}^{-1}$ of methanol permeated across the palladium-modified Nafion ($1.73 \mu\text{g cm}^{-2}$ Pd loading). On the other hand, an unmodified membrane of pure Nafion displayed a relatively higher methanol permeation of $1.4 \times 10^{-7} \text{ mol cm}^{-2} \text{ s}^{-1}$.

6. Future prospects and conclusions

The production of anode electro-catalysts with a satisfactory performance to efficiently and effectively catalyze methanol oxidation reaction is vital for the wider commercialization of DMFC. Various factors should be regarded by researchers to help with their search for new electrocatalysts in future investigations. The introduction of support materials, especially having nanostructured morphology, onto which different metals are loaded can aid in achieving catalysts with enhanced electrical conductivity, mass transport, larger surface area, and stability. The resulting synergistic effects from the combination not only promotes finer performance for the existing catalyst materials, but also help progress the synthesis of new types with optimal performance quality. In addition, the durability of the metal and support composites will also be improved that allows them to be practically used as DMFCs for future applications. It is suggested that the implementation of nonplatinum metals is more preferable than using platinum. Although nonplatinum metals may not perform as well as platinum, the chances of carbon monoxide poisoning can be lowered to enhance the catalytic life cycle. Research should also focus on developing new catalysts for alkaline media. This is due to the possibility of having wider selections of catalyst materials, including supports, for the developments. Another important aspect to consider is to ensure that the materials that have been selected for catalyst synthesis are economical in order to fabricate products that are attractive for commercialization. With the growing market for portable electronic devices it is predicted that a great demand in portable power systems with large power density will be the

norm in coming years. With several studies being performed on DMFC technology, there is a good possibility that it could significantly contribute in this market because of the advantages such as quick refueling and high energy density. However, progress is still required to overcome the technical barriers discussed earlier in previous sections. Here are some of the key considerations for future DMFC catalyst design:

- A higher catalyst loading is helpful in achieving high methanol conversion in MOR in Micro-DMFC consisting of platinum-based catalyst, however, methanol crossover can occur due to higher loading and a prudent approach in catalyst loading is required to generate higher current density, minimize the methanol crossover and lower the overall cost.
- Noble metal catalysts such as Pt, are expensive and tend to deactivate quickly in presence of carbon monoxide generated during methanol oxidation. Alloying Pt with other metals e.g. Ru, or replacing Pt completely using transition metals or alloys could help destabilizing the CO intermediate increasing the life-cycle of the catalysts. Catalysts materials reported for water-gas-shift reaction ($\text{CO} + \text{H}_2\text{O} = \text{CO}_2 + \text{H}_2$), can be particularly helpful for dissociating water and converting the intermediate CO into CO_2 and thereby removing the poisonous effect of CO formation.
- Use of nano-dendrites and porous nanostructures also offer a high mass transfer efficiency along with a large surface area. An optimized approach is required for porosity as the small pores can increase the surface area, they may also reduce the mass transport rate and compromise the overall conversion of methanol. Mesoporous structures with 1-D Pt nanowires, 2-D Pt nano-sheets, 3-D Pt nano-spheres, and nano-dendrites of Pt and Rh have been reported to display great durability owing to their morphology that allows the presence of a large electrochemically active surfaces suitable for methanol oxidation. The mesoporous nano-spheres of Pt are also reported to demonstrate exceptional thermal stability.
- Hybrid electrocatalysts such as Pt@GO, Pt@PVP, and Rh@RGO have shown to be specifically active for MOR by providing dispersed active sites and high conductivity. Use of nitrogen and sulfur doped graphene as a support for Pd has also been reported to perform exceptionally well, showing high current density and very slow deactivation rate.
- Choice of support for DMFCs is critical as they influence the stability, dispersion, and overall conductivity of electrode-catalyst assembly. Resistance to corrosion, interaction with the metal and hydrophobicity are few other important considerations for long term stable performance. So far conductive polymers, carbon based support and mesoporous silica have been the most widely studied support for DMFC applications. A combination of conductive polymer PANi and carbon has shown to improve the MOR current density and CO resistivity

owing to enhanced diffusion of ions, large active surface area and reduced methanol crossover. Partial sulfonation of polyaniline has the potential of better interaction with the active metal sites resulting in superior thermal stability.

- Among the carbon based supports: carbon nanofiber (CNF), carbon nanocoil (CNC), nano carbon black (CB), single/multiwalled carbon nanotubes (SWCNT/MWCNTs), carbon mesoporous (CMS), and graphene/graphene oxides (G/GOs) are the possible choices for enhancing the electrocatalytic activity. A hybrid structure combining two or more forms of carbon also seems promising as the results on blending g-C₃N₄/carbon-black for Pd nanoparticles led to exceptional oxidation current for MOR.

Overall, the information presented in this review, including the recent findings on different materials for anode catalysts as well as the effects of different parameters, is expected to provide a guidance on the advancement of excellent alternative technology for future applications.

Abbreviations

3DGA	Three-Dimensional Graphene Aerogel
3D-NG	Three-Dimensional Hierarchical Nitrogen-Doped Graphene
AAO	Aluminium Anodic Oxide
ACL	Anode Catalyst Layer
aCNT	Activated Carbon Nanotube
ACP	Aromatic Conductive Polymer
AFM	Atomic Force Microscopy
BET	Brunauer-Emmett-Teller
BG	Boron-Doped Graphene
BT	Boiling Temperature-Prepared
CA	Chronoamperometry
CA	Carbon Aerogel
CB	Carbon Black
CBD	Chemical Bath Deposition
CCL	Cathode Catalyst Layer
CF	Carbon Fiber
CMS	Carbon Mesoporous
CNC	Carbon Nanocoil
CNF	Carbon Nano Fibers
CNT	Carbon Nanotube
CN _x -NTs	Nitrogen-Doped Carbon Nanotube
CP	Carbon Paper
CS	Carbon Nanosphere
CSA	Chlorosulfonic Acid
CS-functionalized	Chitosan-functionalized
CTAB	Cetrimonium Bromide
CV	Cyclic Voltammetry
DAFC	Direct Alcohol Fuel Cells
DFT	Density Functional Theory
DMAB	Dimethylamine Borane
DMFC	Direct Methanol Fuel Cell
DPN	Dendritic Platinum Nanoparticles

(Continued)

(Continued).

ECSA	Electrochemical Active Surface Area
EIS	Electrochemical Impedance Spectroscopy
EISA	Evaporation Induced Self-Assembly
EP-F	Nanoflake Nickel Oxide
EP-M	Microspherical Nickel Oxide
FCC	Face Centered Cubic
G/GO	Graphene/Graphene Oxide
GC	Glassy Carbon
GMC	Graphitic Mesoporous Carbon
GO	Graphene Oxide
HAADF- STEM	High-Angle Annular Dark-Field Scanning Transmission Electron Microscopy
HRTEM	High-Resolution Transmission Electron Microscopy
ITO	Indium Tin Oxide
LDH	Layered Double Hydroxide
LSV	Linear Sweep Voltammetry
MA	Mass Activity
MCM-41	Mobil Crystalline Material
MEA	Membrane Electrode Assembly
MOR	Methanol Oxidation Reactions
MPN	Mesoporous Platinum Nanospheres
MSN	Mesoporous Silica Nanoparticles
MWCNTS	Multi Walled Carbon Nanotubes
N-CNF	Nitrogen-Doped Carbon Nano Fiber
ND	Nanodendrite
NG	Nitrogen-Doped Graphene
NGA	Nitrogen-Doped Three-Dimensional Porous Graphene
NLDFT	Nonlocal Density Functional Theory
NMCS	N-doped Mesoporous Carbon Sphere
NN	Nanoneedles
NOMC	Nitrogen-Doped Mesoporous Carbon
NP	Nanoparticles
NR	Nanorod
NRP	Nanorod Pellets
NW	Nanowire
OECD	Organisation For Economic Co-Operation and Development
OMC/WC	Ordered Mesoporous Carbon-Tungsten Carbide
OMCS	Ordered Mesoporous Carbon Sphere
ORR	Oxygen Reduction Reaction
PAN	Polyacrylonitrile
PAni	Polyaniline
PEI	Polyethyleneimine
PpPD	Poly(Para-Phenylenediamine)
PPy	Polypyrrole
PTFE	Polytetrafluoroethylene
PVP	Polyvinylpyrrolidone
RG0	Reduced Graphene Oxide
r-GSH	Reduced Glutathione
RHE	Reversible Hydrogen Electrode
RT	Room Temperature-Prepared
SA	Specific Activity
SAED	Selected Area Electron Diffraction
S-CMS	Sulfur-Doped Carbon Microsphere
SEM	Scanning Electron Microscopy
SEM-EDX	Scanning Electron Microscopy – Energy Dispersive X-Ray Spectroscopy
SPAni	Sulfonated Polyaniline
SWCNTS	Single Walled Carbon Nanotubes
TECNF	Tio ₂ Embedded On Carbon Nanofiber
TEM	Transmission Electron Microscopy
UPD	Underpotential Deposition
WC-CNT	Tungsten Carbide-Carbon Nanotube
XAS	X-Ray Absorption Spectroscopy
XC-72-CQD	Carbon Quantum Dots-Modified Carbon Black
X-NSs	Crossed-X Nanosheets
XPS	X-Ray Photoelectron Spectroscopy
XRD	X-Ray Diffraction

Acknowledgments

This publication was made possible by NPRP grant (NPRP8-145-2-066) from the Qatar National Research Fund (a member of Qatar foundation). The statements made herein are solely the responsibility of the author(s). The author(s) would also like to acknowledge the support from Qatar University internal grant QUCG-CENG-19/20-7. Open Access funding provided by the Qatar National Library.

ORCID

Anand Kumar  <http://orcid.org/0000-0002-9146-979X>

References

- [1] Wolfram, C.; Shelef, O.; Gertler, P. How Will Energy Demand Develop in the Developing World? *J Econ Perspec.* 2012, 26(1), 119–138. DOI: 10.1257/jep.26.1.119.
- [2] Socolow, R.; Hotinski, R.; Greenblatt, J. B.; Pacala, S. Solving the Climate Problem: Technologies Available to Curb CO₂ Emissions. *Environment.* 2004, 46, 8–19.
- [3] Kamarudin, S. K.; Daud, W. R. W.; Ho, S. L.; Hasran, U. A. Overview on the Challenges and Developments of Micro-direct Methanol Fuel Cells (DMFC). *J. Power Sources.* 2007, 163, 743–754. DOI: 10.1016/j.jpowsour.2006.09.081.
- [4] Carrette, L.; Friedrich, K.; Stimming, U. Fuel Cells—fundamentals and Applications. *Fuel Cells.* 2001, 1, 5–39. DOI: 10.1002/1615-6854(200105)1:1<5::AID-FUCE5>3.0.CO;2-G.
- [5] Verma, L.; Studies on Methanol Fuel Cell. *J. Power Sources.* 2000, 86, 464–468. DOI: 10.1016/S0378-7753(99)00403-6.
- [6] Baldauf, M.; Preidel, W. Status of the Development of a Direct Methanol Fuel Cell. *J. Power Sources.* 1999, 84, 161–166. DOI: 10.1016/S0378-7753(99)00332-8.
- [7] Kamarudin, S. K.; Achmad, F.; Daud, W. R. W. Overview on the Application of Direct Methanol Fuel Cell (DMFC) for Portable Electronic Devices. *Int. J. Hydrogen Energy.* 2009, 34, 6902–6916. DOI: 10.1016/j.ijhydene.2009.06.013.
- [8] Chen, A.; Holt-Hindle, P. Platinum-based Nanostructured Materials: Synthesis, Properties, and Applications. *Chem. Rev.* 2010, 110, 3767–3804. DOI: 10.1021/cr9003902.
- [9] Kloke, A.; von Stetten, F.; Zengerle, R.; Kerzenmacher, S. Strategies for the Fabrication of Porous Platinum Electrodes. *Adv. Mater.* 2011, 23, 4976–5008. DOI: 10.1002/adma.201102182.
- [10] Li, C.; Tan, H.; Lin, J.; Luo, X.; Wang, S.; You, J.; Kang, Y.; Bando, Y.; Yamauchi, Y.; Kim, J. Emerging Pt-based Electrocatalysts with Highly Open Nanoarchitectures for Boosting Oxygen Reduction Reaction. *Nano Today.* 2018, 21, 91–105. DOI: 10.1016/j.nantod.2018.06.005.
- [11] Li, C.; Iqbal, M.; Lin, J.; Luo, X.; Jiang, B.; Malgras, V.; Wu, K. C.; Kim, J.; Yamauchi, Y. Electrochemical Deposition: An Advanced Approach for Templated Synthesis of Nanoporous Metal Architectures. *Acc. Chem. Res.* 2018, 51, 1764–1773. DOI: 10.1021/acs.accounts.8b00119.
- [12] Jiang, B.; Li, C.; Malgras, V.; Imura, M.; Tominaka, S.; Yamauchi, Y. Mesoporous Pt Nanospheres with Designed Pore Surface as Highly Active Electrocatalyst. *Chem. Sci.* 2016, 7, 1575–1581. DOI: 10.1039/C5SC03779D.

- [13] Li, C.; Sato, T.; Yamauchi, Y. Electrochemical Synthesis of One-dimensional Mesoporous Pt Nanorods Using the Assembly of Surfactant Micelles in Confined Space. *Angew. Chem. Int. Ed.* **2013**, *52*, 8050–8053. DOI: [10.1002/anie.201303035](https://doi.org/10.1002/anie.201303035).
- [14] Wang, L.; Yamauchi, Y. Strategic Synthesis of Trimetallic Au@ Pd@ Pt Core– Shell Nanoparticles from Poly (Vinylpyrrolidone)-based Aqueous Solution toward Highly Active Electrocatalysts. *Chem. Mater.* **2011**, *23*, 2457–2465. DOI: [10.1021/cm200382s](https://doi.org/10.1021/cm200382s).
- [15] Wang, H.; Jeong, H. Y.; Imura, M.; Wang, L.; Radhakrishnan, L.; Fujita, N.; Castle, T.; Terasaki, O.; Yamauchi, Y. Shape-and Size-controlled Synthesis in Hard Templates: Sophisticated Chemical Reduction for Mesoporous Monocrystalline Platinum Nanoparticles. *J. Am. Chem. Soc.* **2011**, *133*, 14526–14529. DOI: [10.1021/ja2058617](https://doi.org/10.1021/ja2058617).
- [16] Ataee-Esfahani, H.; Wang, L.; Nemoto, Y.; Yamauchi, Y. Synthesis of Bimetallic Au@ Pt Nanoparticles with Au Core and Nanostructured Pt Shell toward Highly Active Electrocatalysts. *Chem. Mater.* **2010**, *22*, 6310–6318. DOI: [10.1021/cm102074w](https://doi.org/10.1021/cm102074w).
- [17] Jha, N.; Reddy, A. L. M.; Shaijumon, M.; Rajalakshmi, N.; Ramaprabhu, S. Pt–Ru/multi-walled Carbon Nanotubes as Electrocatalysts for Direct Methanol Fuel Cell. *Int. J. Hydrogen Energy.* **2008**, *33*, 427–433. DOI: [10.1016/j.ijhydene.2007.07.064](https://doi.org/10.1016/j.ijhydene.2007.07.064).
- [18] Ferrin, P.; Nilekar, A. U.; Greeley, J.; Mavrikakis, M.; Rossmeisl, J. Reactivity Descriptors for Direct Methanol Fuel Cell Anode Catalysts. *Surf. Sci.* **2008**, *602*, 3424–3431. DOI: [10.1016/j.susc.2008.08.011](https://doi.org/10.1016/j.susc.2008.08.011).
- [19] Dinh, H. N.; Ren, X.; Garzon, F. H.; Zelenay, P.; Gottesfeld, S. Electrocatalysis in Direct Methanol Fuel Cells: In-situ Probing of PtRu Anode Catalyst Surfaces. *J. Electroanal. Chem.* **2000**, *491*, 222–233. DOI: [10.1016/S0022-0728\(00\)00271-0](https://doi.org/10.1016/S0022-0728(00)00271-0).
- [20] Hogarth, M.; Hards, G. Direct Methanol Fuel Cells. *Platinum Met. Rev.* **1996**, *40*, 150–159.
- [21] Gokhale, A. A.; Dumesic, J. A.; Mavrikakis, M. On the Mechanism of Low-temperature Water Gas Shift Reaction on Copper. *J. Am. Chem. Soc.* **2008**, *130*, 1402–1414. DOI: [10.1021/ja0768237](https://doi.org/10.1021/ja0768237).
- [22] Grabow, L. C.; Gokhale, A. A.; Evans, S. T.; Dumesic, J. A.; Mavrikakis, M. Mechanism of the Water Gas Shift Reaction on Pt: First Principles, Experiments, and Microkinetic Modeling. *J. Phys. Chem. C.* **2008**, *112*, 4608–4617. DOI: [10.1021/jp7099702](https://doi.org/10.1021/jp7099702).
- [23] Huang, H.; Yang, S.; Vajtai, R.; Wang, X.; Ajayan, P. M. Pt-decorated 3D Architectures Built from Graphene and Graphitic Carbon Nitride Nanosheets as Efficient Methanol Oxidation Catalysts. *Adv. Mater.* **2014**, *26*, 5160–5165. DOI: [10.1002/adma.201401877](https://doi.org/10.1002/adma.201401877).
- [24] Justin, P.; Rao, G. R. Methanol Oxidation on MoO₃ Promoted Pt/C Electrocatalyst. *Int. J. Hydrogen Energy.* **2011**, *36*, 5875–5884. DOI: [10.1016/j.ijhydene.2011.01.122](https://doi.org/10.1016/j.ijhydene.2011.01.122).
- [25] Cui, G.; Shen, P. K.; Meng, H.; Zhao, J.; Wu, G. Tungsten Carbide as Supports for Pt Electrocatalysts with Improved CO Tolerance in Methanol Oxidation. *J. Power Sources.* **2011**, *196*, 6125–6130. DOI: [10.1016/j.jpowsour.2011.03.042](https://doi.org/10.1016/j.jpowsour.2011.03.042).
- [26] Bahrami, H.; Faghri, A. Review and Advances of Direct Methanol Fuel Cells: Part II: Modeling and Numerical Simulation. *J. Power Sources.* **2013**, *230*, 303–320. DOI: [10.1016/j.jpowsour.2012.12.009](https://doi.org/10.1016/j.jpowsour.2012.12.009).
- [27] García-Díaz, B. L.; Patterson, J. R.; Weidner, J. W. Quantifying Individual Losses in a Direct Methanol Fuel Cell. *J. Fuel Cell Sci Technol.* **2012**, *9*. DOI: [10.1115/1.4005394](https://doi.org/10.1115/1.4005394).
- [28] Bard, A. J.; Faulkner, L. R. Fundamentals and Applications. *Electrochem Methods.* **2001**, *2*, 580–632.

- [29] Yang, W.; Zhao, T. Two-phase, Mass-transport Model for Direct Methanol Fuel Cells with Effect of Non-equilibrium Evaporation and Condensation. *J. Power Sources*. 2007, 174, 136–147. DOI: [10.1016/j.jpowsour.2007.08.075](https://doi.org/10.1016/j.jpowsour.2007.08.075).
- [30] Yang, W.; Zhao, T. A Two-dimensional, Two-phase Mass Transport Model for Liquid-feed DMFCs, *Electrochim. Acta*. 2007, 52, 6125–6140.
- [31] Yang, W.; Zhao, T.; He, Y. Modelling of Coupled Electron and Mass Transport in Anisotropic Proton-exchange Membrane Fuel Cell Electrodes. *J. Power Sources*. 2008, 185, 765–775. DOI: [10.1016/j.jpowsour.2008.06.100](https://doi.org/10.1016/j.jpowsour.2008.06.100).
- [32] Xu, C.; Faghri, A. Water Transport Characteristics in a Passive Liquid-feed DMFC. *Int. J. Heat Mass Transfer*. 2010, 53, 1951–1966. DOI: [10.1016/j.ijheatmasstransfer.2009.12.060](https://doi.org/10.1016/j.ijheatmasstransfer.2009.12.060).
- [33] Xu, C.; Faghri, A. Mass Transport Analysis of a Passive Vapor-feed Direct Methanol Fuel Cell. *J. Power Sources*. 2010, 195, 7011–7024. DOI: [10.1016/j.jpowsour.2010.05.003](https://doi.org/10.1016/j.jpowsour.2010.05.003).
- [34] Xu, C.; Faghri, A. Effect of the Capillary Property of Porous Media on the Water Transport Characteristics in a Passive Liquid-feed DMFC. *J. Fuel Cell Sci Technol*. 2010, 7. DOI: [10.1115/1.4001761](https://doi.org/10.1115/1.4001761).
- [35] Yang, W.; Zhao, T. A Transient Two-phase Mass Transport Model for Liquid Feed Direct Methanol Fuel Cells. *J. Power Sources*. 2008, 185, 1131–1140. DOI: [10.1016/j.jpowsour.2008.07.052](https://doi.org/10.1016/j.jpowsour.2008.07.052).
- [36] Yang, W.; Zhao, T.; Xu, C. Three-dimensional Two-phase Mass Transport Model for Direct Methanol Fuel Cells. *Electrochim. Acta*. 2007, 53, 853–862. DOI: [10.1016/j.electacta.2007.07.070](https://doi.org/10.1016/j.electacta.2007.07.070).
- [37] Bahrami, H.; Faghri, A. Transport Phenomena in a Semi-passive Direct Methanol Fuel Cell. *Int. J. Heat Mass Transfer*. 2010, 53, 2563–2578. DOI: [10.1016/j.ijheatmasstransfer.2009.12.050](https://doi.org/10.1016/j.ijheatmasstransfer.2009.12.050).
- [38] Bahrami, H.; Faghri, A. Water Management in a Passive DMFC Using Highly Concentrated Methanol Solution. *J. Fuel Cell Sci Technol*. 2011, 8. DOI: [10.1115/1.4002315](https://doi.org/10.1115/1.4002315).
- [39] Sun, Y.; Xing, L.; Scott, K. Analysis of the Kinetics of Methanol Oxidation in a Porous Pt–Ru Anode. *J. Power Sources*. 2010, 195, 1–10. DOI: [10.1016/j.jpowsour.2009.07.028](https://doi.org/10.1016/j.jpowsour.2009.07.028).
- [40] Shivhare, M.; Allen, R.; Scott, K.; Morris, A.; Martin, E. A Kinetic Model for the Direct Methanol Fuel Cell Anode Based on Surface Coverage. *J. Electroanal. Chem*. 2006, 595, 145–151. DOI: [10.1016/j.jelechem.2006.07.017](https://doi.org/10.1016/j.jelechem.2006.07.017).
- [41] Kareemulla, D.; Jayanti, S. Comprehensive One-dimensional, Semi-analytical, Mathematical Model for Liquid-feed Polymer Electrolyte Membrane Direct Methanol Fuel Cells. *J. Power Sources*. 2009, 188, 367–378. DOI: [10.1016/j.jpowsour.2008.11.138](https://doi.org/10.1016/j.jpowsour.2008.11.138).
- [42] Choi, K.; McFarland, E. W.; Stucky, G. D. Electrocatalytic Properties of Thin Mesoporous Platinum Films Synthesized Utilizing Potential-Controlled Surfactant Assembly. *Adv. Mater*. 2003, 15, 2018–2021. DOI: [10.1002/adma.200304557](https://doi.org/10.1002/adma.200304557).
- [43] Wang, L.; Yamauchi, Y. Block Copolymer Mediated Synthesis of Dendritic Platinum Nanoparticles. *J. Am. Chem. Soc*. 2009, 131, 9152–9153. DOI: [10.1021/ja902485x](https://doi.org/10.1021/ja902485x).
- [44] Teng, X.; Liang, X.; Maksimuk, S.; Yang, H. Synthesis of Porous Platinum Nanoparticles. *small*. 2006, 2, 249–253. DOI: [10.1002/smll.200500244](https://doi.org/10.1002/smll.200500244).
- [45] Yang, S.; Luo, X. Mesoporous Nano/micro Noble Metal Particles: Synthesis and Applications. *Nanoscale*. 2014, 6, 4438–4457. DOI: [10.1039/C3NR06858G](https://doi.org/10.1039/C3NR06858G).
- [46] Atae-Esfahani, H.; Imura, M.; Yamauchi, Y. All-Metal Mesoporous Nanocolloids: Solution-Phase Synthesis of Core-Shell Pd@ Pt Nanoparticles with a Designed

- Concave Surface. *Angew. Chem. Int. Ed.* **2013**, *52*, 13611–13615. DOI: [10.1002/anie.201307126](https://doi.org/10.1002/anie.201307126).
- [47] Liang, H.; Cao, X.; Zhou, F.; Cui, C.; Zhang, W.; Yu, S. A Free-Standing Pt-Nanowire Membrane as A Highly Stable Electrocatalyst for the Oxygen Reduction Reaction. *Adv. Mater.* **2011**, *23*, 1467–1471. DOI: [10.1002/adma.201004377](https://doi.org/10.1002/adma.201004377).
- [48] Xia, B. Y.; Ng, W. T.; Wu, H. B.; Wang, X.; Lou, X. W. Self-supported Interconnected Pt Nanoassemblies as Highly Stable Electrocatalysts for Low-temperature Fuel Cells. *Angew. Chem. Int. Ed.* **2012**, *51*, 7213–7216. DOI: [10.1002/anie.201201553](https://doi.org/10.1002/anie.201201553).
- [49] Li, C.; Imura, M.; Yamauchi, Y. Displacement Plating of a Mesoporous Pt Skin onto Co Nanochains in a Low-Concentration Surfactant Solution. *Chemistry*. **2014**, *20*, 3277–3282. DOI: [10.1002/chem.201303250](https://doi.org/10.1002/chem.201303250).
- [50] Liu, L.; Pippel, E.; Scholz, R.; Gösele, U. Nanoporous Pt– Co Alloy Nanowires: Fabrication, Characterization, and Electrocatalytic Properties. *Nano Lett.* **2009**, *9*, 4352–4358. DOI: [10.1021/nl902619q](https://doi.org/10.1021/nl902619q).
- [51] Alia, S. M.; Zhang, G.; Kisailus, D.; Li, D.; Gu, S.; Jensen, K.; Yan, Y. Porous Platinum Nanotubes for Oxygen Reduction and Methanol Oxidation Reactions. *Adv. Funct. Mater.* **2010**, *20*, 3742–3746. DOI: [10.1002/adfm.201001035](https://doi.org/10.1002/adfm.201001035).
- [52] Chen, Z.; Waje, M.; Li, W.; Yan, Y.; Supportless, P. PtPd Nanotubes as Electrocatalysts for Oxygen-reduction Reactions. *Angew. Chem. Int. Ed.* **2007**, *46*, 4060–4063. DOI: [10.1002/anie.200700894](https://doi.org/10.1002/anie.200700894).
- [53] Wei, J.; Wang, H.; Deng, Y.; Sun, Z.; Shi, L.; Tu, B.; Luqman, M.; Zhao, D. Solvent Evaporation Induced Aggregating Assembly Approach to Three-dimensional Ordered Mesoporous Silica with Ultralarge Accessible Mesopores. *J. Am. Chem. Soc.* **2011**, *133*, 20369–20377. DOI: [10.1021/ja207525e](https://doi.org/10.1021/ja207525e).
- [54] Chen, Y.; Chen, C.; Hung, Y.; Chou, C.; Liu, T.; Liang, M.; Chen, C.; Mou, C. A New Strategy for Intracellular Delivery of Enzyme Using Mesoporous Silica Nanoparticles: Superoxide Dismutase. *J. Am. Chem. Soc.* **2013**, *135*, 1516–1523. DOI: [10.1021/ja3105208](https://doi.org/10.1021/ja3105208).
- [55] Koenigsmann, C.; Zhou, W.; Adzic, R. R.; Sutter, E.; Wong, S. S. Size-dependent Enhancement of Electrocatalytic Performance in Relatively Defect-free, Processed Ultrathin Platinum Nanowires. *Nano Lett.* **2010**, *10*, 2806–2811. DOI: [10.1021/nl100718k](https://doi.org/10.1021/nl100718k).
- [56] Li, H.; Zhao, S.; Gong, M.; Cui, C.; He, D.; Liang, H.; Wu, L.; Yu, S. Ultrathin PtPdTe Nanowires as Superior Catalysts for Methanol Electrooxidation. *Angew. Chem. Int. Ed.* **2013**, *52*, 7472–7476. DOI: [10.1002/anie.201302090](https://doi.org/10.1002/anie.201302090).
- [57] Wang, H.; Wang, L.; Sato, T.; Sakamoto, Y.; Tominaka, S.; Miyasaka, K.; Miyamoto, N.; Nemoto, Y.; Terasaki, O.; Yamauchi, Y. Synthesis of Mesoporous Pt Films with Tunable Pore Sizes from Aqueous Surfactant Solutions. *Chem. Mater.* **2012**, *24*, 1591–1598. DOI: [10.1021/cm300054b](https://doi.org/10.1021/cm300054b).
- [58] Wang, H.; Ishihara, S.; Ariga, K.; Yamauchi, Y. All-metal Layer-by-layer Films: Bimetallic Alternate Layers with Accessible Mesopores for Enhanced Electrocatalysis. *J. Am. Chem. Soc.* **2012**, *134*, 10819–10821. DOI: [10.1021/ja303773z](https://doi.org/10.1021/ja303773z).
- [59] Li, C.; Imura, M.; Yamauchi, Y. A Universal Approach to the Preparation of Colloidal Mesoporous Platinum Nanoparticles with Controlled Particle Sizes in A Wide Range from 20 Nm to 200 Nm. *Phys. Chem. Chem. Phys.* **2014**, *16*, 8787–8790. DOI: [10.1039/C4CP00039K](https://doi.org/10.1039/C4CP00039K).
- [60] Li, C.; Malgras, V.; Alshehri, S. M.; Kim, J. H.; Yamauchi, Y. Electrochemical Synthesis of Mesoporous Pt Nanowires with Highly Electrocatalytic Activity toward Methanol Oxidation Reaction. *Electrochim. Acta.* **2015**, *183*, 107–111. DOI: [10.1016/j.electacta.2015.04.028](https://doi.org/10.1016/j.electacta.2015.04.028).

- [61] Daşdelen, Z.; Yıldız, Y.; Eriş, S.; Şen, F. Enhanced Electrocatalytic Activity and Durability of Pt Nanoparticles Decorated on GO-PVP Hybride Material for Methanol Oxidation Reaction. *Appl. Catal. B Environ.* **2017**, *219*, 511–516. DOI: [10.1016/j.apcatb.2017.08.014](https://doi.org/10.1016/j.apcatb.2017.08.014).
- [62] Wang, L.; Yamauchi, Y. Synthesis of Mesoporous Pt Nanoparticles with Uniform Particle Size from Aqueous Surfactant Solutions toward Highly Active Electrocatalysts. *Chemistry*. **2011**, *17*, 8810–8815. DOI: [10.1002/chem.201100386](https://doi.org/10.1002/chem.201100386).
- [63] Garrick, T. R.; Diao, W.; Tengco, J. M.; Stach, E. A.; Senanayake, S. D.; Chen, D. A.; Monnier, J. R.; Weidner, J. W. The Effect of the Surface Composition of Ru-Pt Bimetallic Catalysts for Methanol Oxidation. *Electrochim. Acta*. **2016**, *195*, 106–111. DOI: [10.1016/j.electacta.2016.02.134](https://doi.org/10.1016/j.electacta.2016.02.134).
- [64] Lu, S.; Eid, K.; Ge, D.; Guo, J.; Wang, L.; Wang, H.; Gu, H. One-pot Synthesis of PtRu Nanodendrites as Efficient Catalysts for Methanol Oxidation Reaction. *Nanoscale*. **2017**, *9*, 1033–1039. DOI: [10.1039/C6NR08895C](https://doi.org/10.1039/C6NR08895C).
- [65] Yang, M.; Catalytic Activities of PtBi Nanoparticles toward Methanol Electrooxidation in Acid and Alkaline Media. *J. Power Sources*. **2013**, *229*, 42–47. DOI: [10.1016/j.jpowsour.2012.11.150](https://doi.org/10.1016/j.jpowsour.2012.11.150).
- [66] Fu, G.; Yan, X.; Cui, Z.; Sun, D.; Xu, L.; Tang, Y.; Goodenough, J. B.; Lee, J. Catalytic Activities for Methanol Oxidation on Ultrathin CuPt₃ Wavy Nanowires With/without Smart Polymer. *Chem. Sci.* **2016**, *7*, 5414–5420. DOI: [10.1039/C6SC01501H](https://doi.org/10.1039/C6SC01501H).
- [67] Yang, H.; Dai, L.; Xu, D.; Fang, J.; Zou, S. Electrooxidation of Methanol and Formic Acid on PtCu Nanoparticles. *Electrochim. Acta*. **2010**, *55*, 8000–8004. DOI: [10.1016/j.electacta.2010.03.026](https://doi.org/10.1016/j.electacta.2010.03.026).
- [68] Xu, C.; Hou, J.; Pang, X.; Li, X.; Zhu, M.; Tang, B. Nanoporous PtCo and PtNi Alloy Ribbons for Methanol Electrooxidation. *Int. J. Hydrogen Energy*. **2012**, *37*, 10489–10498. DOI: [10.1016/j.ijhydene.2012.04.041](https://doi.org/10.1016/j.ijhydene.2012.04.041).
- [69] Ataee-Esfahani, H.; Nemoto, Y.; Imura, M.; Yamauchi, Y. Facile Synthesis of Nanoporous Pt–Ru Alloy Spheres with Various Compositions toward Highly Active Electrocatalysts. *Chemistry–An Asian J.* **2012**, *7*, 876–880. DOI: [10.1002/asia.201200053](https://doi.org/10.1002/asia.201200053).
- [70] Ataee-Esfahani, H.; Liu, J.; Hu, M.; Miyamoto, N.; Tominaka, S.; Wu, K. C.; Yamauchi, Y. Mesoporous Metallic Cells: Design of Uniformly Sized Hollow Mesoporous Pt–Ru Particles with Tunable Shell Thicknesses. *Small*. **2013**, *9*, 1047–1051. DOI: [10.1002/smll.201202539](https://doi.org/10.1002/smll.201202539).
- [71] Franceschini, E. A.; Planes, G. A.; Williams, F. J.; Soler-Illia, G. J.; Corti, H. R.; Mesoporous, P. Pt/Ru Alloy Electrocatalysts for Methanol Oxidation. *J. Power Sources*. **2011**, *196*, 1723–1729. DOI: [10.1016/j.jpowsour.2010.10.016](https://doi.org/10.1016/j.jpowsour.2010.10.016).
- [72] Teng, X.; Maksimuk, S.; Frommer, S.; Yang, H. Three-dimensional PtRu Nanostructures. *Chem. Mater.* **2007**, *19*, 36–41. DOI: [10.1021/cm061979b](https://doi.org/10.1021/cm061979b).
- [73] Zhang, J.; Tang, Y.; Song, C.; Zhang, J.; Wang, H. PEM Fuel Cell Open Circuit Voltage (OCV) in the Temperature Range of 23 C to 120 C. *J. Power Sources*. **2006**, *163*, 532–537. DOI: [10.1016/j.jpowsour.2006.09.026](https://doi.org/10.1016/j.jpowsour.2006.09.026).
- [74] Karatepe, Ö.; Yıldız, Y.; Pamuk, H.; Eris, S.; Dasdelen, Z.; Sen, F. Enhanced Electrocatalytic Activity and Durability of Highly Monodisperse Pt@ PPy–PANI Nanocomposites as a Novel Catalyst for the Electro-oxidation of Methanol. *RSC Adv.* **2016**, *6*, 50851–50857. DOI: [10.1039/C6RA06210E](https://doi.org/10.1039/C6RA06210E).
- [75] Yıldız, Y.; Esirden, İ.; Erken, E.; Demir, E.; Kaya, M.; Şen, F. Microwave (Mw)-assisted Synthesis of 5-Substituted 1H-Tetrazoles via [3 2] Cycloaddition Catalyzed by Mw-Pd/Co Nanoparticles Decorated on Multi-Walled Carbon Nanotubes. *ChemistrySelect*. **2016**, *1*, 1695–1701. DOI: [10.1002/slct.201600265](https://doi.org/10.1002/slct.201600265).

- [76] Çelik, B.; Başkaya, G.; Sert, H.; Karatepe, Ö.; Erken, E.; Şen, F.; Monodisperse, P. (0)/DPA@ GO Nanoparticles as Highly Active Catalysts for Alcohol Oxidation and Dehydrogenation of DMAB. *Int. J. Hydrogen Energy*. 2016, 41, 5661–5669. DOI: 10.1016/j.ijhydene.2016.02.061.
- [77] Heidenreich, R. D.; Hess, W.; Ban, L. A Test Object and Criteria for High Resolution Electron Microscopy. *J. Appl. Crystallogr.* 1968, 1, 1–19. DOI: 10.1107/S0021889868004930.
- [78] Katsnelson, M.; Novoselov, K.; Geim, A. Chiral Tunnelling and the Klein Paradox in Graphene. *Nat. Phys.* 2006, 2, 620. DOI: 10.1038/nphys384.
- [79] Koczkur, K. M.; Mourdikoudis, S.; Polavarapu, L.; Skrabalak, S. E. Polyvinylpyrrolidone (PVP) in Nanoparticle Synthesis. *Dalton Trans.* 2015, 44, 17883–17905. DOI: 10.1039/C5DT02964C.
- [80] Wang, Z.; Yin, G.; Shao, Y.; Yang, B.; Shi, P.; Feng, P. Electrochemical Impedance Studies on Carbon Supported PtRuNi and PtRu Anode Catalysts in Acid Medium for Direct Methanol Fuel Cell. *J. Power Sources*. 2007, 165, 9–15. DOI: 10.1016/j.jpowsour.2006.12.027.
- [81] Antolini, E.; Gonzalez, E. The Electro-oxidation of Carbon Monoxide, Hydrogen/carbon Monoxide and Methanol in Acid Medium on Pt-Sn Catalysts for Low-temperature Fuel Cells: A Comparative Review of the Effect of Pt-Sn Structural Characteristics. *Electrochim. Acta*. 2010, 56, 1–14. DOI: 10.1016/j.electacta.2010.08.077.
- [82] Bianchini, C.; Shen, P. K. Palladium-based Electrocatalysts for Alcohol Oxidation in Half Cells and in Direct Alcohol Fuel Cells. *Chem. Rev.* 2009, 109, 4183–4206. DOI: 10.1021/cr9000995.
- [83] Antolini, E.; Gonzalez, E. Alkaline Direct Alcohol Fuel Cells. *J. Power Sources*. 2010, 195, 3431–3450. DOI: 10.1016/j.jpowsour.2009.11.145.
- [84] Lu, Y.; Jiang, Y.; Gao, X.; Wang, X.; Chen, W. Strongly Coupled Pd Nanotetrahedron/tungsten Oxide Nanosheet Hybrids with Enhanced Catalytic Activity and Stability as Oxygen Reduction Electrocatalysts. *J. Am. Chem. Soc.* 2014, 136, 11687–11697. DOI: 10.1021/ja5041094.
- [85] Shen, M.; Zheng, L.; He, W.; Ruan, C.; Jiang, C.; Ai, K.; Lu, L. High-performance Oxygen Reduction Electrocatalysts Derived from Uniform Cobalt–adenine Assemblies. *Nano Energy*. 2015, 17, 120–130. DOI: 10.1016/j.nanoen.2015.08.007.
- [86] Kang, Y.; Li, F.; Li, S.; Ji, P.; Zeng, J.; Jiang, J.; Chen, Y. Unexpected Catalytic Activity of Rhodium Nanodendrites with Nanosheet Subunits for Methanol Electrooxidation in an Alkaline Medium. *Nano Res.* 2016, 9, 3893–3902. DOI: 10.1007/s12274-016-1258-8.
- [87] Fu, X.; Zhao, Z.; Wan, C.; Wang, Y.; Fan, Z.; Song, F.; Cao, B.; Li, M.; Xue, W.; Huang, Y. Ultrathin Wavy Rh Nanowires as Highly Effective Electrocatalysts for Methanol Oxidation Reaction with Ultrahigh ECSA. *Nano Res.* 2019, 12, 211–215. DOI: 10.1007/s12274-018-2204-8.
- [88] Jiang, B.; Li, C.; Dag, Ö.; Abe, H.; Takei, T.; Imai, T.; Hossain, M. S. A.; Islam, M. T.; Wood, K.; Henzie, J. Mesoporous Metallic Rhodium Nanoparticles. *Nat. Commun.* 2017, 8, 15581. DOI: 10.1038/ncomms15581.
- [89] Huang, X.; Zhao, Z.; Chen, Y.; Chiu, C.; Ruan, L.; Liu, Y.; Li, M.; Duan, X.; Huang, Y. High Density Catalytic Hot Spots in Ultrafine Wavy Nanowires. *Nano Lett.* 2014, 14, 3887–3894. DOI: 10.1021/nl501137a.
- [90] Kang, Y.; Xue, Q.; Jin, P.; Jiang, J.; Zeng, J.; Chen, Y. Rhodium Nanosheets–reduced Graphene Oxide Hybrids: A Highly Active Platinum-alternative Electrocatalyst for the Methanol Oxidation Reaction in Alkaline Media. *ACS Sustainable Chem. Eng.* 2017, 5, 10156–10162. DOI: 10.1021/acssuschemeng.7b02163.

- [91] Xu, C.; Wang, H.; Shen, P. K.; Jiang, S. P. Highly Ordered Pd Nanowire Arrays as Effective Electrocatalysts for Ethanol Oxidation in Direct Alcohol Fuel Cells. *Adv. Mater.* **2007**, *19*, 4256–4259. DOI: [10.1002/adma.200602911](https://doi.org/10.1002/adma.200602911).
- [92] Jia, F.; Wong, K.; Du, R. Direct Growth of Highly Catalytic Palladium Nanoplates Array onto Gold Substrate by a Template-free Electrochemical Route. *Electrochem. Commun.* **2009**, *11*, 519–521. DOI: [10.1016/j.elecom.2008.11.054](https://doi.org/10.1016/j.elecom.2008.11.054).
- [93] Yin, Z.; Zheng, H.; Ma, D.; Bao, X. Porous Palladium Nanoflowers that Have Enhanced Methanol Electro-oxidation Activity. *J. Phys. Chem. C.* **2008**, *113*, 1001–1005. DOI: [10.1021/jp807456j](https://doi.org/10.1021/jp807456j).
- [94] Zhu, Y.; Kang, Y.; Zou, Z.; Zhou, Q.; Zheng, J.; Xia, B.; Yang, H. Facile Preparation of Carbon-supported Pd Nanoparticles for Electrocatalytic Oxidation of Formic Acid. *Fuel Cells Bull.* **2008**, *2008*, 12–15. DOI: [10.1016/S1464-2859\(08\)70286-4](https://doi.org/10.1016/S1464-2859(08)70286-4).
- [95] Jia, F.; Wong, K.; Zhang, L. Electrochemical Synthesis of Nanostructured Palladium of Different Morphology Directly on Gold Substrate through a Cyclic Deposition/dissolution Route. *J. Phys. Chem. C.* **2009**, *113*, 7200–7206. DOI: [10.1021/jp900623t](https://doi.org/10.1021/jp900623t).
- [96] Wang, X.; Wang, W.; Qi, Z.; Zhao, C.; Ji, H.; Zhang, Z. Electrochemical Catalytic Activities of Nanoporous Palladium Rods for Methanol Electro-oxidation. *J. Power Sources.* **2010**, *195*, 6740–6747. DOI: [10.1016/j.jpowsour.2010.03.098](https://doi.org/10.1016/j.jpowsour.2010.03.098).
- [97] Zhao, Y.; Nie, S.; Wang, H.; Tian, J.; Ning, Z.; Li, X. Direct Synthesis of Palladium Nanoparticles on Mn₃O₄ Modified Multi-walled Carbon Nanotubes: A Highly Active Catalyst for Methanol Electro-oxidation in Alkaline Media. *J. Power Sources.* **2012**, *218*, 320–330. DOI: [10.1016/j.jpowsour.2012.07.012](https://doi.org/10.1016/j.jpowsour.2012.07.012).
- [98] Shi, J.; Yang, G.; Zhu, J. Sonochemical Fabrication of PDDA-RGO-PdPt Nanocomposites as Electrocatalyst for DAFCs. *J. Mater. Chem.* **2011**, *21*, 7343–7349. DOI: [10.1039/c1jm10333d](https://doi.org/10.1039/c1jm10333d).
- [99] Gong, X.; Yang, Y.; Huang, S. Mn₃O₄ Catalyzed Growth of Polycrystalline Pt Nanoparticles and Single Crystalline Pt Nanorods with High Index Facets. *Chem. Commun.* **2011**, *47*, 1009–1011. DOI: [10.1039/C0CC03656K](https://doi.org/10.1039/C0CC03656K).
- [100] Zhang, X.; Zhu, J.; Tiwary, C. S.; Ma, Z.; Huang, H.; Zhang, J.; Lu, Z.; Huang, W.; Wu, Y. Palladium Nanoparticles Supported on Nitrogen and Sulfur Dual-doped Graphene as Highly Active Electrocatalysts for Formic Acid and Methanol Oxidation. *ACS Appl. Mater. Interfaces.* **2016**, *8*, 10858–10865. DOI: [10.1021/acsami.6b01580](https://doi.org/10.1021/acsami.6b01580).
- [101] Qin, Y.; Jia, Y.; Jiang, Y.; Niu, D.; Zhang, X.; Zhou, X.; Niu, L.; Yuan, W. Controllable Synthesis of Carbon Nanofiber Supported Pd Catalyst for Formic Acid Electrooxidation. *Int. J. Hydrogen Energy.* **2012**, *37*, 7373–7377. DOI: [10.1016/j.ijhydene.2012.01.124](https://doi.org/10.1016/j.ijhydene.2012.01.124).
- [102] Singh, R.; Singh, A. Electrocatalytic Activity of Binary and Ternary Composite Films of Pd, MWCNT and Ni, Part II: Methanol Electrooxidation in 1 M KOH. *Int. J. Hydrogen Energy.* **2009**, *34*, 2052–2057. DOI: [10.1016/j.ijhydene.2008.12.047](https://doi.org/10.1016/j.ijhydene.2008.12.047).
- [103] Zhang, Y.; Shu, H.; Chang, G.; Ji, K.; Oyama, M.; Liu, X.; He, Y. Facile Synthesis of Palladium-graphene Nanocomposites and Their Catalysis for Electro-oxidation of Methanol and Ethanol. *Electrochim. Acta.* **2013**, *109*, 570–576. DOI: [10.1016/j.electacta.2013.07.068](https://doi.org/10.1016/j.electacta.2013.07.068).
- [104] Wang, X.; Wang, W.; Qi, Z.; Zhao, C.; Ji, H.; Zhang, Z. High Catalytic Activity of Ultrafine Nanoporous Palladium for Electro-oxidation of Methanol, Ethanol, and Formic Acid. *Electrochem. Commun.* **2009**, *11*, 1896–1899. DOI: [10.1016/j.elecom.2009.08.011](https://doi.org/10.1016/j.elecom.2009.08.011).
- [105] Liang, R.; Hu, A.; Persic, J.; Zhou, Y. N. Palladium Nanoparticles Loaded on Carbon Modified TiO₂ Nanobelts for Enhanced Methanol Electrooxidation. *Nano-Micro Lett.* **2013**, *5*, 202–212. DOI: [10.1007/BF03353751](https://doi.org/10.1007/BF03353751).

- [106] Qiao-Hui, G.; Huang, J.; Tian-Yan, Y. Electrospun Palladium Nanoparticle-loaded Carbon Nanofiber for Methanol Electro-oxidation. *Chin. J. Anal. Chem.* **2013**, *41*, 210–214. DOI: [10.1016/S1872-2040\(13\)60629-5](https://doi.org/10.1016/S1872-2040(13)60629-5).
- [107] Xiong, Q.; Tu, J.; Xia, X.; Zhao, X.; Gu, C.; Wang, X. A Three-dimensional Hierarchical Fe₂O₃ @ NiO Core/shell Nanorod Array on Carbon Cloth: A New Class of Anode for High-performance Lithium-ion Batteries. *Nanoscale*. **2013**, *5*, 7906–7912. DOI: [10.1039/c3nr02258g](https://doi.org/10.1039/c3nr02258g).
- [108] Xia, X.; Tu, J.; Zhang, Y.; Wang, X.; Gu, C.; Zhao, X.; Fan, H. J. High-quality Metal Oxide Core/shell Nanowire Arrays on Conductive Substrates for Electrochemical Energy Storage. *ACS Nano*. **2012**, *6*, 5531–5538. DOI: [10.1021/nn301454q](https://doi.org/10.1021/nn301454q).
- [109] Gu, C.; Huang, M.; Ge, X.; Zheng, H.; Wang, X.; Tu, J. NiO Electrode for Methanol Electro-oxidation: Mesoporous Vs. Nanoparticulate. *Int. J. Hydrogen Energy*. **2014**, *39*, 10892–10901. DOI: [10.1016/j.ijhydene.2014.05.028](https://doi.org/10.1016/j.ijhydene.2014.05.028).
- [110] Ge, X.; Gu, C.; Wang, X.; Tu, J. Anomalous Self-reduction of Layered Double Hydroxide (LDH): From α -Ni(OH)₂ to Hexagonal Close Packing (HCP) Ni/NiO by Annealing without a Reductant. *Chem. Commun.* **2015**, *51*, 1004–1007. DOI: [10.1039/C4CC07767A](https://doi.org/10.1039/C4CC07767A).
- [111] Azurdia, J. A.; McCrum, A.; Laine, R. M. Systematic Synthesis of Mixed-metal Oxides in NiO–Co₃O₄, NiO–MoO₃, and NiO–CuO Systems via Liquid-feed Flame Spray Pyrolysis. *J. Mater. Chem.* **2008**, *18*, 3249–3258. DOI: [10.1039/b801745j](https://doi.org/10.1039/b801745j).
- [112] Chen, W.; Rakhi, R.; Alshareef, H. N. High Energy Density Supercapacitors Using Macroporous Kitchen Sponges. *J. Mater. Chem.* **2012**, *22*, 14394–14402. DOI: [10.1039/c2jm32030d](https://doi.org/10.1039/c2jm32030d).
- [113] Tong, Y.; Gu, C.; Zhang, J.; Tang, H.; Wang, X.; Tu, J. Thermal Growth of NiO on Interconnected Ni–P Tube Network for Electrochemical Oxidation of Methanol in Alkaline Medium. *Int. J. Hydrogen Energy*. **2016**, *41*, 6342–6352. DOI: [10.1016/j.ijhydene.2016.03.018](https://doi.org/10.1016/j.ijhydene.2016.03.018).
- [114] Liu, J.; Du, S.; Wei, L.; Liu, H.; Tian, Y.; Chen, Y. Template-free Synthesis of NiO Hollow Microspheres Covered with Nanoflakes. *Mater. Lett.* **2006**, *60*, 3601–3604. DOI: [10.1016/j.matlet.2006.03.068](https://doi.org/10.1016/j.matlet.2006.03.068).
- [115] Al-Enizi, A. M.; Ghanem, M. A.; El-Zatahry, A. A.; Al-Deyab, S. S. Nickel Oxide/nitrogen Doped Carbon Nanofibers Catalyst for Methanol Oxidation in Alkaline Media. *Electrochim. Acta*. **2014**, *137*, 774–780. DOI: [10.1016/j.electacta.2014.05.150](https://doi.org/10.1016/j.electacta.2014.05.150).
- [116] Das, S.; Dutta, K.; Kundu, P. P. Nickel Nanocatalysts Supported on Sulfonated Polyaniline: Potential toward Methanol Oxidation and as Anode Materials for DMFCs. *J. Mater. Chem. A*. **2015**, *3*, 11349–11357. DOI: [10.1039/C5TA01837D](https://doi.org/10.1039/C5TA01837D).
- [117] Hatchett, D. W.; Millick, N. M.; Kinyanjui, J. M.; Pookpanratana, S.; Bär, M.; Hofmann, T.; Luinetti, A.; Heske, C. The Electrochemical Reduction of PdCl₄²⁻ and PdCl₆²⁻ in Polyaniline: Influence of Pd Deposit Morphology on Methanol Oxidation in Alkaline Solution. *Electrochim. Acta*. **2011**, *56*, 6060–6070. DOI: [10.1016/j.electacta.2011.04.083](https://doi.org/10.1016/j.electacta.2011.04.083).
- [118] Wang, Y.; Chen, W.; Pan, D.; Xu, Q.; Ma, J.; Zheng, J.; Li, R. Methanol Electrooxidation Reaction in Alkaline Medium on Glassy Carbon Electrode Modified with Ordered Mesoporous Ni/Al₂O₃. *Int.J.Electrochem.Sci.* **2017**, *12*, 2194–2206. DOI: [10.20964/2017.03.47](https://doi.org/10.20964/2017.03.47).
- [119] Jafarian, M.; Mahjani, M.; Heli, H.; Gobal, F.; Khajehsharifi, H.; Hamed, M. A Study of the Electro-catalytic Oxidation of Methanol on A Cobalt Hydroxide Modified Glassy Carbon Electrode. *Electrochim. Acta*. **2003**, *48*, 3423–3429. DOI: [10.1016/S0013-4686\(03\)00399-2](https://doi.org/10.1016/S0013-4686(03)00399-2).

- [120] Xia, Y.; Dai, H.; Jiang, H.; Zhang, L. Three-dimensional Ordered Mesoporous Cobalt Oxides: Highly Active Catalysts for the Oxidation of Toluene and Methanol. *Catal. Commun.* **2010**, *11*, 1171–1175. DOI: [10.1016/j.catcom.2010.07.005](https://doi.org/10.1016/j.catcom.2010.07.005).
- [121] Zafeiratos, S.; Dintzer, T.; Teschner, D.; Blume, R.; Hävecker, M.; Knop-Gericke, A.; Schlögl, R. Methanol Oxidation over Model Cobalt Catalysts: Influence of the Cobalt Oxidation State on the Reactivity. *J. Catal.* **2010**, *269*, 309–317. DOI: [10.1016/j.jcat.2009.11.013](https://doi.org/10.1016/j.jcat.2009.11.013).
- [122] Thamer, B. M.; El-Newehy, M. H.; Al-Deyab, S. S.; Abdelkareem, M. A.; Kim, H. Y.; Barakat, N. A. Cobalt-incorporated, Nitrogen-doped Carbon Nanofibers as Effective Non-precious Catalyst for Methanol Electrooxidation in Alkaline Medium. *Appl. Catal., A* **2015**, *498*, 230–240. DOI: [10.1016/j.apcata.2015.03.042](https://doi.org/10.1016/j.apcata.2015.03.042).
- [123] Shahid, M. M.; Pandikumar, A.; Golsheikh, A. M.; Huang, N. M.; Lim, H. N. Enhanced Electrocatalytic Performance of Cobalt Oxide Nanocubes Incorporating Reduced Graphene Oxide as a Modified Platinum Electrode for Methanol Oxidation. *RSC Adv.* **2014**, *4*, 62793–62801. DOI: [10.1039/C4RA08952A](https://doi.org/10.1039/C4RA08952A).
- [124] Shenashen, M. A.; Hassen, D.; El-Safty, S. A.; Isago, H.; Elmarakbi, A.; Yamaguchi, H. Axially Oriented Tubercle Vein and X-crossed Sheet of N-Co₃O₄@ C Hierarchical Mesoarchitectures as Potential Heterogeneous Catalysts for Methanol Oxidation Reaction. *Chem. Eng. J.* **2017**, *313*, 83–98. DOI: [10.1016/j.cej.2016.12.003](https://doi.org/10.1016/j.cej.2016.12.003).
- [125] Asgari, M.; Maragheh, M. G.; Davarkhah, R.; Lohrasbi, E.; Golikand, A. N. Electrocatalytic Oxidation of Methanol on the Nickel–cobalt Modified Glassy Carbon Electrode in Alkaline Medium. *Electrochim. Acta* **2012**, *59*, 284–289. DOI: [10.1016/j.electacta.2011.10.091](https://doi.org/10.1016/j.electacta.2011.10.091).
- [126] Yu, M.; Wang, S.; Hu, J.; Chen, Z.; Bai, Y.; Wu, L.; Chen, J.; Weng, X. Additive-free Macroscopic-scale Synthesis of Coral-like Nickel Cobalt Oxides with Hierarchical Pores and Their Electrocatalytic Properties for Methanol Oxidation. *Electrochim. Acta* **2014**, *145*, 300–306. DOI: [10.1016/j.electacta.2014.07.131](https://doi.org/10.1016/j.electacta.2014.07.131).
- [127] Sun, S.; Xu, Z. J. Composition Dependence of Methanol Oxidation Activity in Nickel–cobalt Hydroxides and Oxides: An Optimization toward Highly Active Electrodes. *Electrochim. Acta* **2015**, *165*, 56–66. DOI: [10.1016/j.electacta.2015.03.008](https://doi.org/10.1016/j.electacta.2015.03.008).
- [128] Rajeshkhanna, G.; Rao, G. R. Micro and Nano-architectures of Co₃O₄ on Ni Foam for Electro-oxidation of Methanol. *Int. J. Hydrogen Energy* **2018**, *43*, 4706–4715. DOI: [10.1016/j.ijhydene.2017.10.110](https://doi.org/10.1016/j.ijhydene.2017.10.110).
- [129] Wang, W.; Chu, Q.; Zhang, Y.; Zhu, W.; Wang, X.; Liu, X. Nickel Foam Supported Mesoporous NiCo₂O₄ Arrays with Excellent Methanol Electro-oxidation Performance. *New J. Chem.* **2015**, *39*, 6491–6497. DOI: [10.1039/C5NJ00766F](https://doi.org/10.1039/C5NJ00766F).
- [130] Ko, T.; Devarayan, K.; Seo, M.; Kim, H.; Kim, B. Facile Synthesis of Core/shell-like NiCo₂O₄-decorated MWCNTs and Its Excellent Electrocatalytic Activity for Methanol Oxidation. *Sci. Rep.* **2016**, *6*, 20313. DOI: [10.1038/srep20313](https://doi.org/10.1038/srep20313).
- [131] Tong, Y.; Gu, C.; Zhang, J.; Tang, H.; Li, Y.; Wang, X.; Tu, J. Urchin-like Ni-Co-PO Nanocomposite as Novel Methanol Electro-oxidation Materials in Alkaline Environment. *Electrochim. Acta* **2016**, *187*, 11–19. DOI: [10.1016/j.electacta.2015.10.195](https://doi.org/10.1016/j.electacta.2015.10.195).
- [132] Vernickaite, E.; Tsyttsaru, N.; Cesiulis, H. Electrodeposited Co-W Alloys and Their Prospects as Effective Anode for Methanol Oxidation in Acidic Media. *Surf. Coat. Technol.* **2016**, *307*, 1322–1328. DOI: [10.1016/j.surfcoat.2016.07.049](https://doi.org/10.1016/j.surfcoat.2016.07.049).
- [133] Barakat, N. A.; Abdelkareem, M. A.; Yousef, A.; Al-Deyab, S. S.; El-Newehy, M.; Kim, H. Y. Cadmium-doped Cobalt/carbon Nanoparticles as Novel Nonprecious Electrocatalyst for Methanol Oxidation. *Int. J. Hydrogen Energy* **2013**, *38*, 3387–3394. DOI: [10.1016/j.ijhydene.2012.12.097](https://doi.org/10.1016/j.ijhydene.2012.12.097).

- [134] Zhang, M.; Li, Y.; Yan, Z.; Jing, J.; Xie, J.; Chen, M. Improved Catalytic Activity of Cobalt Core–platinum Shell Nanoparticles Supported on Surface Functionalized Graphene for Methanol Electro-oxidation. *Electrochim. Acta.* **2015**, *158*, 81–88. DOI: [10.1016/j.electacta.2015.01.160](https://doi.org/10.1016/j.electacta.2015.01.160).
- [135] Zeng, J.; Lee, J. Y. Ruthenium-free, Carbon-supported Cobalt and Tungsten Containing Binary & Ternary Pt Catalysts for the Anodes of Direct Methanol Fuel Cells. *Int. J. Hydrogen Energy.* **2007**, *32*, 4389–4396. DOI: [10.1016/j.ijhydene.2007.03.012](https://doi.org/10.1016/j.ijhydene.2007.03.012).
- [136] Huang, H.; Hu, X.; Zhang, J.; Su, N.; Cheng, J. Facile Fabrication of Platinum-cobalt Alloy Nanoparticles with Enhanced Electrocatalytic Activity for a Methanol Oxidation Reaction. *Sci. Rep.* **2017**, *7*, 45555. DOI: [10.1038/srep45555](https://doi.org/10.1038/srep45555).
- [137] Zhang, M.; Yan, Z.; Li, Y.; Jing, J.; Xie, J. Preparation of Cobalt Silicide on Graphene as Pt Electrocatalyst Supports for Highly Efficient and Stable Methanol Oxidation in Acidic Media. *Electrochim. Acta.* **2015**, *161*, 48–54. DOI: [10.1016/j.electacta.2015.01.221](https://doi.org/10.1016/j.electacta.2015.01.221).
- [138] Qin, Y.; Zhang, X.; Dai, X.; Sun, H.; Yang, Y.; Shi, Q.; Gao, D.; Wang, H. Platinum–cobalt Nanocrystals Synthesized under Different Atmospheres for High Catalytic Performance in Methanol Electro-oxidation. *J. Mater. Chem. A.* **2015**, *3*, 10671–10676. DOI: [10.1039/C5TA01950H](https://doi.org/10.1039/C5TA01950H).
- [139] Schimka, L.; Harl, J.; Stroppa, A.; Grüneis, A.; Marsman, M.; Mittendorfer, F.; Kresse, G. Accurate Surface and Adsorption Energies from Many-body Perturbation Theory. *Nat. Mater.* **2010**, *9*, 741. DOI: [10.1038/nmat2806](https://doi.org/10.1038/nmat2806).
- [140] Hori, Y.; Murata, A.; Yoshinami, Y. Adsorption of CO, Intermediately Formed in Electrochemical Reduction of CO₂, at a Copper Electrode. *J Chem Soc Faraday Trans.* **1991**, *87*, 125–128. DOI: [10.1039/ft9918700125](https://doi.org/10.1039/ft9918700125).
- [141] Carugno, S.; Chassaing, E.; Rosso, M.; González, G. A. Enhanced Electrochemical Oxidation of Methanol on Copper Electrodes Modified by Electrocorrosion and Electrodeposition. *Mater. Chem. Phys.* **2014**, *143*, 1012–1017. DOI: [10.1016/j.matchemphys.2013.10.039](https://doi.org/10.1016/j.matchemphys.2013.10.039).
- [142] Han, L.; Cui, P.; He, H.; Liu, H.; Peng, Z.; Yang, J. A Seed-mediated Approach to the Morphology-controlled Synthesis of Bimetallic Copper–platinum Alloy Nanoparticles with Enhanced Electrocatalytic Performance for the Methanol Oxidation Reaction. *J. Power Sources.* **2015**, *286*, 488–494. DOI: [10.1016/j.jpowsour.2015.04.003](https://doi.org/10.1016/j.jpowsour.2015.04.003).
- [143] Ren, Y.; Zhang, S.; Lin, R.; Wei, X. Electro-catalytic Performance of Pd Decorated Cu Nanowires Catalyst for the Methanol Oxidation. *Int. J. Hydrogen Energy.* **2015**, *40*, 2621–2630. DOI: [10.1016/j.ijhydene.2014.12.005](https://doi.org/10.1016/j.ijhydene.2014.12.005).
- [144] Chen, D.; Zhao, Y.; Peng, X.; Wang, X.; Hu, W.; Jing, C.; Tian, S.; Tian, J. Star-like PtCu Nanoparticles Supported on Graphene with Superior Activity for Methanol Electro-oxidation. *Electrochim. Acta.* **2015**, *177*, 86–92. DOI: [10.1016/j.electacta.2015.03.066](https://doi.org/10.1016/j.electacta.2015.03.066).
- [145] Xu, W.; Zhu, S.; Li, Z.; Cui, Z.; Yang, X. Evolution of Palladium/copper Oxide–titanium Dioxide Nanostructures by Dealloying and Their Catalytic Performance for Methanol Electro-oxidation. *J. Power Sources.* **2015**, *274*, 1034–1042. DOI: [10.1016/j.jpowsour.2014.10.147](https://doi.org/10.1016/j.jpowsour.2014.10.147).
- [146] Yang, L.; Yan, D.; Liu, C.; Song, H.; Tang, Y.; Luo, S.; Liu, M. Vertically Oriented Reduced Graphene Oxide Supported Dealloyed Palladium–copper Nanoparticles for Methanol Electrooxidation. *J. Power Sources.* **2015**, *278*, 725–732. DOI: [10.1016/j.jpowsour.2014.12.141](https://doi.org/10.1016/j.jpowsour.2014.12.141).
- [147] Arulmani, S.; Krishnamoorthy, S.; Wu, J. J.; Anandan, S. High-Performance Electrocatalytic Activity of Palladium–Copper Nanoalloy Towards Methanol Electro-oxidation in an Alkaline Medium. *Electroanalysis.* **2017**, *29*, 433–440. DOI: [10.1002/elan.201600164](https://doi.org/10.1002/elan.201600164).

- [148] Chang, R.; Zheng, L.; Wang, C.; Yang, D.; Zhang, G.; Sun, S. Synthesis of Hierarchical Platinum-palladium-copper Nanodendrites for Efficient Methanol Oxidation. *Appl. Catal. B Environ.* **2017**, *211*, 205–211. DOI: [10.1016/j.apcatb.2017.04.040](https://doi.org/10.1016/j.apcatb.2017.04.040).
- [149] Shi, X.; Wen, Y.; Guo, X.; Pan, Y.; Ji, Y.; Ying, Y.; Yang, H. Dendritic CuPtPd Catalyst for Enhanced Electrochemical Oxidation of Methanol. *ACS Appl. Mater. Interfaces.* **2017**, *9*, 25995–26000. DOI: [10.1021/acsami.7b06296](https://doi.org/10.1021/acsami.7b06296).
- [150] Zheng, J.; Cullen, D. A.; Forest, R. V.; Wittkopf, J. A.; Zhuang, Z.; Sheng, W.; Chen, J. G.; Yan, Y. Platinum–ruthenium Nanotubes and Platinum–ruthenium Coated Copper Nanowires as Efficient Catalysts for Electro-oxidation of Methanol. *ACS Catal.* **2015**, *5*, 1468–1474. DOI: [10.1021/cs501449y](https://doi.org/10.1021/cs501449y).
- [151] Liu, F.; Dang, D.; Tian, X. Platinum-decorated Three Dimensional Titanium Copper Nitride Architectures with Durable Methanol Oxidation Reaction Activity. *Int. J. Hydrogen Energy.* **2019**, *44*, 8415–8424. DOI: [10.1016/j.ijhydene.2019.02.059](https://doi.org/10.1016/j.ijhydene.2019.02.059).
- [152] Fu, S.; Zhu, C.; Du, D.; Lin, Y. Enhanced Electrocatalytic Activities of PtCuCoNi Three-dimensional Nanoporous Quaternary Alloys for Oxygen Reduction and Methanol Oxidation Reactions. *ACS Appl. Mater. Interfaces.* **2016**, *8*, 6110–6116. DOI: [10.1021/acsami.6b00424](https://doi.org/10.1021/acsami.6b00424).
- [153] Chen, X.; Si, C.; Gao, Y.; Frenzel, J.; Sun, J.; Eggeler, G.; Zhang, Z. Multi-component Nanoporous Platinum–ruthenium–copper–osmium–iridium Alloy with Enhanced Electrocatalytic Activity Towards Methanol Oxidation and Oxygen Reduction. *J. Power Sources.* **2015**, *273*, 324–332. DOI: [10.1016/j.jpowsour.2014.09.076](https://doi.org/10.1016/j.jpowsour.2014.09.076).
- [154] Chen, X.; Wang, H.; Wang, Y.; Bai, Q.; Gao, Y.; Zhang, Z. Synthesis and Electrocatalytic Performance of Multi-component Nanoporous PtRuCuW Alloy for Direct Methanol Fuel Cells. *Catalysts.* **2015**, *5*, 1003–1015. DOI: [10.3390/catal5031003](https://doi.org/10.3390/catal5031003).
- [155] Döner, A.; Solmaz, R.; Kardaş, G. Fabrication and Characterization of Alkaline Leached CuZn/Cu Electrode as Anode Material for Direct Methanol Fuel Cell. *Energy.* **2015**, *90*, 1144–1151. DOI: [10.1016/j.energy.2015.06.058](https://doi.org/10.1016/j.energy.2015.06.058).
- [156] Sun, Y.; Zhou, Y.; Zhu, C.; Tu, W.; Wang, H.; Huang, H.; Liu, Y.; Shao, M.; Zhong, J.; Lee, S. Synergistic Cu@CoOx Core-cage Structure on Carbon Layers as Highly Active and Durable Electrocatalysts for Methanol Oxidation. *Appl. Catal. B Environ.* **2019**, *244*, 795–801. DOI: [10.1016/j.apcatb.2018.12.017](https://doi.org/10.1016/j.apcatb.2018.12.017).
- [157] Cao, H.; Fan, Z.; Hou, G.; Tang, Y.; Zheng, G. Ball-flower-shaped Ni Nanoparticles on Cu Modified TiO₂ Nanotube Arrays for Electrocatalytic Oxidation of Methanol. *Electrochim. Acta.* **2014**, *125*, 275–281. DOI: [10.1016/j.electacta.2014.01.101](https://doi.org/10.1016/j.electacta.2014.01.101).
- [158] Ehsani, A.; Jaleh, B.; Nasrollahzadeh, M. Electrochemical Properties and Electrocatalytic Activity of Conducting Polymer/copper Nanoparticles Supported on Reduced Graphene Oxide Composite. *J. Power Sources.* **2014**, *257*, 300–307. DOI: [10.1016/j.jpowsour.2014.02.010](https://doi.org/10.1016/j.jpowsour.2014.02.010).
- [159] Sun, J.; Shi, J.; Xu, J.; Chen, X.; Zhang, Z.; Peng, Z. Enhanced Methanol Electro-oxidation and Oxygen Reduction Reaction Performance of Ultrafine Nanoporous Platinum–copper Alloy: Experiment and Density Functional Theory Calculation. *J. Power Sources.* **2015**, *279*, 334–344. DOI: [10.1016/j.jpowsour.2015.01.025](https://doi.org/10.1016/j.jpowsour.2015.01.025).
- [160] Na, H.; Zhang, L.; Qiu, H.; Wu, T.; Chen, M.; Yang, N.; Li, L.; Xing, F.; Gao, J. A Two Step Method to Synthesize Palladium–copper Nanoparticles on Reduced Graphene Oxide and Their Extremely High Electrocatalytic Activity for the Electrooxidation of Methanol and Ethanol. *J. Power Sources.* **2015**, *288*, 160–167. DOI: [10.1016/j.jpowsour.2015.04.116](https://doi.org/10.1016/j.jpowsour.2015.04.116).

- [161] Liao, Y.; Yu, G.; Zhang, Y.; Guo, T.; Chang, F.; Zhong, C. Composition-tunable PtCu Alloy Nanowires and Electrocatalytic Synergy for Methanol Oxidation Reaction. *J. Phys. Chem. C*. **2016**, *120*, 10476–10484. DOI: [10.1021/acs.jpcc.6b02630](https://doi.org/10.1021/acs.jpcc.6b02630).
- [162] Huang, M.; Guan, L. Facile Synthesis of Carbon Supported Pt–Cu Nanomaterials with Surface Enriched Pt as Highly Active Anode Catalyst for Methanol Oxidation. *Int. J. Hydrogen Energy*. **2015**, *40*, 6546–6551. DOI: [10.1016/j.ijhydene.2015.03.099](https://doi.org/10.1016/j.ijhydene.2015.03.099).
- [163] Tang, Y.; Cheng, W. Nanoparticle-modified Electrode with Size-and Shape-dependent Electrocatalytic Activities. *Langmuir*. **2013**, *29*, 3125–3132. DOI: [10.1021/la304616k](https://doi.org/10.1021/la304616k).
- [164] Hosseini, M. G.; Abdolmaleki, M.; Ashrafpoor, S. Methanol Electro-oxidation on a Porous Nanostructured Ni/Pd-Ni Electrode in Alkaline Media. *Chin. J. Catal.* **2013**, *34*, 1712–1719. DOI: [10.1016/S1872-2067\(12\)60643-3](https://doi.org/10.1016/S1872-2067(12)60643-3).
- [165] Telli, E.; Solmaz, R.; Kardaş, G. Electrocatalytic Oxidation of Methanol on Pt/NiZn Electrode in Alkaline Medium. *Russian J. Electrochem.* **2011**, *47*, 811–818. DOI: [10.1134/S1023193511070135](https://doi.org/10.1134/S1023193511070135).
- [166] Sheikh, A.; Abd-Allfah, K. E.; Malfatti, C. On Reviewing the Catalyst Materials for Direct Alcohol Fuel Cells (Dafcs). *energy*. **2014**, *1*, 1–10.
- [167] Serov, A.; Kwak, C. Review of Non-platinum Anode Catalysts for DMFC and PEMFC Application. *Appl. Catal. B Environ.* **2009**, *90*, 313–320. DOI: [10.1016/j.apcatb.2009.03.030](https://doi.org/10.1016/j.apcatb.2009.03.030).
- [168] Rahim, M. A.; Hameed, R. A.; Khalil, M. Nickel as a Catalyst for the Electro-oxidation of Methanol in Alkaline Medium. *J. Power Sources*. **2004**, *134*, 160–169. DOI: [10.1016/j.jpowsour.2004.02.034](https://doi.org/10.1016/j.jpowsour.2004.02.034).
- [169] OGUMI, Z.; MATSUOKA, K.; CHIBA, S.; MATSUOKA, M.; IRIYAMA, Y.; ABE, T.; INABA, M. Preliminary Study on Direct Alcohol Fuel Cells Employing Anion Exchange Membrane. *Electrochemistry*. **2002**, *70*, 980–983. DOI: [10.5796/electrochemistry.70.980](https://doi.org/10.5796/electrochemistry.70.980).
- [170] Danks, T. N.; Slade, R. C.; Varcoe, J. R. Comparison of PVDF-and FEP-based Radiation-grafted Alkaline Anion-exchange Membranes for Use in Low Temperature Portable DMFCs. *J. Mater. Chem.* **2002**, *12*, 3371–3373. DOI: [10.1039/b208627a](https://doi.org/10.1039/b208627a).
- [171] Danks, T. N.; Slade, R. C.; Varcoe, J. R. Alkaline Anion-exchange Radiation-grafted Membranes for Possible Electrochemical Application in Fuel Cells. *J. Mater. Chem.* **2003**, *13*, 712–721. DOI: [10.1039/b212164f](https://doi.org/10.1039/b212164f).
- [172] McLean, G.; Niet, T.; Prince-Richard, S.; Djilali, N. An Assessment of Alkaline Fuel Cell Technology. *Int. J. Hydrogen Energy*. **2002**, *27*, 507–526. DOI: [10.1016/S0360-3199\(01\)00181-1](https://doi.org/10.1016/S0360-3199(01)00181-1).
- [173] Agel, E.; Bouet, J.; Fauvarque, J. Characterization and Use of Anionic Membranes for Alkaline Fuel Cells. *J. Power Sources*. **2001**, *101*, 267–274. DOI: [10.1016/S0378-7753\(01\)00759-5](https://doi.org/10.1016/S0378-7753(01)00759-5).
- [174] Xing, B.; Savadogo, O. Hydrogen/oxygen Polymer Electrolyte Membrane Fuel Cells (Pemfcs) Based on Alkaline-doped Polybenzimidazole (PBI). *Electrochem. Commun.* **2000**, *2*, 697–702. DOI: [10.1016/S1388-2481\(00\)00107-7](https://doi.org/10.1016/S1388-2481(00)00107-7).
- [175] Tripković, A. V.; Popović, K. D.; Grgur, B. N.; Blizanac, B.; Ross, P.; Marković, N. Methanol Electrooxidation on Supported Pt and PtRu Catalysts in Acid and Alkaline Solutions. *Electrochim. Acta*. **2002**, *47*, 3707–3714. DOI: [10.1016/S0013-4686\(02\)00340-7](https://doi.org/10.1016/S0013-4686(02)00340-7).
- [176] Wang, Y.; Li, L.; Hu, L.; Zhuang, L.; Lu, J.; Xu, B. A Feasibility Analysis for Alkaline Membrane Direct Methanol Fuel Cell: Thermodynamic Disadvantages versus Kinetic Advantages. *Electrochem. Commun.* **2003**, *5*, 662–666. DOI: [10.1016/S1388-2481\(03\)00148-6](https://doi.org/10.1016/S1388-2481(03)00148-6).

- [177] Sata, T.; Tsujimoto, M.; Yamaguchi, T.; Matsusaki, K. Change of Anion Exchange Membranes in an Aqueous Sodium Hydroxide Solution at High Temperature. *J. Membr. Sci.* **1996**, *112*, 161–170. DOI: [10.1016/0376-7388\(95\)00292-8](https://doi.org/10.1016/0376-7388(95)00292-8).
- [178] Kim, S.; Park, S. Electroactivity of Pt–Ru/polyaniline Composite Catalyst-electrodes Prepared by Electrochemical Deposition Methods. *Solid State Ionics.* **2008**, *178*, 1915–1921.
- [179] Choi, J.; Kim, Y.; Lee, J.; Cho, K.; Jung, H.; Park, J.; Park, I.; Sung, Y. A Polyaniline Supported PtRu Nanocomposite Anode and A Pd-impregnated Nanocomposite Nafion Membrane for DMFCs. *Solid State Ionics.* **2005**, *176*, 3031–3034. DOI: [10.1016/j.ssi.2005.09.041](https://doi.org/10.1016/j.ssi.2005.09.041).
- [180] Amani, M.; Kazemeini, M.; Hamedanian, M.; Pahlavanzadeh, H.; Gharibi, H. Investigation of Methanol Oxidation on a Highly Active and Stable Pt–Sn Electrocatalyst Supported on Carbon–polyaniline Composite for Application in a Passive Direct Methanol Fuel Cell. *Mater. Res. Bull.* **2015**, *68*, 166–178. DOI: [10.1016/j.materresbull.2015.02.053](https://doi.org/10.1016/j.materresbull.2015.02.053).
- [181] Dutta, K.; Kumar, P.; Das, S.; Kundu, P. P. Utilization of Conducting Polymers in Fabricating Polymer Electrolyte Membranes for Application in Direct Methanol Fuel Cells. *Polym. Rev.* **2014**, *54*, 1–32. DOI: [10.1080/15583724.2013.839566](https://doi.org/10.1080/15583724.2013.839566).
- [182] Mahale, R. Y.; Arulkashmir, A.; Dutta, K.; Krishnamoorthy, K. Band Edge Modulated Conjugated Polymers for Oxidation Prevention. *Phys. Chem. Chem. Phys.* **2012**, *14*, 4577–4583. DOI: [10.1039/c2cp23544g](https://doi.org/10.1039/c2cp23544g).
- [183] Dutta, K.; Kundu, P. P. Amphiphiles as Hydrophobicity Regulator: Fine Tuning the Surface Hydrophobicity of an Electropolymerized Film. *J. Colloid Interface Sci.* **2013**, *397*, 192–198. DOI: [10.1016/j.jcis.2013.01.045](https://doi.org/10.1016/j.jcis.2013.01.045).
- [184] Dutta, K.; Kundu, P. P. Interaction between Oxidized Polyaniline and Oppositely Charged Amphiphilic Assemblies in an Aqueous/organic Biphase System. *J. Colloid Interface Sci.* **2013**, *407*, 516–523. DOI: [10.1016/j.jcis.2013.06.038](https://doi.org/10.1016/j.jcis.2013.06.038).
- [185] Dutta, K.; Kundu, P. P. Reversible Assembly and Disassembly of Amphiphilic Assemblies by Electropolymerized Polyaniline Films: Effects Rendered by Varying the Electropolymerization Potential. *J. Phys. Chem. B.* **2013**, *117*, 7797–7805. DOI: [10.1021/jp402748w](https://doi.org/10.1021/jp402748w).
- [186] Dutta, K.; Kumar, P.; Das, S.; Kundu, P. P. Effects of Various Factors on the Interfacial Mass Transfer Phenomenon and Dispersion of Polyaniline in an Aqueous/organic Bi-/tri-phasic System. *Colloids Surf. Physicochem. Eng. Aspects.* **2013**, *436*, 830–838. DOI: [10.1016/j.colsurfa.2013.07.046](https://doi.org/10.1016/j.colsurfa.2013.07.046).
- [187] Selvaraj, V.; Alagar, M. Pt and Pt–Ru Nanoparticles Decorated Polypyrrole/multiwalled Carbon Nanotubes and Their Catalytic Activity Towards Methanol Oxidation. *Electrochem. Commun.* **2007**, *9*, 1145–1153. DOI: [10.1016/j.elecom.2007.01.011](https://doi.org/10.1016/j.elecom.2007.01.011).
- [188] Zhang, L.; Wang, Z.; Zhang, J.; Sui, X.; Zhao, L.; Gu, D. Honeycomb-like Mesoporous Nitrogen-doped Carbon Supported Pt Catalyst for Methanol Electrooxidation. *Carbon.* **2015**, *93*, 1050–1058. DOI: [10.1016/j.carbon.2015.06.022](https://doi.org/10.1016/j.carbon.2015.06.022).
- [189] Yin, S.; Shen, P. K.; Song, S.; Jiang, S. P. Functionalization of Carbon Nanotubes by an Effective Intermittent Microwave Heating-assisted HF/H₂O₂ Treatment for Electrocatalyst Support of Fuel Cells. *Electrochim. Acta.* **2009**, *54*, 6954–6958. DOI: [10.1016/j.electacta.2009.07.009](https://doi.org/10.1016/j.electacta.2009.07.009).
- [190] Carmo, M.; Linardi, M.; Poco, J. G. R. H₂O₂ Treated Carbon Black as Electrocatalyst Support for Polymer Electrolyte Membrane Fuel Cell Applications. *Int. J. Hydrogen Energy.* **2008**, *33*, 6289–6297. DOI: [10.1016/j.ijhydene.2008.08.021](https://doi.org/10.1016/j.ijhydene.2008.08.021).
- [191] Salgado, J.; Paganin, V.; Gonzalez, E.; Montemor, M.; Tacchini, I.; Ansón, A.; Salvador, M.; Ferreira, P.; Figueiredo, F.; Ferreira, M. Characterization and

- Performance Evaluation of Pt–Ru Electrocatalysts Supported on Different Carbon Materials for Direct Methanol Fuel Cells. *Int. J. Hydrogen Energy*. 2013, 38, 910–920. DOI: [10.1016/j.ijhydene.2012.10.079](https://doi.org/10.1016/j.ijhydene.2012.10.079).
- [192] Hameed, R. A.; El-Sherif, R. M. Microwave Irradiated Nickel Nanoparticles on Vulcan XC-72R Carbon Black for Methanol Oxidation Reaction in KOH Solution. *Appl. Catal. B Environ*. 2015, 162, 217–226. DOI: [10.1016/j.apcatb.2014.06.057](https://doi.org/10.1016/j.apcatb.2014.06.057).
- [193] Qian, H.; Huang, H.; Wang, X. Design and Synthesis of Palladium/graphitic Carbon Nitride/carbon Black Hybrids as High-performance Catalysts for Formic Acid and Methanol Electrooxidation. *J. Power Sources*. 2015, 275, 734–741. DOI: [10.1016/j.jpowsour.2014.10.109](https://doi.org/10.1016/j.jpowsour.2014.10.109).
- [194] Li, Y.; Liu, C.; Liu, Y.; Feng, B.; Li, L.; Pan, H.; Kellogg, W.; Higgins, D.; Wu, G. Sn-doped TiO₂ Modified Carbon to Support Pt Anode Catalysts for Direct Methanol Fuel Cells. *J. Power Sources*. 2015, 286, 354–361. DOI: [10.1016/j.jpowsour.2015.03.155](https://doi.org/10.1016/j.jpowsour.2015.03.155).
- [195] Amin, R.; Hameed, R. A.; El-Khatib, K.; Youssef, M. E. Electrocatalytic Activity of Nanostructured Ni and Pd–Ni on Vulcan XC-72R Carbon Black for Methanol Oxidation in Alkaline Medium. *Int. J. Hydrogen Energy*. 2014, 39, 2026–2041. DOI: [10.1016/j.ijhydene.2013.11.033](https://doi.org/10.1016/j.ijhydene.2013.11.033).
- [196] Huang, X.; Chen, Y.; Zhu, E.; Xu, Y.; Duan, X.; Huang, Y. Monodisperse Cu@ PtCu Nanocrystals and Their Conversion into hollow-PtCu Nanostructures for Methanol Oxidation. *J. Mater. Chem. A*. 2013, 1, 14449–14454. DOI: [10.1039/c3ta13903d](https://doi.org/10.1039/c3ta13903d).
- [197] Calvillo, L.; Gangeri, M.; Perathoner, S.; Centi, G.; Moliner, R.; Lázaro, M. Synthesis and Performance of Platinum Supported on Ordered Mesoporous Carbons as Catalyst for PEM Fuel Cells: Effect of the Surface Chemistry of the Support. *Int. J. Hydrogen Energy*. 2011, 36, 9805–9814. DOI: [10.1016/j.ijhydene.2011.03.023](https://doi.org/10.1016/j.ijhydene.2011.03.023).
- [198] Soo, L. T.; Loh, K. S.; Mohamad, A. B.; Daud, W. R. W.; Wong, W. Y. An Overview of the Electrochemical Performance of Modified Graphene Used as an Electrocatalyst and as a Catalyst Support in Fuel Cells. *Appl. Catal., A*. 2015, 497, 198–210. DOI: [10.1016/j.apcata.2015.03.008](https://doi.org/10.1016/j.apcata.2015.03.008).
- [199] An, H.; An, G.; Ahn, H. Octahedral Co₃O₄/carbon Nanofiber Composite-supported Pt Catalysts for Improved Methanol Electrooxidation. *J. Alloys Compounds*. 2015, 645, 317–321. DOI: [10.1016/j.jallcom.2015.05.105](https://doi.org/10.1016/j.jallcom.2015.05.105).
- [200] Ito, Y.; Takeuchi, T.; Tsujiguchi, T.; Abdelkareem, M. A.; Nakagawa, N. Ultrahigh Methanol Electro-oxidation Activity of PtRu Nanoparticles Prepared on TiO₂-embedded Carbon Nanofiber Support. *J. Power Sources*. 2013, 242, 280–288. DOI: [10.1016/j.jpowsour.2013.05.064](https://doi.org/10.1016/j.jpowsour.2013.05.064).
- [201] Chen, J.; Niu, Q.; Chen, G.; Nie, J.; Ma, G. Electrooxidation of Methanol on Pt@ Ni Bimetallic Catalyst Supported on Porous Carbon Nanofibers. *J. Phys. Chem. C*. 2017, 121, 1463–1471. DOI: [10.1021/acs.jpcc.6b10882](https://doi.org/10.1021/acs.jpcc.6b10882).
- [202] Mu, X.; Xu, Z.; Xie, Y.; Mi, H.; Ma, J. Pt Nanoparticles Supported on Co Embedded Coal-based Carbon Nanofiber for Enhanced Electrocatalytic Activity Towards Methanol Electro-oxidation. *J. Alloys Compounds*. 2017, 711, 374–380. DOI: [10.1016/j.jallcom.2017.04.008](https://doi.org/10.1016/j.jallcom.2017.04.008).
- [203] Singh, B.; Dempsey, E. Exceptional Pt Nanoparticle Decoration of Functionalised Carbon Nanofibers: A Strategy to Improve the Utility of Pt and Support Material for Direct Methanol Fuel Cell Applications. *RSC Adv*. 2013, 3, 2279–2287. DOI: [10.1039/c2ra21862c](https://doi.org/10.1039/c2ra21862c).
- [204] Barakat, N. A.; El-Newehy, M.; Al-Deyab, S. S.; Kim, H. Y. Cobalt/copper-decorated Carbon Nanofibers as Novel Non-precious Electrocatalyst for Methanol Electrooxidation. *Nanoscale Res. Lett*. 2014, 9, 2. DOI: [10.1186/1556-276X-9-2](https://doi.org/10.1186/1556-276X-9-2).

- [205] Ghouri, Z. K.; Barakat, N. A.; Park, M.; Kim, B.; Kim, H. Y. Synthesis and Characterization of Co/SrCO₃ Nanorods-decorated Carbon Nanofibers as Novel Electrocatalyst for Methanol Oxidation in Alkaline Medium. *Ceram. Int.* **2015**, *41*, 6575–6582. DOI: [10.1016/j.ceramint.2015.01.103](https://doi.org/10.1016/j.ceramint.2015.01.103).
- [206] Ghouri, Z. K.; Barakat, N. A.; Obaid, M.; Lee, J. H.; Kim, H. Y. Co/CeO₂-decorated Carbon Nanofibers as Effective Non-precious Electro-catalyst for Fuel Cells Application in Alkaline Medium. *Ceram. Int.* **2015**, *41*, 2271–2278. DOI: [10.1016/j.ceramint.2014.10.031](https://doi.org/10.1016/j.ceramint.2014.10.031).
- [207] Elbasri, M.; Perrot, H.; Sel, O.; Lafdi, K.; El Rhazi, M. Synthesis of Carbon Nanofibers/poly (Para-phenylenediamine)/nickel Particles Nanocomposite for Enhanced Methanol Electrooxidation. *Int. J. Hydrogen Energy.* **2019**, *44*, 24534–24545. DOI: [10.1016/j.ijhydene.2019.07.141](https://doi.org/10.1016/j.ijhydene.2019.07.141).
- [208] Titirici, M. M.; Thomas, A.; Yu, S.; Müller, J.; Antonietti, M. A Direct Synthesis of Mesoporous Carbons with Bicontinuous Pore Morphology from Crude Plant Material by Hydrothermal Carbonization. *Chem. Mater.* **2007**, *19*, 4205–4212. DOI: [10.1021/cm0707408](https://doi.org/10.1021/cm0707408).
- [209] Liang, C.; Li, Z.; Dai, S. Mesoporous Carbon Materials: Synthesis and Modification. *Angew. Chem. Int. Ed.* **2008**, *47*, 3696–3717. DOI: [10.1002/anie.200702046](https://doi.org/10.1002/anie.200702046).
- [210] Tamai, H.; Kakii, T.; Hirota, Y.; Kumamoto, T.; Yasuda, H. Synthesis of Extremely Large Mesoporous Activated Carbon and Its Unique Adsorption for Giant Molecules. *Chem. Mater.* **1996**, *8*, 454–462. DOI: [10.1021/cm950381t](https://doi.org/10.1021/cm950381t).
- [211] Zhou, T.; Wang, H.; Ji, S.; Linkov, V.; Wang, R. Soybean-derived Mesoporous Carbon as an Effective Catalyst Support for Electrooxidation of Methanol. *J. Power Sources.* **2014**, *248*, 427–433. DOI: [10.1016/j.jpowsour.2013.09.108](https://doi.org/10.1016/j.jpowsour.2013.09.108).
- [212] Qi, J.; Jiang, L.; Tang, Q.; Zhu, S.; Wang, S.; Yi, B.; Sun, G. Synthesis of Graphitic Mesoporous Carbons with Different Surface Areas and Their Use in Direct Methanol Fuel Cells. *Carbon.* **2012**, *50*, 2824–2831. DOI: [10.1016/j.carbon.2012.02.049](https://doi.org/10.1016/j.carbon.2012.02.049).
- [213] Wang, Y.; He, C.; Brouzgou, A.; Liang, Y.; Fu, R.; Wu, D.; Tsiakaras, P.; Song, S. A Facile Soft-template Synthesis of Ordered Mesoporous Carbon/tungsten Carbide Composites with High Surface Area for Methanol Electrooxidation. *J. Power Sources.* **2012**, *200*, 8–13. DOI: [10.1016/j.jpowsour.2011.10.037](https://doi.org/10.1016/j.jpowsour.2011.10.037).
- [214] Zhang, C.; Xu, L.; Shan, N.; Sun, T.; Chen, J.; Yan, Y. Enhanced Electrocatalytic Activity and Durability of Pt Particles Supported on Ordered Mesoporous Carbon Spheres. *ACS Catal.* **2014**, *4*, 1926–1930. DOI: [10.1021/cs500107t](https://doi.org/10.1021/cs500107t).
- [215] Long, G.; Li, X.; Wan, K.; Liang, Z.; Piao, J.; Tsiakaras, P. Pt/CN-doped Electrocatalysts: Superior Electrocatalytic Activity for Methanol Oxidation Reaction and Mechanistic Insight into Interfacial Enhancement. *Appl. Catal. B Environ.* **2017**, *203*, 541–548. DOI: [10.1016/j.apcatb.2016.10.055](https://doi.org/10.1016/j.apcatb.2016.10.055).
- [216] Tan, Q.; Shu, C. Y.; Abbott, J.; Zhao, Q.; Liu, L.; Qu, T.; Chen, Y.; Zhu, H.; Liu, Y.; Wu, G. Highly Dispersed Pd-CeO₂ Nanoparticles Supported on N-doped Core-Shell Structured Mesoporous Carbon for Methanol Oxidation in Alkaline Media. *ACS Catal.* **2019**. DOI: [10.1021/acscatal.9b00726](https://doi.org/10.1021/acscatal.9b00726).
- [217] Xiang, D.; Yin, L. Well-dispersed and Size-tuned Bimetallic PtFe X Nanoparticle Catalysts Supported on Ordered Mesoporous Carbon for Enhanced Electrocatalytic Activity in Direct Methanol Fuel Cells. *J. Mater. Chem.* **2012**, *22*, 9584–9593. DOI: [10.1039/c2jm16641k](https://doi.org/10.1039/c2jm16641k).
- [218] Li, F.; Chan, K.; Yung, H.; Yang, C.; Ting, S. W. Uniform Dispersion of 1: 1 PtRu Nanoparticles in Ordered Mesoporous Carbon for Improved Methanol Oxidation. *Phys. Chem. Chem. Phys.* **2013**, *15*, 13570–13577. DOI: [10.1039/c3cp00153a](https://doi.org/10.1039/c3cp00153a).

- [219] Yan, Z.; Zhang, M.; Xie, J.; Wang, H.; Wei, W. Smaller Pt Particles Supported on Mesoporous Bowl-like Carbon for Highly Efficient and Stable Methanol Oxidation and Oxygen Reduction Reaction. *J. Power Sources*. 2013, 243, 48–53. DOI: [10.1016/j.jpowsour.2013.06.008](https://doi.org/10.1016/j.jpowsour.2013.06.008).
- [220] Tang, J.; Wang, T.; Pan, X.; Sun, X.; Fan, X.; Guo, Y.; Xue, H.; He, J. Synthesis and Electrochemical Characterization of N-doped Partially Graphitized Ordered Mesoporous carbon-Co Composite. *J. Phys. Chem. C*. 2013, 117, 16896–16906. DOI: [10.1021/jp405775x](https://doi.org/10.1021/jp405775x).
- [221] Dicks, A. L.; The Role of Carbon in Fuel Cells. *J. Power Sources*. 2006, 156, 128–141. DOI: [10.1016/j.jpowsour.2006.02.054](https://doi.org/10.1016/j.jpowsour.2006.02.054).
- [222] Wang, L.; Wang, Y.; Li, A.; Yang, Y.; Wang, J.; Zhao, H.; Du, X.; Qi, T. Electrocatalysis of Carbon Black-or Chitosan-functionalized Activated Carbon Nanotubes-supported Pd with a Small Amount of La₂O₃ Towards Methanol Oxidation in Alkaline Media. *Int. J. Hydrogen Energy*. 2014, 39, 14730–14738. DOI: [10.1016/j.ijhydene.2014.07.076](https://doi.org/10.1016/j.ijhydene.2014.07.076).
- [223] Yang, G.; Zhou, Y.; Pan, H.; Zhu, C.; Fu, S.; Wai, C. M.; Du, D.; Zhu, J.; Lin, Y. Ultrasonic-assisted Synthesis of Pd-Pt/carbon Nanotubes Nanocomposites for Enhanced Electro-oxidation of Ethanol and Methanol in Alkaline Medium, Ultrason. *Sonochem*. 2016, 28, 192–198. DOI: [10.1016/j.ultsonch.2015.07.021](https://doi.org/10.1016/j.ultsonch.2015.07.021).
- [224] Lou, X.; Chen, J.; Wang, M.; Gu, J.; Wu, P.; Sun, D.; Tang, Y. Carbon Nanotubes Supported Cerium Dioxide and Platinum Nanohybrids: Layer-by-layer Synthesis and Enhanced Electrocatalytic Activity for Methanol Oxidation. *J. Power Sources*. 2015, 287, 203–210. DOI: [10.1016/j.jpowsour.2015.04.046](https://doi.org/10.1016/j.jpowsour.2015.04.046).
- [225] Zhan, G.; Fu, Z.; Sun, D.; Pan, Z.; Xiao, C.; Wu, S.; Chen, C.; Hu, G.; Wei, Z. Platinum Nanoparticles Decorated Robust Binary Transition Metal Nitride-carbon Nanotubes Hybrid as an Efficient Electrocatalyst for the Methanol Oxidation Reaction. *J. Power Sources*. 2016, 326, 84–92. DOI: [10.1016/j.jpowsour.2016.06.112](https://doi.org/10.1016/j.jpowsour.2016.06.112).
- [226] Wang, Y.; He, Q.; Guo, J.; Wei, H.; Ding, K.; Lin, H.; Bhana, S.; Huang, X.; Luo, Z.; Shen, T. Carboxyl Multiwalled Carbon-nanotube-stabilized Palladium Nanocatalysts toward Improved Methanol Oxidation Reaction. *ChemElectroChem*. 2015, 2, 559–570. DOI: [10.1002/celec.201402378](https://doi.org/10.1002/celec.201402378).
- [227] Huang, X.; Luo, L.; Chen, G.; Li, Q. Dual Role of Hemin in Pt Nanoparticle Deposition on Carbon Nanotubes for Methanol Electro-oxidation and Oxygen Reduction. *Mater. Lett.* 2019, 241, 51–54. DOI: [10.1016/j.matlet.2019.01.073](https://doi.org/10.1016/j.matlet.2019.01.073).
- [228] Huang, L.; Luo, X.; Jiang, Y.; Mao, X.; Shi, M. Oxygen Deficiency Assisted Synthesis of Network-like Tungsten Carbide-carbon Nanotubes Composites for Methanol Oxidation. *Ceram. Int.* 2019, 45, 16976–16981. DOI: [10.1016/j.ceramint.2019.05.246](https://doi.org/10.1016/j.ceramint.2019.05.246).
- [229] Yang, X.; Jia, Q.; Duan, F.; Hu, B.; Wang, M.; He, L.; Song, Y.; Zhang, Z. Multiwall Carbon Nanotubes Loaded with MoS₂ Quantum Dots and MXene Quantum Dots: Non-Pt Bifunctional Catalyst for the Methanol Oxidation and Oxygen Reduction Reactions in Alkaline Solution. *Appl. Surf. Sci.* 2019, 464, 78–87. DOI: [10.1016/j.apsusc.2018.09.069](https://doi.org/10.1016/j.apsusc.2018.09.069).
- [230] Zhou, Y.; Xu, X.; Shan, B.; Wen, Y.; Jiang, T.; Lu, J.; Zhang, S.; Wilkinson, D. P.; Zhang, J.; Huang, Y. Tuning and Understanding the Supercapacitance of Heteroatom-doped Graphene. *Energy Storage Mater.* 2015, 1, 103–111. DOI: [10.1016/j.ensm.2015.09.002](https://doi.org/10.1016/j.ensm.2015.09.002).
- [231] Xu, X.; Yuan, T.; Zhou, Y.; Li, Y.; Lu, J.; Tian, X.; Wang, D.; Wang, J. Facile Synthesis of Boron and Nitrogen-doped Graphene as Efficient Electrocatalyst for the Oxygen Reduction Reaction in Alkaline Media. *Int. J. Hydrogen Energy*. 2014, 39, 16043–16052. DOI: [10.1016/j.ijhydene.2013.12.079](https://doi.org/10.1016/j.ijhydene.2013.12.079).

- [232] Zhang, L.; Sui, X.; Zhao, L.; Zhang, J.; Gu, D.; Wang, Z. Nitrogen-doped Carbon Nanotubes for High-performance Platinum-based Catalysts in Methanol Oxidation Reaction. *Carbon*. 2016, 108, 561–567. DOI: [10.1016/j.carbon.2016.07.059](https://doi.org/10.1016/j.carbon.2016.07.059).
- [233] Zhou, Y.; Yang, G.; Pan, H.; Zhu, C.; Fu, S.; Shi, Q.; Du, D.; Cheng, X.; Yang, J.; Wai, C. M. Ultrasonic-assisted Synthesis of Carbon Nanotube Supported Bimetallic Pt–Ru Nanoparticles for Effective Methanol Oxidation. *J. Mater. Chem. A*. 2015, 3, 8459–8465. DOI: [10.1039/C5TA00695C](https://doi.org/10.1039/C5TA00695C).
- [234] Zhang, J.; Sun, S.; Li, Y.; Zhang, X.; Zhang, P.; Fan, Y. A Strategy in Deep Eutectic Solvents for Carbon Nanotube-supported PtCo Nanocatalysts with Enhanced Performance toward Methanol Electrooxidation. *Int. J. Hydrogen Energy*. 2017, 42, 26744–26751. DOI: [10.1016/j.ijhydene.2017.09.090](https://doi.org/10.1016/j.ijhydene.2017.09.090).
- [235] Ali, S.; Ahmed, R.; Sohail, M.; Khan, S. A.; Ansari, M. S. Co@ Pt Core-shell Nanoparticles Supported on Carbon Nanotubes as Promising Catalyst for Methanol Electro-oxidation. *J. Ind. Eng. Chem*. 2015, 28, 344–350. DOI: [10.1016/j.jiec.2015.03.014](https://doi.org/10.1016/j.jiec.2015.03.014).
- [236] Zhou, Y.; Liu, C.; Liu, J.; Cai, X.; Lu, Y.; Zhang, H.; Sun, X.; Wang, S. Self-decoration of PtNi Alloy Nanoparticles on Multiwalled Carbon Nanotubes for Highly Efficient Methanol Electro-oxidation. *Nano-Micro Lett*. 2016, 8, 371–380. DOI: [10.1007/s40820-016-0096-2](https://doi.org/10.1007/s40820-016-0096-2).
- [237] Ning, L.; Liu, X.; Deng, M.; Huang, Z.; Zhu, A.; Zhang, Q.; Liu, Q. Palladium-based Nanocatalysts Anchored on CNT with High Activity and Durability for Ethanol Electro-oxidation. *Electrochim. Acta*. 2019, 297, 206–214. DOI: [10.1016/j.electacta.2018.11.188](https://doi.org/10.1016/j.electacta.2018.11.188).
- [238] Satyanarayana, M.; Rajeshkhanna, G.; Sahoo, M. K.; Rao, G. R. Electrocatalytic Activity of Pd_{20-x}Ag_x Nanoparticles Embedded in Carbon Nanotubes for Methanol Oxidation in Alkaline Media. *ACS Appl. Energy Mater*. 2018, 1, 3763–3770. DOI: [10.1021/acsaem.8b00544](https://doi.org/10.1021/acsaem.8b00544).
- [239] Zhao, Y.; Zhou, Y.; Xiong, B.; Wang, J.; Chen, X.; O’Hayre, R.; Shao, Z. Facile Single-step Preparation of Pt/N-graphene Catalysts with Improved Methanol Electrooxidation Activity. *J. Solid State Electrochem*. 2013, 17, 1089–1098. DOI: [10.1007/s10008-012-1968-0](https://doi.org/10.1007/s10008-012-1968-0).
- [240] Zhao, S.; Yin, H.; Du, L.; Yin, G.; Tang, Z.; Liu, S. Three Dimensional N-doped graphene/PtRu Nanoparticle Hybrids as High Performance Anode for Direct Methanol Fuel Cells. *J. Mater. Chem. A*. 2014, 2, 3719–3724. DOI: [10.1039/c3ta14809b](https://doi.org/10.1039/c3ta14809b).
- [241] Zhao, L.; Sui, X.; Li, J.; Zhang, J.; Zhang, L.; Huang, G.; Wang, Z. Supramolecular Assembly Promoted Synthesis of Three-dimensional Nitrogen Doped Graphene Frameworks as Efficient Electrocatalyst for Oxygen Reduction Reaction and Methanol Electrooxidation. *Appl. Catal. B Environ*. 2018, 231, 224–233. DOI: [10.1016/j.apcatb.2018.03.020](https://doi.org/10.1016/j.apcatb.2018.03.020).
- [242] Liu, M.; Peng, C.; Yang, W.; Guo, J.; Zheng, Y.; Chen, P.; Huang, T.; Xu, J. Pd Nanoparticles Supported on Three-dimensional Graphene Aerogels as Highly Efficient Catalysts for Methanol Electrooxidation. *Electrochim. Acta*. 2015, 178, 838–846. DOI: [10.1016/j.electacta.2015.08.063](https://doi.org/10.1016/j.electacta.2015.08.063).
- [243] Xiong, B.; Zhou, Y.; Zhao, Y.; Wang, J.; Chen, X.; O’Hayre, R.; Shao, Z. The Use of Nitrogen-doped Graphene Supporting Pt Nanoparticles as a Catalyst for Methanol Electrocatalytic Oxidation. *Carbon*. 2013, 52, 181–192. DOI: [10.1016/j.carbon.2012.09.019](https://doi.org/10.1016/j.carbon.2012.09.019).
- [244] Lu, J.; Zhou, Y.; Tian, X.; Xu, X.; Zhu, H.; Zhang, S.; Yuan, T. Synthesis of Boron and Nitrogen Doped Graphene Supporting PtRu Nanoparticles as Catalysts for Methanol Electrooxidation. *Appl. Surf. Sci*. 2014, 317, 284–293. DOI: [10.1016/j.apsusc.2014.08.083](https://doi.org/10.1016/j.apsusc.2014.08.083).

- [245] Hofstead-Duffy, A. M.; Chen, D.; Sun, S.; Tong, Y. J. Origin of the Current Peak of Negative Scan in the Cyclic Voltammetry of Methanol Electro-oxidation on Pt-based Electrocatalysts: A Revisit to the Current Ratio Criterion. *J. Mater. Chem.* **2012**, *22*, 5205–5208. DOI: [10.1039/c2jm15426a](https://doi.org/10.1039/c2jm15426a).
- [246] Xu, X.; Zhou, Y.; Lu, J.; Tian, X.; Zhu, H.; Liu, J. Single-step Synthesis of PtRu/N-doped Graphene for Methanol Electrocatalytic Oxidation. *Electrochim. Acta.* **2014**, *120*, 439–451. DOI: [10.1016/j.electacta.2013.12.062](https://doi.org/10.1016/j.electacta.2013.12.062).
- [247] Zhao, L.; Sui, X.; Li, J.; Zhang, J.; Zhang, L.; Wang, Z. 3D Hierarchical Pt-nitrogen-doped-graphene-carbonized Commercially Available Sponge as a Superior Electrocatalyst for Low-temperature Fuel Cells. *ACS Appl. Mater. Interfaces.* **2016**, *8*, 16026–16034. DOI: [10.1021/acscami.6b03520](https://doi.org/10.1021/acscami.6b03520).
- [248] Khosravi, M.; Amini, M. K. Carbon Paper Supported Pt/Au Catalysts Prepared via Cu Underpotential Deposition-redox Replacement and Investigation of Their Electrocatalytic Activity for Methanol Oxidation and Oxygen Reduction Reactions. *Int. J. Hydrogen Energy.* **2010**, *35*, 10527–10538. DOI: [10.1016/j.ijhydene.2010.07.136](https://doi.org/10.1016/j.ijhydene.2010.07.136).
- [249] Wei, S.; Wu, D.; Shang, X.; Fu, R. Studies on the Structure and Electrochemical Performance of Pt/carbon Aerogel Catalyst for Direct Methanol Fuel Cells. *Energy Fuels.* **2009**, *23*, 908–911. DOI: [10.1021/ef8006432](https://doi.org/10.1021/ef8006432).
- [250] Zhang, Y.; Jiang, L.; Li, H.; Fan, L.; Hu, W.; Wang, C.; Li, Y.; Yang, S. Single-Crystalline C₆₀ Nanostructures by Sonophysical Preparation: Tuning Hollow Nanobowls as Catalyst Supports for Methanol Oxidation. *Chemistry.* **2011**, *17*, 4921–4926. DOI: [10.1002/chem.201002719](https://doi.org/10.1002/chem.201002719).
- [251] Liu, Y.; Yang, H.; Li, X.; Mao, L. Pt Nanoparticles Supported on Monodisperse Carbon Spheres for Methanol Oxidation in Alkaline Media. *Mater. Lett.* **2013**, *106*, 287–289. DOI: [10.1016/j.matlet.2013.05.011](https://doi.org/10.1016/j.matlet.2013.05.011).
- [252] Zhang, Y.; Liu, Y.; Liu, W.; Li, X.; Mao, L. Synthesis of Honeycomb-like Mesoporous Nitrogen-doped Carbon Nanospheres as Pt Catalyst Supports for Methanol Oxidation in Alkaline Media. *Appl. Surf. Sci.* **2017**, *407*, 64–71. DOI: [10.1016/j.apsusc.2017.02.158](https://doi.org/10.1016/j.apsusc.2017.02.158).
- [253] Xie, F.; Ma, L.; Gan, M.; He, H.; Hu, L.; Jiang, M.; Zhang, H. One-pot Construction of the Carbon Spheres Embellished by Layered Double Hydroxide with Abundant Hydroxyl Groups for Pt-based Catalyst Support in Methanol Electrooxidation. *J. Power Sources.* **2019**, *420*, 73–81. DOI: [10.1016/j.jpowsour.2019.02.088](https://doi.org/10.1016/j.jpowsour.2019.02.088).
- [254] Niu, X.; Xiong, Q.; Pan, J.; Li, X.; Zhang, W.; Qiu, F.; Yan, Y. Highly Active and Durable Methanol Electro-oxidation Catalyzed by Small Palladium Nanoparticles inside Sulfur-doped Carbon Microsphere. *Fuel.* **2017**, *190*, 174–181. DOI: [10.1016/j.fuel.2016.11.033](https://doi.org/10.1016/j.fuel.2016.11.033).
- [255] Pan, D.; Li, X.; Zhang, A. Platinum Assisted by Carbon Quantum Dots for Methanol Electro-oxidation. *Appl. Surf. Sci.* **2018**, *427*, 715–723.
- [256] Sui, X.; Li, C.; Zhao, L.; Wang, Z.; Gu, D.; Huang, G. Mesoporous g-C₃N₄ Derived Nano-titanium Nitride Modified Carbon Black as Ultra-fine PtRu Catalyst Support for Methanol Electro-oxidation. *Int. J. Hydrogen Energy.* **2018**, *43*, 5153–5162. DOI: [10.1016/j.ijhydene.2018.01.137](https://doi.org/10.1016/j.ijhydene.2018.01.137).
- [257] Li, C.; Wang, Z.; Sui, X.; Zhang, L.; Gu, D.; Gu, S. Graphitic Carbon Nitride Nanosheet Coated Carbon Black as a High-performance PtRu Catalyst Support Material for Methanol Electrooxidation. *J. Mater. Chem. A.* **2014**, *2*, 20139–20146. DOI: [10.1039/C4TA04594G](https://doi.org/10.1039/C4TA04594G).
- [258] Cao, R.; Xia, T.; Zhu, R.; Liu, Z.; Guo, J.; Chang, G.; Zhang, Z.; Liu, X.; He, Y. Novel Synthesis of Core-shell Au-Pt Dendritic Nanoparticles Supported on Carbon Black for

- Enhanced Methanol Electro-oxidation. *Appl. Surf. Sci.* **2018**, *433*, 840–846. DOI: [10.1016/j.apsusc.2017.10.104](https://doi.org/10.1016/j.apsusc.2017.10.104).
- [259] Eris, S.; Daşdelen, Z.; Sen, F. Investigation of Electrocatalytic Activity and Stability of Pt@ f-VC Catalyst Prepared by In-situ Synthesis for Methanol Electrooxidation. *Int. J. Hydrogen Energy.* **2018**, *43*, 385–390. DOI: [10.1016/j.ijhydene.2017.11.063](https://doi.org/10.1016/j.ijhydene.2017.11.063).
- [260] Chang, X.; Dong, F.; Yang, S.; Tang, Z.; Zha, F. Well Dispersed Pt Nanoparticles on Commercial Carbon Black Oxidized by Ozone Possess Significantly High Electro-catalytic Activity for Methanol Oxidation. *Int. J. Hydrogen Energy.* **2019**, *44*, 21559–21568. DOI: [10.1016/j.ijhydene.2019.06.084](https://doi.org/10.1016/j.ijhydene.2019.06.084).
- [261] Jiang, M.; Ma, L.; Gan, M.; Hu, L.; He, H.; Xie, F.; Zhang, H. Worm-like PtP Nanocrystals Supported on NiCo₂P_x/C Composites for Enhanced Methanol Electrooxidation Performance. *Electrochim. Acta.* **2019**, *293*, 30–39. DOI: [10.1016/j.electacta.2018.10.022](https://doi.org/10.1016/j.electacta.2018.10.022).
- [262] Comignani, V.; Sieben, J. M.; Brigante, M. E.; Duarte, M. M. Manganese (II, III) Oxide-Activated Carbon Black Supported PtRu Nanoparticles for Methanol Electrooxidation in Acid Medium. *ChemElectroChem.* **2018**, *5*, 2118–2125. DOI: [10.1002/celec.201800413](https://doi.org/10.1002/celec.201800413).
- [263] Qian, H.; Chen, S.; Fu, Y.; Wang, X. Platinum–palladium Bimetallic Nanoparticles on Graphitic Carbon Nitride Modified Carbon Black: A Highly Electroactive and Durable Catalyst for Electrooxidation of Alcohols. *J. Power Sources.* **2015**, *300*, 41–48. DOI: [10.1016/j.jpowsour.2015.09.051](https://doi.org/10.1016/j.jpowsour.2015.09.051).
- [264] Zhang, Y.; Zang, J.; Jia, S.; Tian, P.; Han, C.; Wang, Y. Low Content of Pt Supported on Ni-MoC_x/carbon Black as a Highly Durable and Active Electrocatalyst for Methanol Oxidation, Oxygen Reduction and Hydrogen Evolution Reactions in Acidic Condition. *Appl. Surf. Sci.* **2017**, *412*, 327–334. DOI: [10.1016/j.apsusc.2017.03.284](https://doi.org/10.1016/j.apsusc.2017.03.284).
- [265] Hameed, R. A.; Optimization of Manganese Oxide Amount on Vulcan XC-72R Carbon Black as a Promising Support of Ni Nanoparticles for Methanol Electro-oxidation Reaction. *Int. J. Hydrogen Energy.* **2015**, *40*, 13979–13993. DOI: [10.1016/j.ijhydene.2015.08.065](https://doi.org/10.1016/j.ijhydene.2015.08.065).
- [266] Calderón, J.; Nieto-Monge, M.; Pérez-Rodríguez, S.; Pardo, J.; Moliner, R.; Lázaro, M. Palladium–nickel Catalysts Supported on Different Chemically-treated Carbon Blacks for Methanol Oxidation in Alkaline Media. *Int. J. Hydrogen Energy.* **2016**, *41*, 19556–19569. DOI: [10.1016/j.ijhydene.2016.07.121](https://doi.org/10.1016/j.ijhydene.2016.07.121).
- [267] Gu, Z.; Xu, H.; Bin, D.; Yan, B.; Li, S.; Xiong, Z.; Zhang, K.; Du, Y. Preparation of PdNi Nanospheres with Enhanced Catalytic Performance for Methanol Electrooxidation in Alkaline Medium. *Colloids Surf. Physicochem. Eng. Aspects.* **2017**, *529*, 651–658. DOI: [10.1016/j.colsurfa.2017.06.044](https://doi.org/10.1016/j.colsurfa.2017.06.044).
- [268] Zhao, L.; Wang, Z.; Li, J.; Zhang, J.; Sui, X.; Zhang, L. Hybrid of Carbon-supported Pt Nanoparticles and Three Dimensional Graphene Aerogel as High Stable Electrocatalyst for Methanol Electrooxidation. *Electrochim. Acta.* **2016**, *189*, 175–183. DOI: [10.1016/j.electacta.2015.12.072](https://doi.org/10.1016/j.electacta.2015.12.072).
- [269] Kim, H. J.; Ruqia, B.; Kang, M. S.; Lim, S. B.; Choi, R.; Nam, K. M.; Seo, W. S.; Lee, G.; Choi, S. Shape-controlled Pt Nanocubes Directly Grown on Carbon Supports and Their Electrocatalytic Activity toward Methanol Oxidation. *Sci. Bull.* **2017**, *62*, 943–949. DOI: [10.1016/j.scib.2017.05.029](https://doi.org/10.1016/j.scib.2017.05.029).
- [270] An, G.; Ahn, H. Well-dispersed Pt Catalysts Supported on Porous Carbon Nanofibers for Improved Methanol Oxidation in Direct Methanol Fuel Cells. *ECS Solid State Lett.* **2014**, *3*, M29–M32. DOI: [10.1149/2.0061407ssl](https://doi.org/10.1149/2.0061407ssl).
- [271] Calderón, J.; Calvillo, L.; Lázaro, M.; Rodríguez, J.; Pastor, E. Effect of the Dendrimer Generation Used in the Synthesis of Pt-Ru Nanoparticles Supported on Carbon Nanofibers on the Catalytic Activity Towards Methanol Oxidation. *Energies.* **2017**, *10*, 159. DOI: [10.3390/en10020159](https://doi.org/10.3390/en10020159).

- [272] Shanmugapriya, S.; Zhu, P.; Yan, C.; Asiri, A. M.; Zhang, X.; Selvan, R. K. Multifunctional High-Performance Electrocatalytic Properties of Nb₂O₅ Incorporated Carbon Nanofibers as Pt Support Catalyst. *Adv Mater Interfaces*. 2019, 6, 1900565. DOI: [10.1002/admi.201900565](https://doi.org/10.1002/admi.201900565).
- [273] Mu, X.; Xu, Z.; Ma, Y.; Xie, Y.; Mi, H.; Ma, J. Graphene-carbon Nanofiber Hybrid Supported Pt Nanoparticles with Enhanced Catalytic Performance for Methanol Oxidation and Oxygen Reduction. *Electrochim. Acta*. 2017, 253, 171–177. DOI: [10.1016/j.electacta.2017.09.029](https://doi.org/10.1016/j.electacta.2017.09.029).
- [274] Kim, D. H.; Shin, D.; Lee, Y.; An, G.; Han, J. H.; Ahn, H.; Choi, B. J. Effects of SnO₂ Layer Coated on Carbon Nanofiber for the Methanol Oxidation Reaction. *Ceram. Int*. 2018, 44, 19554–19559. DOI: [10.1016/j.ceramint.2018.07.199](https://doi.org/10.1016/j.ceramint.2018.07.199).
- [275] Al-Enizi, A. M.; Brooks, R. M.; El-Halwany, M.; Yousef, A.; Nafady, A.; Hameed, R. A. CoCr₇C₃-like Nanorods Embedded on Carbon Nanofibers as Effective Electrocatalyst for Methanol Electro-oxidation. *Int. J. Hydrogen Energy*. 2018, 43, 9943–9953. DOI: [10.1016/j.ijhydene.2018.04.069](https://doi.org/10.1016/j.ijhydene.2018.04.069).
- [276] Wang, M.; Ma, Z.; Li, R.; Tang, B.; Bao, X.; Zhang, Z.; Wang, X. Novel Flower-like PdAu (Cu) Anchoring on a 3D rGO-CNT Sandwich-stacked Framework for Highly Efficient Methanol and Ethanol Electro-oxidation. *Electrochim. Acta*. 2017, 227, 330–344. DOI: [10.1016/j.electacta.2017.01.046](https://doi.org/10.1016/j.electacta.2017.01.046).
- [277] Song, H.; Yang, L.; Tang, Y.; Yan, D.; Liu, C.; Luo, S. Three-Dimensional Nitrogen-Doped Reduced Graphene Oxide–Carbon Nanotubes Architecture Supporting Ultrafine Palladium Nanoparticles for Highly Efficient Methanol Electrooxidation. *Chemistry*. 2015, 21, 16631–16638. DOI: [10.1002/chem.201502804](https://doi.org/10.1002/chem.201502804).
- [278] Bedolla-Valdez, Z.; Verde-Gómez, Y.; Valenzuela-Muñiz, A.; Gochi-Ponce, Y.; Oropeza-Guzmán, M.; Berhault, G.; Alonso-Núñez, G. Sonochemical Synthesis and Characterization of Pt/CNT, Pt/TiO₂, and Pt/CNT/TiO₂ Electrocatalysts for Methanol Electro-oxidation. *Electrochim. Acta*. 2015, 186, 76–84. DOI: [10.1016/j.electacta.2015.10.084](https://doi.org/10.1016/j.electacta.2015.10.084).
- [279] Huang, M.; Zhang, J.; Wu, C.; Guan, L. Networks of Connected Pt Nanoparticles Supported on Carbon Nanotubes as Superior Catalysts for Methanol Electrooxidation. *J. Power Sources*. 2017, 342, 273–278. DOI: [10.1016/j.jpowsour.2016.12.054](https://doi.org/10.1016/j.jpowsour.2016.12.054).
- [280] Wang, R.; Fan, Y.; Wang, L.; Wu, L.; Sun, S.; Sun, S. Pt Nanocatalysts on a Polyindole-functionalized Carbon Nanotube Composite with High Performance for Methanol Electrooxidation. *J. Power Sources*. 2015, 287, 341–348. DOI: [10.1016/j.jpowsour.2015.03.181](https://doi.org/10.1016/j.jpowsour.2015.03.181).
- [281] Maya-Cornejo, J.; Garcia-Bernabé, A.; Compañ, V. Bimetallic Pt-M Electrocatalysts Supported on Single-wall Carbon Nanotubes for Hydrogen and Methanol Electrooxidation in Fuel Cells Applications. *Int. J. Hydrogen Energy*. 2018, 43, 872–884. DOI: [10.1016/j.ijhydene.2017.10.097](https://doi.org/10.1016/j.ijhydene.2017.10.097).
- [282] Yang, Z.; Luo, F. Pt Nanoparticles Deposited on Dihydroxy-polybenzimidazole Wrapped Carbon Nanotubes Shows a Remarkable Durability in Methanol Electro-oxidation. *Int. J. Hydrogen Energy*. 2017, 42, 507–514. DOI: [10.1016/j.ijhydene.2016.10.148](https://doi.org/10.1016/j.ijhydene.2016.10.148).
- [283] Fard, L. A.; Ojani, R.; Raouf, J. B. Electrodeposition of Three-dimensional Pd Nanoflowers on a PPy@ MWCNTs with Superior Electrocatalytic Activity for Methanol Electrooxidation. *Int. J. Hydrogen Energy*. 2016, 41, 17987–17994. DOI: [10.1016/j.ijhydene.2016.08.010](https://doi.org/10.1016/j.ijhydene.2016.08.010).
- [284] Huang, H.; Ye, G.; Yang, S.; Fei, H.; Tiwary, C. S.; Gong, Y.; Vajtai, R.; Tour, J. M.; Wang, X.; Ajayan, P. M. Nanosized Pt Anchored onto 3D Nitrogen-doped Graphene

- Nanoribbons Towards Efficient Methanol Electrooxidation. *J. Mater. Chem. A.* **2015**, *3*, 19696–19701. DOI: [10.1039/C5TA05372B](https://doi.org/10.1039/C5TA05372B).
- [285] Rodriguez, J.; Fuentes-Moyado, S.; Zepeda, T.; De León, J. D.; Cruz-Reyes, J.; Oropeza-Guzman, M.; Berhault, G.; Alonso-Núñez, G. Methanol Electro-oxidation with Alloy Nanoparticles of Pt_{10-x}-Fe_x Supported on CNTs. *Fuel.* **2016**, *182*, 1–7. DOI: [10.1016/j.fuel.2016.05.070](https://doi.org/10.1016/j.fuel.2016.05.070).
- [286] Sun, J.; Dou, M.; Zhang, Z.; Ji, J.; Wang, F. Carbon Nanotubes Supported Pt-Co-P Ultrafine Nanoparticle Electrocatalysts with Superior Activity and Stability for Methanol Electro-oxidation. *Electrochim. Acta.* **2016**, *215*, 447–454. DOI: [10.1016/j.electacta.2016.08.133](https://doi.org/10.1016/j.electacta.2016.08.133).
- [287] Deng, Z.; Yi, Q.; Zhang, Y.; Nie, H. NiCo/CN/CNT Composite Catalysts for Electro-catalytic Oxidation of Methanol and Ethanol. *J. Electroanal. Chem.* **2017**, *803*, 95–103. DOI: [10.1016/j.jelechem.2017.09.025](https://doi.org/10.1016/j.jelechem.2017.09.025).
- [288] Su, N.; Hu, X.; Zhang, J.; Huang, H.; Cheng, J.; Yu, J.; Ge, C. Plasma-induced Synthesis of Pt Nanoparticles Supported on TiO₂ Nanotubes for Enhanced Methanol Electro-oxidation. *Appl. Surf. Sci.* **2017**, *399*, 403–410. DOI: [10.1016/j.apsusc.2016.12.095](https://doi.org/10.1016/j.apsusc.2016.12.095).
- [289] Yan, H.; Meng, M.; Wang, L.; Wu, A.; Tian, C.; Zhao, L.; Fu, H. Small-sized Tungsten Nitride Anchoring into a 3D CNT-rGO Framework as a Superior Bifunctional Catalyst for the Methanol Oxidation and Oxygen Reduction Reactions. *Nano Res.* **2016**, *9*, 329–343. DOI: [10.1007/s12274-015-0912-x](https://doi.org/10.1007/s12274-015-0912-x).
- [290] Huang, M.; Zhang, J.; Wu, C.; Guan, L. Pt Nanoparticles Densely Coated on SnO₂-covered Multiwalled Carbon Nanotubes with Excellent Electrocatalytic Activity and Stability for Methanol Oxidation. *ACS Appl. Mater. Interfaces.* **2017**, *9*, 26921–26927. DOI: [10.1021/acsami.7b07866](https://doi.org/10.1021/acsami.7b07866).
- [291] Zhang, J.; Yi, X.; Liu, S.; Fan, H.; Ju, W.; Wang, Q.; Ma, J. Vertically Aligned Carbon Nanotubes/carbon Fiber Paper Composite to Support Pt Nanoparticles for Direct Methanol Fuel Cell Application. *J. Phys. Chem. Solids.* **2017**, *102*, 99–104. DOI: [10.1016/j.jpjcs.2016.11.006](https://doi.org/10.1016/j.jpjcs.2016.11.006).
- [292] Peng, X.; Chen, D.; Yang, X.; Wang, D.; Li, M.; Tseng, C.; Panneerselvam, R.; Wang, X.; Hu, W.; Tian, J. Microwave-assisted Synthesis of Highly Dispersed PtCu Nanoparticles on Three-dimensional Nitrogen-doped Graphene Networks with Remarkably Enhanced Methanol Electrooxidation. *ACS Appl. Mater. Interfaces.* **2016**, *8*, 33673–33680. DOI: [10.1021/acsami.6b11800](https://doi.org/10.1021/acsami.6b11800).
- [293] Nouralishahi, A.; Rashidi, A. M.; Mortazavi, Y.; Khodadadi, A. A.; Choolaei, M. Enhanced Methanol Electro-oxidation Reaction on Pt-CoO_x/MWCNTs Hybrid Electro-catalyst. *Appl. Surf. Sci.* **2015**, *335*, 55–64. DOI: [10.1016/j.apsusc.2015.02.011](https://doi.org/10.1016/j.apsusc.2015.02.011).
- [294] Zhang, J.; Wang, Z.; Li, C.; Zhao, L.; Liu, J.; Zhang, L.; Gu, D. Multiwall-carbon Nanotube Modified by N-doped Carbon Quantum Dots as Pt Catalyst Support for Methanol Electrooxidation. *J. Power Sources.* **2015**, *289*, 63–70. DOI: [10.1016/j.jpowsour.2015.04.150](https://doi.org/10.1016/j.jpowsour.2015.04.150).
- [295] Yousaf, A. B.; Imran, M.; Zaidi, S. J.; Kasak, P. Engineering and Understanding of Synergistic Effects in the Interfaces of rGO-CNTs/PtPd Nanocomposite Revealed Fast Electro-oxidation of Methanol. *J. Electroanal. Chem.* **2019**, *832*, 343–352. DOI: [10.1016/j.jelechem.2018.11.033](https://doi.org/10.1016/j.jelechem.2018.11.033).
- [296] Huang, W.; Wang, H.; Zhou, J.; Wang, J.; Duchesne, P. N.; Muir, D.; Zhang, P.; Han, N.; Zhao, F.; Zeng, M. Highly Active and Durable Methanol Oxidation Electrocatalyst Based on the Synergy of Platinum–nickel Hydroxide–graphene. *Nat. Commun.* **2015**, *6*, 10035. DOI: [10.1038/ncomms10035](https://doi.org/10.1038/ncomms10035).

- [297] Zhang, L.; Wang, H.; Li, X.; Xia, F.; Liu, Y.; Xu, X.; Gao, J.; Xing, F. One-step Synthesis of Palladium-gold-silver Ternary Nanoparticles Supported on Reduced Graphene Oxide for the Electrooxidation of Methanol and Ethanol. *Electrochim. Acta.* **2015**, *172*, 42–51. DOI: [10.1016/j.electacta.2014.11.152](https://doi.org/10.1016/j.electacta.2014.11.152).
- [298] Kiyani, R.; Rowshanzamir, S.; Parnian, M. J. Nitrogen Doped Graphene Supported Palladium-cobalt as a Promising Catalyst for Methanol Oxidation Reaction: Synthesis, Characterization and Electrocatalytic Performance. *Energy.* **2016**, *113*, 1162–1173. DOI: [10.1016/j.energy.2016.07.143](https://doi.org/10.1016/j.energy.2016.07.143).
- [299] Zhang, J.; He, J.; Wang, X.; Fan, Y.; Zhang, X.; Zhong, J.; Chen, W.; Sun, S. One-step Synthesis in Deep Eutectic Solvents of PtV Alloy Nanonetworks on Carbon Nanotubes with Enhanced Methanol Electrooxidation Performance. *Int. J. Hydrogen Energy.* **2019**, *44*, 28709–28719. DOI: [10.1016/j.ijhydene.2019.09.104](https://doi.org/10.1016/j.ijhydene.2019.09.104).
- [300] Askari, M. B.; Salarizadeh, P.; Seifi, M.; Rozati, S. M. Ni/NiO Coated on Multi-walled Carbon Nanotubes as a Promising Electrode for Methanol Electro-oxidation Reaction in Direct Methanol Fuel Cell. *Solid State Sci.* **2019**, *97*, 106012. DOI: [10.1016/j.solidstatesciences.2019.106012](https://doi.org/10.1016/j.solidstatesciences.2019.106012).
- [301] Yang, F.; Zhang, B.; Dong, S.; Wang, C.; Feng, A.; Fan, X.; Li, Y. Reduced Graphene Oxide Supported Pd-Cu-Co Trimetallic Catalyst: Synthesis, Characterization and Methanol Electrooxidation Properties. *J. Energy Chem.* **2019**, *29*, 72–78. DOI: [10.1016/j.jechem.2018.02.007](https://doi.org/10.1016/j.jechem.2018.02.007).
- [302] He, M.; Fei, G.; Zheng, Z.; Cheng, Z.; Wang, Z.; Xia, H. Pt Nanoparticle-Loaded Graphene Aerogel Microspheres with Excellent Methanol Electro-Oxidation Performance. *Langmuir.* **2019**, *35*, 3694–3700. DOI: [10.1021/acs.langmuir.9b00021](https://doi.org/10.1021/acs.langmuir.9b00021).
- [303] Oskueyan, G.; Lakouraj, M. M. Electrodeposition of Nanostructured Pt–Pd Bimetallic Catalyst on Polyaniline-camphorsulfonic Acid/graphene Nanocomposites for Methanol Electrooxidation. *J. Appl. Electrochem.* **2019**, *49*, 755–765.
- [304] Zhang, Q.; Yue, F.; Xu, L.; Yao, C.; Priestley, R. D.; Hou, S. Based Porous Graphene/Single-Walled Carbon Nanotubes Supported Pt Nanoparticles as Freestanding Catalyst for Electro-oxidation of Methanol. *Appl. Catal. B Environ.* **2019**, 117886. doi:[10.1016/j.apcatb.2019.117886](https://doi.org/10.1016/j.apcatb.2019.117886).
- [305] Ullah, N.; Xie, M.; Oluigbo, C. J.; Xu, Y.; Xie, J.; Rasheed, H. U.; Zhang, M. Nickel and Cobalt in Situ Grown in 3-dimensional Hierarchical Porous Graphene for Effective Methanol Electro-oxidation Reaction. *J. Electroanal. Chem.* **2019**, *838*, 7–15. DOI: [10.1016/j.jelechem.2019.02.022](https://doi.org/10.1016/j.jelechem.2019.02.022).
- [306] Chen, D.; He, Z.; Pei, S.; Huang, L.; Shao, H.; Jin, Y.; Wang, J. Pd Nanoparticles Supported on N and P Dual-doped Graphene as an Excellent Composite Catalyst for Methanol Electro-oxidation. *J. Alloys Compounds.* **2019**, *785*, 781–788. DOI: [10.1016/j.jallcom.2019.01.246](https://doi.org/10.1016/j.jallcom.2019.01.246).
- [307] An, M.; Du, L.; Du, C.; Sun, Y.; Wang, Y.; Yin, G.; Gao, Y. Pt Nanoparticles Supported by Sulfur and Phosphorus Co-doped Graphene as Highly Active Catalyst for Acidic Methanol Electrooxidation. *Electrochim. Acta.* **2018**, *285*, 202–213. DOI: [10.1016/j.electacta.2018.07.237](https://doi.org/10.1016/j.electacta.2018.07.237).
- [308] Zhang, K.; Chen, X.; Wang, L.; Zhang, D.; Xue, Z.; Zhou, X.; Lu, X. PtPd Nanoparticles Supported on Sulfonated Nitrogen Sulfur Co-doped Graphene for Methanol Electro-oxidation. *Int. J. Hydrogen Energy.* **2018**, *43*, 15931–15940. DOI: [10.1016/j.ijhydene.2018.06.157](https://doi.org/10.1016/j.ijhydene.2018.06.157).
- [309] Song, N.; Yang, Y. Molecular and Supramolecular Switches on Mesoporous Silica Nanoparticles. *Chem. Soc. Rev.* **2015**, *44*, 3474–3504. DOI: [10.1039/C5CS00243E](https://doi.org/10.1039/C5CS00243E).
- [310] Dos Santos, S. M. L.; Nogueira, K. A. B.; de Souza Gama, M.; Lima, J. D. F.; da Silva Júnior, I. J.; de Azevedo, D. C. S. Synthesis and Characterization of Ordered Mesoporous

- Silica (SBA-15 and SBA-16) for Adsorption of Biomolecules. *Microporous Mesoporous Mater.* **2013**, *180*, 284–292. DOI: [10.1016/j.micromeso.2013.06.043](https://doi.org/10.1016/j.micromeso.2013.06.043).
- [311] Azizi, S.; Ghasemi, S.; Yazdani-Sheldarrei, H. Synthesis of Mesoporous Silica (SBA-16) Nanoparticles Using Silica Extracted from Stem Cane Ash and Its Application in Electrocatalytic Oxidation of Methanol. *Int. J. Hydrogen Energy.* **2013**, *38*, 12774–12785. DOI: [10.1016/j.ijhydene.2013.07.086](https://doi.org/10.1016/j.ijhydene.2013.07.086).
- [312] Kim, T.; Ryoo, R.; Gierszal, K. P.; Jaroniec, M.; Solovyov, L. A.; Sakamoto, Y.; Terasaki, O. Characterization of Mesoporous Carbons Synthesized with SBA-16 Silica Template. *J. Mater. Chem.* **2005**, *15*, 1560–1571. DOI: [10.1039/b417804a](https://doi.org/10.1039/b417804a).
- [313] Mesa, M.; Sierra, L.; Guth, J. Contribution to the Study of the Formation Mechanism of Mesoporous SBA-15 and SBA-16 Type Silica Particles in Aqueous Acid Solutions. *Microporous Mesoporous Mater.* **2008**, *112*, 338–350. DOI: [10.1016/j.micromeso.2007.10.008](https://doi.org/10.1016/j.micromeso.2007.10.008).
- [314] Lin, C.; Pang, Y.; Chao, M.; Chen, B.; Lin, H.; Tang, C.; Lin, C. Synthesis of SBA-16 and SBA-15 Mesoporous Silica Crystals Templated with Neutral Block Copolymer Surfactants. *J. Phys. Chem. Solids.* **2008**, *69*, 415–419. DOI: [10.1016/j.jpacs.2007.07.006](https://doi.org/10.1016/j.jpacs.2007.07.006).
- [315] Kleitz, F.; Kim, T.; Ryoo, R. Phase Domain of the Cubic Im $\bar{3}m$ Mesoporous Silica in the EO₁₀₆PO₇₀EO₁₀₆–Butanol–H₂O System. *Langmuir.* **2006**, *22*, 440–445.
- [316] Irum, M.; Zaheer, M.; Friedrich, M.; Kempe, R. Mesoporous Silica Nanosphere Supported Platinum Nanoparticles (Pt@ MSN): One-pot Synthesis and Catalytic Hydrogen Generation. *RSC Adv.* **2016**, *6*, 10438–10441. DOI: [10.1039/C5RA25243A](https://doi.org/10.1039/C5RA25243A).
- [317] Hassan, H.; Rahim, M. A.; Khalil, M.; Mohammed, R. Ni Modified MCM-41 as a Catalyst for Direct Methanol Fuel Cells. *Int. J. Electrochem. Sci.* **2014**, *9*, 760–777.
- [318] Dubau, L.; Hahn, F.; Coutanceau, C.; Léger, J.; Lamy, C. On the Structure Effects of Bimetallic PtRu Electrocatalysts Towards Methanol Oxidation. *J. Electroanal. Chem.* **2003**, *554*, 407–415. DOI: [10.1016/S0022-0728\(03\)00308-5](https://doi.org/10.1016/S0022-0728(03)00308-5).
- [319] Jusys, Z.; Kaiser, J.; Behm, R. J. Composition and Activity of High Surface Area PtRu Catalysts Towards Adsorbed CO and Methanol Electrooxidation—: A DEMS Study. *Electrochim. Acta.* **2002**, *47*, 3693–3706. DOI: [10.1016/S0013-4686\(02\)00339-0](https://doi.org/10.1016/S0013-4686(02)00339-0).
- [320] Paulus, U.; Endruschat, U.; Feldmeyer, G.; Schmidt, T.; Bönnemann, H.; Behm, R. New PtRu Alloy Colloids as Precursors for Fuel Cell Catalysts. *J. Catal.* **2000**, *195*, 383–393.
- [321] Zhou, W.; Zhou, B.; Li, W.; Zhou, Z.; Song, S.; Sun, G.; Xin, Q.; Douvartzides, S.; Goula, M.; Tsiakaras, P. Performance Comparison of Low-temperature Direct Alcohol Fuel Cells with Different Anode Catalysts. *J. Power Sources.* **2004**, *126*, 16–22. DOI: [10.1016/j.jpowsour.2003.08.009](https://doi.org/10.1016/j.jpowsour.2003.08.009).
- [322] El-Shafei, A.; Electrocatalytic Oxidation of Methanol at a Nickel Hydroxide/glassy Carbon Modified Electrode in Alkaline Medium. *J. Electroanal. Chem.* **1999**, *471*, 89–95. DOI: [10.1016/S0022-0728\(99\)00235-1](https://doi.org/10.1016/S0022-0728(99)00235-1).
- [323] Nagashree, K.; Ahmed, M. Electrocatalytic Oxidation of Methanol on Ni Modified Polyaniline Electrode in Alkaline Medium. *J. Solid State Electrochem.* **2010**, *14*, 2307–2320.
- [324] Kubisztal, J.; Budniok, A. Study of the Oxygen Evolution Reaction on Nickel-based Composite Coatings in Alkaline Media. *Int. J. Hydrogen Energy.* **2008**, *33*, 4488–4494. DOI: [10.1016/j.ijhydene.2008.06.023](https://doi.org/10.1016/j.ijhydene.2008.06.023).
- [325] Danaee, I.; Jafarian, M.; Forouzandeh, F.; Gobal, F.; Mahjani, M. Electrocatalytic Oxidation of Methanol on Ni and NiCu Alloy Modified Glassy Carbon Electrode. *Int. J. Hydrogen Energy.* **2008**, *33*, 4367–4376. DOI: [10.1016/j.ijhydene.2008.05.075](https://doi.org/10.1016/j.ijhydene.2008.05.075).

- [326] Wu, M.; Yang, C.; Wang, M. Morphological and Structural Studies of Nanoporous Nickel Oxide Films Fabricated by Anodic Electrochemical Deposition Techniques. *Electrochim. Acta.* **2008**, *54*, 155–161. DOI: [10.1016/j.electacta.2008.08.027](https://doi.org/10.1016/j.electacta.2008.08.027).
- [327] Golikand, A. N.; Shahrokhian, S.; Asgari, M.; Maragheh, M. G.; Irannejad, L.; Khanchi, A. Electrocatalytic Oxidation of Methanol on a Nickel Electrode Modified by Nickel Dimethylglyoxime Complex in Alkaline Medium. *J. Power Sources.* **2005**, *144*, 21–27. DOI: [10.1016/j.jpowsour.2004.12.017](https://doi.org/10.1016/j.jpowsour.2004.12.017).
- [328] Casella, I. G.; Gatta, M. Electrodeposition and Characterization of Nickel-copper Alloy Films as Electrode Material in Alkaline Media. *J. Electrochem. Soc.* **2002**, *149*, B465–B471. DOI: [10.1149/1.1504717](https://doi.org/10.1149/1.1504717).
- [329] Estellé, J.; Salagre, P.; Cesteros, Y.; Serra, M.; Medina, F.; Sueiras, J. Comparative Study of the Morphology and Surface Properties of Nickel Oxide Prepared from Different Precursors. *Solid State Ionics.* **2003**, *156*, 233–243. DOI: [10.1016/S0167-2738\(02\)00612-4](https://doi.org/10.1016/S0167-2738(02)00612-4).
- [330] Liu, C.; Li, Y. Synthesis and Characterization of Amorphous α -nickel Hydroxide. *J. Alloys Compounds.* **2009**, *478*, 415–418. DOI: [10.1016/j.jallcom.2008.11.049](https://doi.org/10.1016/j.jallcom.2008.11.049).
- [331] Wang, C.; Gau, G.; Gau, S.; Tang, C.; Bi, J. Preparation and Characterization of Nanosized Nickel Oxide. *Catal. Lett.* **2005**, *101*, 241–247. DOI: [10.1007/s10562-005-4899-x](https://doi.org/10.1007/s10562-005-4899-x).
- [332] Song, Q.; Li, Y.; Chan, S. Physical and Electrochemical Characteristics of Nanostructured Nickel Hydroxide Powder. *J. Appl. Electrochem.* **2005**, *35*, 157–162. DOI: [10.1007/s10800-004-6301-x](https://doi.org/10.1007/s10800-004-6301-x).
- [333] Ramesh, T.; Kamath, P. V. Synthesis of Nickel Hydroxide: Effect of Precipitation Conditions on Phase Selectivity and Structural Disorder. *J. Power Sources.* **2006**, *156*, 655–661. DOI: [10.1016/j.jpowsour.2005.05.050](https://doi.org/10.1016/j.jpowsour.2005.05.050).
- [334] Spinner, N.; Mustain, W. E. Effect of Nickel Oxide Synthesis Conditions on Its Physical Properties and Electrocatalytic Oxidation of Methanol. *Electrochim. Acta.* **2011**, *56*, 5656–5666. DOI: [10.1016/j.electacta.2011.04.023](https://doi.org/10.1016/j.electacta.2011.04.023).
- [335] Soulantica, K.; Maisonnat, A.; Fromen, M.; Casanove, M.; Lecante, P.; Chaudret, B. Synthesis and Self-Assembly of Monodisperse Indium Nanoparticles Prepared from the Organometallic Precursor [In (η^5 -C₅H₅)]. *Angew. Chem. Int. Ed.* **2001**, *40*, 448–451.
- [336] Esumi, K.; Tano, T.; Meguro, K. Preparation of Organo Palladium Particles from Thermal Decomposition of Its Organic Complex in Organic Solvents. *Langmuir.* **1989**, *5*, 268–270. DOI: [10.1021/la00085a051](https://doi.org/10.1021/la00085a051).
- [337] Reetz, M. T.; Helbig, W. Size-selective Synthesis of Nanostructured Transition Metal Clusters. *J. Am. Chem. Soc.* **1994**, *116*, 7401–7402.
- [338] Esumi, K.; Suzuki, A.; Yamahira, A.; Torigoe, K. Role of Poly (Amidoamine) Dendrimers for Preparing Nanoparticles of Gold, Platinum, and Silver. *Langmuir.* **2000**, *16*, 2604–2608. DOI: [10.1021/la991291w](https://doi.org/10.1021/la991291w).
- [339] Ahmadi, T. S.; Wang, Z. L.; Green, T. C.; Henglein, A.; El-Sayed, M. A. Shape-Controlled Synthesis of Colloidal Platinum Nanoparticles. *Science.* **1996**, *272*, 1924–1926. DOI: [10.1126/science.272.5270.1924](https://doi.org/10.1126/science.272.5270.1924).
- [340] Turkevich, J.; Kim, G. Palladium: Preparation and Catalytic Properties of Particles of Uniform Size. *Science.* **1970**, *169*, 873–879.
- [341] Klabunde, K. J.; Li, Y. X.; Tan, B. J. Solvated Metal Atom Dispersed Catalysts. *Chem. Mater.* **1991**, *3*, 30–39. DOI: [10.1021/cm00013a013](https://doi.org/10.1021/cm00013a013).
- [342] Deivaraj, T.; Lee, J. Y. Preparation of Carbon-supported PtRu Nanoparticles for Direct Methanol Fuel Cell Applications—a Comparative Study. *J. Power Sources.* **2005**, *142*, 43–49. DOI: [10.1016/j.jpowsour.2004.10.010](https://doi.org/10.1016/j.jpowsour.2004.10.010).

- [343] Park, G.; Yang, T.; Yoon, Y.; Lee, W.; Kim, C. Pore Size Effect of the DMFC Catalyst Supported on Porous Materials. *Int. J. Hydrogen Energy*. 2003, 28, 645–650. DOI: 10.1016/S0360-3199(02)00140-4.
- [344] Scibioh, M. A.; Kim, S.; Cho, E. A.; Lim, T.; Hong, S.; Ha, H. Y. Pt-CeO₂/C Anode Catalyst for Direct Methanol Fuel Cells. *Appl. Catal. B Environ.* 2008, 84, 773–782. DOI: 10.1016/j.apcatb.2008.06.017.
- [345] Ye, J.; Liu, J.; Zou, Z.; Gu, J.; Yu, T. Preparation of Pt Supported on WO₃-C with Enhanced Catalytic Activity by Microwave-pyrolysis Method. *J. Power Sources*. 2010, 195, 2633–2637. DOI: 10.1016/j.jpowsour.2009.11.055.
- [346] Amin, R.; Hameed, R. A.; El-Khatib, K.; Youssef, M. E.; Elzatahry, A. Pt-NiO/C Anode Electrocatalysts for Direct Methanol Fuel Cells. *Electrochim. Acta*. 2012, 59, 499–508. DOI: 10.1016/j.electacta.2011.11.013.
- [347] Amin, R.; Hameed, R. A.; El-Khatib, K.; El-Abd, H.; Souaya, E. R. Effect of Preparation Conditions on the Performance of Nano Pt-CuO/C Electrocatalysts for Methanol Electro-oxidation. *Int. J. Hydrogen Energy*. 2012, 37, 18870–18881. DOI: 10.1016/j.ijhydene.2012.10.009.
- [348] Ahmad, M.; Kamarudin, S. K.; Daud, W. R. W.; Yaakub, Z. High Power Passive μ DMFC with Low Catalyst Loading for Small Power Generation. *Energy Conversion Manage.* 2010, 51, 821–825. DOI: 10.1016/j.enconman.2009.11.017.
- [349] Knights, S. D.; Colbow, K. M.; St-Pierre, J.; Wilkinson, D. P. Aging Mechanisms and Lifetime of PEFC and DMFC. *J. Power Sources*. 2004, 127, 127–134. DOI: 10.1016/j.jpowsour.2003.09.033.
- [350] Hahn, R.; Wagner, S.; Schmitz, A.; Reichl, H. Development of a Planar Micro Fuel Cell with Thin Film and Micro Patterning Technologies. *J. Power Sources*. 2004, 131, 73–78. DOI: 10.1016/j.jpowsour.2004.01.015.
- [351] Shimizu, T.; Momma, T.; Mohamedi, M.; Osaka, T.; Sarangapani, S. Design and Fabrication of Pumpless Small Direct Methanol Fuel Cells for Portable Applications. *J. Power Sources*. 2004, 137, 277–283. DOI: 10.1016/j.jpowsour.2004.06.008.
- [352] Chen, C.; Yang, P. Performance of an Air-breathing Direct Methanol Fuel Cell. *J. Power Sources*. 2003, 123, 37–42. DOI: 10.1016/S0378-7753(03)00434-8.
- [353] Lim, C.; Wang, C. Development of High-power Electrodes for a Liquid-feed Direct Methanol Fuel Cell. *J. Power Sources*. 2003, 113, 145–150. DOI: 10.1016/S0378-7753(02)00541-4.
- [354] Liu, J.; Zhao, T.; Liang, Z.; Chen, R. Effect of Membrane Thickness on the Performance and Efficiency of Passive Direct Methanol Fuel Cells. *J. Power Sources*. 2006, 153, 61–67. DOI: 10.1016/j.jpowsour.2005.03.190.
- [355] Liu, J.; Sun, G.; Zhao, F.; Wang, G.; Zhao, G.; Chen, L.; Yi, B.; Xin, Q. Study of Sintered Stainless Steel Fiber Felt as Gas Diffusion Backing in Air-breathing DMFC. *J. Power Sources*. 2004, 133, 175–180. DOI: 10.1016/j.jpowsour.2004.02.009.
- [356] Broussely, M.; Archdale, G. Li-ion Batteries and Portable Power Source Prospects for the Next 5–10 Years. *J. Power Sources*. 2004, 136, 386–394. DOI: 10.1016/j.jpowsour.2004.03.031.
- [357] Yao, S.; Tang, X.; Hsieh, C.; Alyousef, Y.; Vladimer, M.; Fedder, G. K.; Amon, C. H. Micro-electro-mechanical Systems (Mems)-based Micro-scale Direct Methanol Fuel Cell Development. *Energy*. 2006, 31, 636–649. DOI: 10.1016/j.energy.2005.10.016.
- [358] Bae, B.; Kho, B. K.; Lim, T.; Oh, I.; Hong, S.; Ha, H. Y. Performance Evaluation of Passive DMFC Single Cells. *J. Power Sources*. 2006, 158, 1256–1261. DOI: 10.1016/j.jpowsour.2005.10.024.

- [359] Jung, D. H.; Lee, C. H.; Kim, C. S.; Shin, D. R. Performance of a Direct Methanol Polymer Electrolyte Fuel Cell. *J. Power Sources*. 1998, 71, 169–173. DOI: [10.1016/S0378-7753\(97\)02793-6](https://doi.org/10.1016/S0378-7753(97)02793-6).
- [360] Ren, X.; Wilson, M. S.; Gottesfeld, S. High Performance Direct Methanol Polymer Electrolyte Fuel Cells. *J. Electrochem. Soc.* 1996, 143, L12. DOI: [10.1149/1.1836375](https://doi.org/10.1149/1.1836375).
- [361] Jewett, G.; Guo, Z.; Faghri, A. Water and Air Management Systems for a Passive Direct Methanol Fuel Cell. *J. Power Sources*. 2007, 168, 434–446. DOI: [10.1016/j.jpowsour.2007.03.052](https://doi.org/10.1016/j.jpowsour.2007.03.052).
- [362] Jörissen, L.; Gogel, V.; Kerres, J.; Garche, J. New Membranes for Direct Methanol Fuel Cells. *J. Power Sources*. 2002, 105, 267–273.
- [363] Kerres, J. A.; Development of Ionomer Membranes for Fuel Cells. *J. Membr. Sci.* 2001, 185, 3–27. DOI: [10.1016/S0376-7388\(00\)00631-1](https://doi.org/10.1016/S0376-7388(00)00631-1).
- [364] Schaffer, T.; Hacker, V.; Hejze, T.; Tschinder, T.; Besenhard, J.; Prenninger, P. Introduction of an Improved Gas Chromatographic Analysis and Comparison of Methods to Determine Methanol Crossover in DMFCs. *J. Power Sources*. 2005, 145, 188–198. DOI: [10.1016/j.jpowsour.2004.11.074](https://doi.org/10.1016/j.jpowsour.2004.11.074).
- [365] Ren, X.; Zelenay, P.; Thomas, S.; Davey, J.; Gottesfeld, S. Recent Advances in Direct Methanol Fuel Cells at Los Alamos National Laboratory. *J. Power Sources*. 2000, 86, 111–116. DOI: [10.1016/S0378-7753\(99\)00407-3](https://doi.org/10.1016/S0378-7753(99)00407-3).
- [366] Bauer, F.; Willert-Porada, M. Microstructural Characterization of Zr-phosphate-Nafion® Membranes for Direct Methanol Fuel Cell (DMFC) Applications. *J. Membr. Sci.* 2004, 233, 141–149. DOI: [10.1016/j.memsci.2004.01.010](https://doi.org/10.1016/j.memsci.2004.01.010).
- [367] Tang, H. L.; Pan, M.; Jiang, S. P.; Yuan, R. Z. Modification of Nafion™ Membrane to Reduce Methanol Crossover via Self-assembled Pd Nanoparticles. *Mater. Lett.* 2005, 59, 3766–3770. DOI: [10.1016/j.matlet.2005.07.013](https://doi.org/10.1016/j.matlet.2005.07.013).